NOTICE

The quality of this microform is heavily dependent upon the quality of the original thesis submitted for microfilming. Every effort has been made to ensure the highest quality of reproduction possible.

If pages are missing, contact the university which granted the degree.

Some pages may have indistinct print especially if the original pages were typed with a poor typewriter ribbon or if the university sent us an inferior photocopy.

Reproduction in full or in part of this microform is governed by the Canadian Copyright Act, R.S.C. 1970, c. C-30, and subsequent amendments.

AVIS

La qualité de cette microforme dépend grandement de la qualité de la thèse soumise au microfilmage. Nous avons tout fait pour assurer une qualité supérieure de reproduction.

S'il manque des pages, veuillez communiquer avec l'université qui a conféré le grade.

La qualité d'impression de certaines pages peut laisser à désirer, surtout si les pages originales ont été dactylographiées à l'aide d'un ruban usé ou si l'université nous a fait parvenir une photocopie de qualité inférieure.

La reproduction, même partielle, de cette microforme est soumise à la Loi canadienne sur le droit d'auteur, SRC 1970, c. C-30, et ses amendements subséquents.

NUMERICAL MODELLING OF THE SEDIMENTATION AND CONSOLIDATION OF TAILINGS

Nilo Cesar Consoli

A Thesis
in
The Department of Civil Engineering

Presented in Partial Fulfillment of the Requirements
for the Degree of Doctor of Philosophy
at
Concordia University
Montreal, Quebec, Canada

September, 1991

ISBN 0-315-73681-X

Canada

ABSTRACT

Numerical Modelling of The Sedimentation and Consolidation of Tailings

Nilo Cesar Consoli, Ph. D.
Concordia University, 1991

The byproduct of processing rocks for the purpose of extraction of minerals is a waste which is generally referred to as tailings. These byproducts are impounded behind dams specially designed for this objective and are known as tailings deposits.

The objective of this study is to investigate the true capacity of a reservoir when waste material is impounded. The process consists of dispersion, sedimentation and consolidation, which take place simultaneously. It is the purpose of the present study to analyze these coupled phenomena of soil formation to estimate the volume of waste that can be impounded. This is an important factor from a financial and ecological view point.

A theory is proposed which contains the sedimentation and consolidation processes. In order to have a complete modelling of the problem an Implicit Finite Difference Code was developed. The code is based on the use of the Preissmann Scheme and the Double Sweep Method to solve the system of partial differential equations that form the sedimentation part of the problem. A new constitutive model for the characterization of the stress-strain behavior of the solid skeleton, considering the changes in the state of the material is developed. This forms an important part of the basic equation of the consolidation process coupling pore-pressure dissipation and deformation of the soil mass. A Finite Element Code is developed incorporating both nonlinearities, i.e. those arising

from the material response (Elasto-Plastic Model) and those due to geometrical (Eulerian System) nonlinearities.

To complement the study, the case of the disposal of a bauxite mine in a reservoir located in Saramenha, district of Ouro Preto, Minas Gerais, Brazil is considered.

Comparison between numerical analysis and field measurements is made based on total and effective stresses profiles, void ratio profile and vertical displacements through the soil formation profile. The numerical analysis successfully predicts the filling of the reservoir, which helps build confidence in the numerical procedure developed in this study.

" Is mathematical analysis...only a vain play of the mind? It can give to the physicist only a convenient language; is this not a mediocre service, which, strictly speaking, could be done without; and even is it not to be feared that this artificial language may be a veil interpose between reality and the eye of the physicist? Far from it; without this language most of the intimate analogies of things would have remained forever unknown to us; and we should forever have been ignorant of the internal harmony of the world, which is...the only true objective reality. "

Henri Poincaré

ACKNOWLEDGEMENTS

- First, I would like to thank Dr. Hormoz B. Poorooshasb, for his guidance, support, advice, inspiration and friendship during this important period of my life. Special thanks to Dr. Matthew M. Douglass for his kindness, encouragement and support and to Dr. Roberto F. de Azevedo for his encouragement and friendship in decisive periods like the time when I was deciding to come to Montreal, as well as, the period of definition of the thesis topic.

- I must express my gratitude to my colleagues and friends Dr. Q. S. Yang for helpful discussions throughout the development of this work and Dr. M. Z. Emir for his patience in teaching me new skills with the Macintosh.

- Financial support provided by Brazilian Government Agency for Improvement of Personnel with University Degree Level (CAPES) and Federal University of Rio Grande do Sul (UFRGS) are gratefully acknowledged.

- I am grateful to the special friends that I made here, in particular Maria Helena, Robert, Geraldo, Maria Agueda, Qi Fu, Annemarie, Tim Kilbourn, Kazuko Akamatsu, Chico and Norma.

- Thanks to my family, Seu Nilo, Dona Leda, Lenice, Rafael, Sérgio and Ieda, for their support and their unlimited effort that brought my education to this point. Without their love I would not be here.

- Last, but not least, I want to thank the person who was always at my side, in sickness and in health, in good and bad times, my wife, Liselena, for her love, understanding, patience and encouragement during these past three years in Montreal.

TABLE OF CONTENTS

CHAPTER 3

CHAPTER 4

CHAPTER 5

CHAPTER 6

CHAPTER 7

CHAPTER 8

LIST OF FIGURES

LIST OF TABLES

LIST OF SIMBOLS

A ..... Cross Sectional Area of the Sediment-Fluid Mixture

A, ν, R, S, T, ζ ..... Parameters of the Constitutive Relation

A_c ..... Cross Sectional Area of the Sediment Deposited Layer

$A_j, B_j, C_j, D_j, E_j, F_j, G_j$ ..... Preissmann Scheme Coefficients

α ..... Coriolis Coefficient

C ..... Concentration of Solids in the Fluid

C_c ..... Concentration of Solids in the Top Layer of the Deposited Sediments

C_{ijkl} ..... Elastic Tensor

C_v ..... Coefficient of Consolidation

D_{ijkl}^{ep} ..... Elasto-Plastic Matrix

$d\varepsilon^p_{ij}$ ..... Increment of Plastic Strain

dF_i^b ..... Incremental Boundary Force

dS ..... Incremental Surface

$d\Gamma$ ..... Scalar responsible for the magnitude of the Plastic Strain

dv_i ..... Fictitious Incremental Vector of the Velocities of the Material Skeleton

Δt ..... Time Step Grid

Δx ..... Spatial Grid

δ_{kl} ..... Kronecker Delta

E ..... Young's Modulus

e ..... Void Ratio

$e_{Casagrande}$ ..... Casagrande's Void Ratio

e^p ..... Plastic Distortion

e' ..... Effective Void Ratio

ε_{ij} ..... Strain Tensor

F ..... Yield Function

F_i ..... Components of the Body Force

f ..... Internal Yield Function

f_x ..... Deposition Flux

g ..... Acceleration of Gravity

$g(\theta)$ ..... Function which defines the Cross Sectional Shape of the State Boundary Surface in the π-Plane

γ^f ..... Unit Weight of the Fluid

γ^t ..... Total Unit Weight of the Soil

γ^w ..... Unit Weight of the Water

H_p ..... Plastic Hardening Parameter

I ..... Inflow

I_c ..... Slope of the Channel Bed

I_1 ..... First Invariant of the Stress Tensor

J_2, J_3 ..... Second and Third Invariants of the Stress Deviation Tensor

K_{ij} ..... Permeability Tensor

K_o ..... Coefficient of Earth Pressure at Rest

k ..... Permeability Coefficient

κ ..... Von Karman Constant

L ..... Width of the Control Volume

Λ ..... Plastic Potential Function

Λ^f ..... Internal Plastic Potential Function

$\mu, \delta, W, e_o, L, E_o$ ..... Parameters of the Constituitive Relation

N_d, N_p ..... Shape Functions

n ..... Manning Coefficient

n ..... Porosity

ν ..... Poisson's Ratio

ν_i ..... Normal Vector to dS

Ω ..... Weighting Factor for Space

p ..... Pore-Pressure

p^N ..... Nodal Pore-Pressure

p_a ..... Atmospheric Pressure

p,q,θ ..... Quantities Derived from the Invariants of Stress

ϕ ..... Mohr-Coulomb Angle of Friction

$\Psi(e^p)$ ..... Function which records the history of the Plastic Flow

R_{ij}, W_{ij} ..... Components of Rotation

ρ ..... Density of the Sediment-Laden Fluid

ρ_c ..... Density of the Deposited Material

ρ_s ..... Density of the Sediments

ρ_w ..... Density of the Fluid

S ..... Surface

S_f ..... Friction Slope

S_{ij} ..... Stress Deviation Tensor

S_{ij} ..... Kirchoff Stress

ST ..... Average Concentration of Suspended Sediments

σ_{ij} ..... Stress Tensor

σ_{ij} ..... Cauchy Stress Tensor

σ_{v}' ..... Vertical Effective Stress

T_i ..... Traction

T_{ij} ..... Lagrange Stress Tensor

T_s ..... Incremental Thickness of Sediments

t ..... Time

Θ ..... Weighting Factor for Time

U_z ..... Consolidation Ratio

u_i ..... Displacements

u_i^N ..... Nodal Displacements

V ..... Mean Velocity of the Flow

V ..... Volume

v_i ..... Velocity of the Material Skeleton

v_i^f ..... Velocity of the Fluid

v_i^N ..... Nodal Velocity of the Material Skeleton

v^f_{kl} ..... Unit Tensor to the Internal Yield Surface

v^P_{ij} ..... Unit Tensor to the Internal Plastic Potential Surface

ϑ, ϑ_o ..... Spatial Angles

w ..... Sediment Fall Velocity

X_j ..... Original System of Coordinates

x_j ..... Current System of Coordinates

Y ..... Depth of the Flow

Z ..... Coordinate at the Bottom of the Channel

CHAPTER 1

INTRODUCTION

1.1. Motivation for the Study

The increasing necessity of mineral resources for the maintenance of technological development poses an environmental problem: the demand for storage space for its waste.

The waste, a fine grained cohesionless assembly of particles generally known as tailings, is a complicated material to deal with in view of the lack of understanding of its mechanical behavior and the fact that often it carries toxic matter with it.

To start with, the mode of deformation of the waste material (tailings) is not well understood. Hence the volume required for its impounding, generally disposed in valleys or reservoirs behind dams, can not be evaluated with ease. The process is further complicated by the fact that the deposition is originally in a state of suspension and after sedimentation undergoes a process of consolidation. These factors are mainly responsible for making the situation extremely complex from an engineering and analytical viewpoint.

1.2. Purpose of Study

The objectives of the present study are:

• To develop and calibrate an appropriate constitutive law to describe the flow of the material.

• To study the processes of transportation of sediments, sedimentation and consolidation of the material, which take place simultaneously.

• To outline the needs for further research in this field.

1.3. Methodology

The solution of the nonlinear partial differential equations (the governing equations of the problem) will be solved through the following special techniques :

1 - It is demonstrated that the problem of elasto-plastic finite deformation is governed by a quasi-linear model irrespective of deformation magnitude. This follows from the adoption of a rate viewpoint towards finite deformation finite element method based in the Eulerian Coordinate System and Kirchoff Stresses, which is developed by application of the Gauss Theorem and Galerkin Method to the instantaneously linear governing differential equations, where the constitutive model is introduced.

2 - In the study of the sedimentation process, in order to have a complete modelling of the problem an Implicit Finite Difference Code is developed employing the Preissmann Scheme and the Double Sweep Method.

3 - A study is made to establish a level of confidence in the analysis through a case study of the situation prevailing in Saramenha, Brazil.

1.4. Thesis Outline

In Chapter 2, a review is made of the work previously completed linking the processes of sedimentation and consolidation.

In Chapter 3, a description of the case history, with geotechnical characteristics of the bauxite tailings, special laboratory tests and field instrumentation are presented.

Chapter 4 discusses the sedimentation model developed, where the system of partial differential equations that are the foundation of the physical problem, are codified in an Implicit Finite Difference Code.

In Chapter 5, a new constitutive model is developed, based on State Parameters (Poorooshasb, 1961). The stress-strain relation are described, by calibrating the model using test results performed on samples of a cohesionless soil. The stress-strain curves and stress paths are analytically reconstituted for monotonic and cyclic loading.

In Chapter 6, the development of a finite deformation finite element method to deal with the Coupled Consolidation Theory is presented. The code employs the Eulerian System of Coordinates.

In Chapter 7 numerical solutions are compared with the exact solutions to examine the accuracy of the model proposed.

A study of Saramenha's Case History is presented in Chapter 8, and comparisons are made between the field data measurements and the numerical results.

Finally, in Chapter 9, conclusions are presented and suggestions for further research proposed.

CHAPTER 2

REVIEW OF PREVIOUS WORK

2.1. Introduction

Since the research on the motion of a solid particle in a fluid was started in the middle of the nineteenth century by Stokes, relative flow of the fluid and solid phases have been studied in several fields as sedimentology, chemical engineering, hydraulic engineering, geotechnical engineering and environmental engineering.

Almost all the work on the behavior of solid-liquid mixtures is divided into a theoretical basis between sedimentation of dispersions and consolidation of sediments. Consequently this review will concentrate on the themes of sedimentation, consolidation and the link between the two.

2.2. Sedimentation

Sedimentation processes have been used for centuries. However, it was Stokes, in 1851, who first proposed a law to explain the relative flow established between a continuous fluid phase and a discontinuous solid phase. This law is known as Stokes Law, and states that the settling velocity of a dispersion was considered to be a material property of the mixture, which, in turn, depends on the velocity of a single particle and the porosity of the mixture.

Lewis et al. (1949) studied the fluidazation of glass spheres and found that their results could best be correlated by an expression where the fluidazation velocity of the liquid phase was directly related to the Stokes velocity of a single particle and the porosity.

This was followed by Kinch (1952), who realized that the settling process of uniform dispersions is a transient process. This theory, however, ignores the continuity of the mixture and focuses its attention on the continuity of the solid phase. The effective stresses in the sediment which is formed at the bottom of the dispersion are ignored so that the velocity of the solid particles is a function of the porosity only.

Experimental studies of sedimentation are reported by McRoberts and Nixon (1976), Been (1980), Imai (1980), Schiffman et al (1984) and Abreu (1989).

Tan et al., (1990) have studied the behavior of clay slurry and concluded that it is sensitive to the environment the slurry is in. For a dilute slurry, viscometric study indicates that it has zero strength, but as soon the void ratio is reduced below certain value, there is a dramatic gain in strength.

2.2.1. Considerations of Sediment Transport

The study of a real life sedimentation problem is not restricted to the understanding of the deposition of the sediments, but also to its transportation: both are parts of the natural process which occurs simultaneously.

Most of the work done in this area was basically in the development of methods for the prediction of the amount of sediments carried into a reservoir as a function of watershed characteristics. This is a stochastic problem and thus a model to predict the amount of sediment storage in reservoirs should involve the theory of probability.

Iwagaki (1956) explained the process of sedimentation in a reservoir using the equation of motion and continuity for clear water flowing in a channel, together with a sediment load equation.

A review of the literature shows that in the beginning empirical methods were introduced to obtain the distribution of storage sediment in reservoirs. As an example there is the case of the Empirical Area-Reduction Method developed by Borland and Miller (1960), but the use of their method is limited because the

effects of the flow characteristics are not considered. After that, deterministic methods were developed to predict the amount of sediments carried into a reservoir as a function of watershed characteristics, e.g. the studies of Paulet (1971). Chang and Richards (1971) developed a numerical method based on the method of characteristics for the solution of the process of sedimentation. Soares (1975) discusses a deterministic model to evaluate sediment deposition in a reservoir, and the results of this analysis are then given as inputs to the stochastic model in order to obtain the mean value and the variance of the sediment storage as a function of time. Lyn (1987) has studied standard one-dimensional equations of unsteady sediment transport. Rahuel et al. (1989) introduced a methodology for simulation of water and sediment movement in mobile-bed alluvial rivers, treating bedload transport of nonuniform sediment mixtures.

2.3. Consolidation

A rapid application of load to a saturated mass of soil generates a pore-pressure distribution which triggers a field of relative velocities between soil particles and the surrounding liquid. At this moment, a transitory process of flow begins, during which variation of the displacement, stress and deformation occur. This process induces a volume change, linked to a transference of pressure from the liquid to the soil skeleton: the process is referred to as consolidation.

This physical phenomena is modelled by a complex mathematical formulation, which is solved in its most general form by time and spatial integration of a system of non-linear partial differential equations, with appropriate initial and boundary conditions.

The first coherent theoretical formulation of the consolidation phenomena was developed by Terzaghi in 1923. Even though his theory was only in unidimensional terms it founded the mathematical basis of many theories which followed. The main hypotheses of the unidimensional theory of Terzaghi are:

- Complete saturation of the soil;

- Incompressibility of the soil grains and interstitial liquid;

- Validity of Darcy's Law;

- Liquid flowing only in one (vertical) direction;

- Validity of hypothesis of infinitesimal strain;

- Strains in the same direction as drainage;

- Permeability coefficient independent of void ratio;

- Void ratio dependent only on effective stress and through a linear relation;

- Total stresses constant with time;

The above simplified assumptions restricted the use of this theory considerably. For this reason, new formulations have appeared since then. Davis and Raymond (1965), extended the pioneer theory, considering the effects of non-linearity in the relation between void ratio and effective stress. Mikasa (1965) and Poskitt (1969), went further and developed a theory in which permeability and compressibility coefficients were non-linear functions of the void ratio. However, still considering a unidimensional theory, Gibson, England and Hussey (1967), added to the previous theories the consideration of finite strain in the Lagrangean System. In reality, as shown by Schiffman (1980) all unidimensional theories of consolidation are particular cases of the theory developed by Gibson, England and Hussey (1967).

In 1936, Rendulic created a theory which considered multidimensional consolidation and was an extension of the Terzaghi's theory and due to this was named Terzaghi-Rendulic or Pseudo-Multidimentional Theory. The name Pseudo-Multidimensional Theory is due to the fact that this theory was still based in the hypotheses that the total stresses remain constant during the complete process of consolidation in the case where loading remain unchanged. Following the previous hypotheses it is possible to formulate the problems of multidimensional consolidation from a diffusion type equation where the only unknown is the excess pore-pressure. In this way, the dissipation of the excess

pore-pressure is studied separately from the phenomena of the deformation of the soil skeleton.

Biot (1941) formulated the first general and coherent multidimentional consolidation theory, taking into consideration the interdependency between the deformation of the soil skeleton and the flow of the interstitial fluid.

One of the most interesting characteristics of the Biot's Theory is that in some regions of the porous media submitted to a process of consolidation with external loading constant, the pore-pressure can rise to higher values than the initial ones, without any volume change in the region. This phenomena was studied in some detail by Mandel (1953) and Cryer (1963), and is referred to as the Mandel-Cryer Effect.

Unfortunately, due to mathematical complexity, only simple problems have been solved analytically using Biot's Theory. These include the consolidation of a sphere subjected to hydrostatic pressure (Cryer, 1963) and an infinite strip uniformly loaded in a semi-infinite media (Schiffman et al, 1969). It is emphasized again that all these solutions are for a homogeneous, linear elastic and isotropic media. Real life problems have to be analyzed removing as many of the above restrictive assumptions as possible.

2.3.1. Finite Element Analysis of Consolidation

With the development of the Finite Element Method the solution of more realistic boundary problems with the Biot's Coupled Consolidation Theory became possible.

Sandhu and Wilson (1969) were the first to obtain a solution of the Biot's Theory using the Variational Principles. The numerical solution of Terzaghi's unidimensional consolidation and the consolidation of a linear elastic semi-space medium due to a distributed load were verified against exact solutions with good agreement.

Osaimi and Clough (1979) extended the work of Sandhu and Wilson considering the material non-linearity through the use of the Hyperbolic Model (Duncan and Chang, 1970), as well as, introducing incremental construction.

Sandhu and Liu (1979) studied the consolidation of soils which exhibit secondary compression considering visco-elastic material behavior.

Adachi et al. (1982) studied the consolidation behavior of saturated clay using a visco-elasto-plastic model combining the Cam-Clay concept and Perzyna's description.

Chang and Duncan (1983) developed the formulation of the consolidation theory in finite elements in partially saturated soil.

Lately, several analyses obtained with the use of finite element method in the study of case histories have been documented. As an example, the case analyzed by Magnan et al. (1982) , where an experimental embankment built by the Laboratory Des Ponts et Chaussees in Cubzak-les-Ponts, France, showed good agreement in comparison between the numerical analyzis and the field data.

Almeida and Ortigão (1982), using the Modified Cam-Clay Model implemented in the coupled consolidation finite element code analyzed successfully the behavior of an experimental embankment laying over a thick layer of soft clay in Sarapui, Rio de Janeiro, Brazil.

Another case history was analyzed by Zeng and Gong (1985), where material non-linearity and anisotropy were considered in the Biot's theory finite element code. In this case the behavior of a soft clay deposit, over which two oil tanks where built, was successfully predicted.

Consoli (1987) using the Modified CamClay Model, as well as, the Hyperbolic Model analyzed successfully the behavior of an experimental excavation in a soft clay deposit situated in a river shore near Sarapui, Rio de Janeiro, Brazil. The analytical and field data comparisons include horizontal displacements, surficial displacements, pore-pressure and vertical displacements at several depths.

Yang (1990) using a model capable of simulating monotonic and cyclic loading succesfully predicted the susceptibility of liquefaction of the seafloor under storm waves at the Ekofisk tank site in the North Sea.

Emir (1991) studied the effect of vibration in the consolidation of very soft clays using an elasto-viscoplastic constitutive equation.

2.3.1.1 Finite Deformation Finite Element Analysis

Investigation of problems involving geometrical nonlinear behavior has been a subject of study for some time.

Much of the earlier work (Kirchoff, 1883) was developed due to the difficulty in the analysis of many practical problems, as the deformation of the spiral spring, where the displacements are not small. Since that time, many investigators have developed the general theory of elasticity which incorporates the possibility of finite displacements, strains and rotations. An historical account of large elastic deformation theory and applications has been given by Truesdell (1952).

The problem of finite deformation of an elasto-plastic continuum has received much attention. Initially, attempts were made to examine the conditions necessary for a rigorous solution (Hill, 1962).

Several researchers considered various ways of decomposing the strain rate into elastic and plastic parts, among them were Green and Naghdi (1965) and Lee (1969).

The invention of the digital computer has given rise to a great amount of activity in this area. Many incremental formulations have been put forward to make use of the numerical capabilities of computers. Most have utilized finite element schemes and these include diverse formulations of both Lagrangian (material) and Eulerian (spatial) type. Further details of the Lagrangian and Eulerian approaches are given in Chapter 6.

Most of the work done has been devoted to formulating analysis for plate and shell problems including large displacement but small strains. These

formulations are inappropriate for applications to bulky geometries encountered in most problems in soil mechanics.

Hibbit et al. (1970) used a Lagrangian scheme to derive finite element rate equilibrium equations from the principle of virtual work for large deformations.

Zienkiewicz and Nayak (1971) presented a unified formulation for large deformation and plasticity problems. A Lagrangian system was used in conjunction with an isoparametric finite element code to solve a thick cantilever problem.

An Eulerian system was developed by Osias and Swedlow (1974), where derivation of the finite elernent equations was made by the use of the Galerkin Method. A rate viewpoint was adopted and objectivity of formulation was preserved by the introduction of the Jaumann stress rate.

Meeking and Rice (1975) adopted an Eulerian formulation and derived governing equations based on variational principles. The analysis of a bar in plane strain tension is presented as a numerical example.

In the field of soil mechanics a few attempts have been made at the application of a finite deformation analysis to soil behavior, even though it is well known that large deformations occur when very soft soils are loaded and during the process of soil formation.

One of the first attempts in this area was made by Fernandez and Christian (1971) who performed an analytical study of a strip footing on undrained clay with both material and geometric nonlinearities included in the formulation.

The study of one-dimensional elastic finite consolidation and bidimensional elastic finite deformation consolidation of a rigid footing was made by Carter et al., (1976), showing the importance of geometrical non-linearity compared to infinitesimal theory. In this work an Eulerian rate viewpoint was adopted, as it was previously used by Osias and Swedlow (1974). The same authors presented a paper in 1977 in which the loading surface of an initially stressed free elastic-perfectly plastic cohesive soil is studied.

Yamada and Wifi (1977) have studied the behavior of shallow foundations of homogeneous and multilayer soils through a rational approach to the finite strain analysis based on a variational principle. The influence of different footing size is shown.

An Eulerian formulation of the finite element method for predicting the stresses and pore water pressure around a driven pile was developed by Banerjee and Fathallah (1979). The analysis had been applied reasonably to the problem of expanding a cylindrical cavity to twenty times its original radius.

Meijer (1984) studied the comparison of elastic finite and infinitesimal strain consolidation by numerical experiments. The field equations were formulated on a Lagrangian coordinate system. The conclusions of Meijer's work were that for the case of a vertically loaded half plane, despite the assumption of a weak material the differences of the results were not spectacular.

Burd et al. (1986) using an Eulerian Scheme with an elastic-perfectly plastic constitutive model have studied the behavior of reinforcement of a layer of granular fill on a soft clay subgrade. Model tests were analytically reproduced with accuracy.

Kiousis et al. (1986), presented an incremental finite element formulation for elastic-perfectly plastic bodies subjected to large deformation. The formulation is in Lagrangian coordinates and the plasticity model employed is the extended Von Mises.

Dluzewski (1988) developed a total Eulerian finite element formulation with the hyperbolic (non-linear elastic) model as the stress-strain model where the solution of the boundary value problems can be sought via an iterating process. The main shortcoming is that no history of the process can be taken into consideration and the analysis is limited to monotonic loadings only.

The above mentioned theories of finite deformation finite element analysis of consolidation assume that the soil skeleton is elastic, non-linear elastic or elastic-perfectly plastic. Furthermore only monotonic behavior is considered.

2.3.1.2 Simulation of Incremental Construction

Incremental construction procedures must be modeled in order to simulate the performance of typical geotechnical engineering problems. Sequential construction was first analytically modeled by King (1965) who employed the finite element method to simulate the incremental construction of concrete gravity dams. In his procedure the building layer is assumed to be placed in a liquid state where the material has weight but is unable of carry shear stresses. When the next layer is placed, in the same way that the previous layer was, the first layer is assumed to be able to resist shear stresses. This process continues until all layers are constructed.

2.3.2. Stress-Strain Behavior of Soils

The stress-strain behavior of soils is dependent on several factors such as drainage conditions, stress history, loading conditions and is highly nonlinear and inelastic. The history of soil modelling started with the linear elastic model, followed by nonlinear elastic models and finally models based on the plasticity theory.

2.3.2.1 Elastic Linear Relation

The first stress-strain relation to be proposed for materials in general was the linear elastic relation developed by Hooke, and known nowadays as Hooke's Law. This relation presumes a unique relation between stress tensor (σ_{ij}) and strain tensor (ε_{ij}) and may be expressed by the equation

$$\sigma_{ij} = C_{ijkl}\ \varepsilon_{kl} \qquad (2.1)$$

where C_{ijkl} is a forth order tensor representing the elastic constants.

2.3.2.2 Pseudo-Elastic Non-Linear Relation

The development of non-linear elastic relations started in 1963 with the work of Kondner and Zelasko, which proposed that stress-strain curves for soils could be determined by hyperbolas. Duncan and Chang (1970) developed the Hyperbolic Model, which was based on the suggestions of Kondner and Zelasko (1963) and on the relation proposed by Janbu (1963) in which Young's Modulus is related to the confining pressure through a logarithmic relation. The shear strength of the soil is characterized by the Mohr-Coulomb criterion.

Zienkiewicz and Naylor (1971) and Consoli (1987) approached non-linear elasticity by directly relating Young's Modulus to the mean stresses of the soil.

The main shortcomings of this kind of approach are that no history of loading can be taken into consideration, its inability to represent dilatancy and the impossibility of considering the influence of the void ratio and its variation in the formulation.

2.3.2.3 Models Based on the Plasticity Theory

The first attempts to analyze the behavior of plastic materials were made by Coulomb in 1773 and Rankine in 1857, in earth pressure calculations.

The scientific study of plasticity of metals began with the work of Tresca (1864), followed by Saint-Vënant (1870), Levy (1870), Von Mises (1913), Prandtl (1924) and Hencky (1924). During this early period there seemed to be little appreciation of the necessity of considering the strain rate behavior of plastic materials.

After 1950, there was a period of fast advances when Drucker and Prager (1951) developed the fundamental theorems of limit analysis for perfect plastic materials and Drucker(1951) launched the definition of work-hardening material and the concept of associated flow rule.

Drucker, Gibson and Henkel (1957) introduced the concept of work hardening into soil mechanics.

Roscoe et al (1958, 1963 and 1968) introduced isotropic hardening plasticity into soil mechanics through the development of the strain hardening CamClay Model and Modified CamClay Model, where in both models normality was ensured.

The concepts of State and State Parameters were introduced by Poorooshasb (1961) and it was in this work that the concept of Critical State Line as the locus where shear deformations continue, without further volume change was introduced.

Poorooshasb et al. (1966, 1967) extended the plasticity ideas for cohesionless soil to a non-associated form in which the yield surface and the plastic potential were defined separately.

Lade and Duncan (1975) and Lade (1977) developed and later modified a work hardening model able to describe the behavior of the cohesionless media. The latest version of the model has two yield surfaces, a cone and a cap, both hardening isotropically. A non associated flow rule was used in the conical yield surface and an associated flow rule was used for the cap yield surface.

Mroz (1967) and Prevost (1978) have proposed a kinematic hardening type of model known as nested yield surface or multisurface plasticity, where instead of using a single yield surface in stress space, it postulates the existence of a family of yield surfaces with each surface translating independently, obeying a linear work hardening model.

Linking the Bounding Surface concept (Dafalias and Popov, 1975) to a yield surface, Mroz (1979) proposed the two surface model, where the yield surface was allowed to translate within the domain enclosed by the bounding surface, hardening isotropically.

Poorooshasb and Pietruszczak (1985, 1986) developed a two surface model for sand which is based on the bounding surface concept incorporating a non - associated flow rule and the idea of reflected plastic potential.

Yang (1990) developed a simple constitutive model in terms of effective stress and based on the concepts of generalized plasticity and bounding surface formulation with the ability to deal with monotonic and cyclic loading.

2.4 Link Between Sedimentation and Consolidation Processes

Almost all of the literature cited above recognizes the simultaneous presence of sedimentation and consolidation in the deposition phenomena, both inland and offshore. These processes are coupled with mass transport and erosion.

However, little work has been done towards linking sedimentation and consolidation in a single framework.

Been (1980) pointed out the relation which existed between the theories of Kinch (1952) and Gibson, England and Hussey (1967).

Somasundaran (1981) studied the process of sedimentation and consolidation from an experimental viewpoint.

Schiffman et al., (1984) presented a single theoretical basis for sedimentation and consolidation processes of solid-water mixtures. The behavior of the mixture as a whole is governed by the same material properties during both processes and the link is provided by a modified effective stress principle.

It is important to point out that all the work done this far has been restricted to the solution of unidimensional problems. The theory presented in this thesis, however, provides an extension of the concept to deal with multidimensional problems as they occur in practice.

CHAPTER 3

SARAMENHA' S CASE HISTORY DESCRIPTION

3.1. Introduction

The field problem consists of the sedimentation and consolidation characteristics of bauxite tailings impounded behind Marzagão Dam located in Saramenha, district of Ouro Preto, province of Minas Gerais, Brazil.

The Dam is located at a distance of 3000 meters from the production area of the ALCAN DO BRASIL bauxite plant, a subsidiary of the ALCAN ALUMINUM LIMITED, a Canadian Enterprise which operates in Brazil. A plan view of the region can be seen in Figure 3.1. The length of reservoir is approximately 1000 meters, with an average inclination of 1%. The cross sections of the reservoir are variable. The annual rainfall causes an average inflow into the reservoir of 9.5 m^3/s. The predominant flow patterns are presented in Figure 3.2.

The utilization of the Marzagão Dam for storage of residuals started in 1974. In the beginning there was a concrete dam which later was incorporated in the core of the earth dam that is under construction at present. When completed this dam will have a section as shown in Figure 3.3. The present crest is at altitude level 1182 meters above the sea level, with its spillway at the level 1177.5. This level is the first of four stages forecasted to the completion of the dam.

In Figure 3.2 are shown the three inlet points at which the waste was disposed in accordance with the following scheme:

- First Disposal Point (1974 to 1979), with a yearly average of 125000 tons of solid waste;

- Second Disposal Point (1979 to August/1988), with a yearly average of 175000 tons of solid waste;

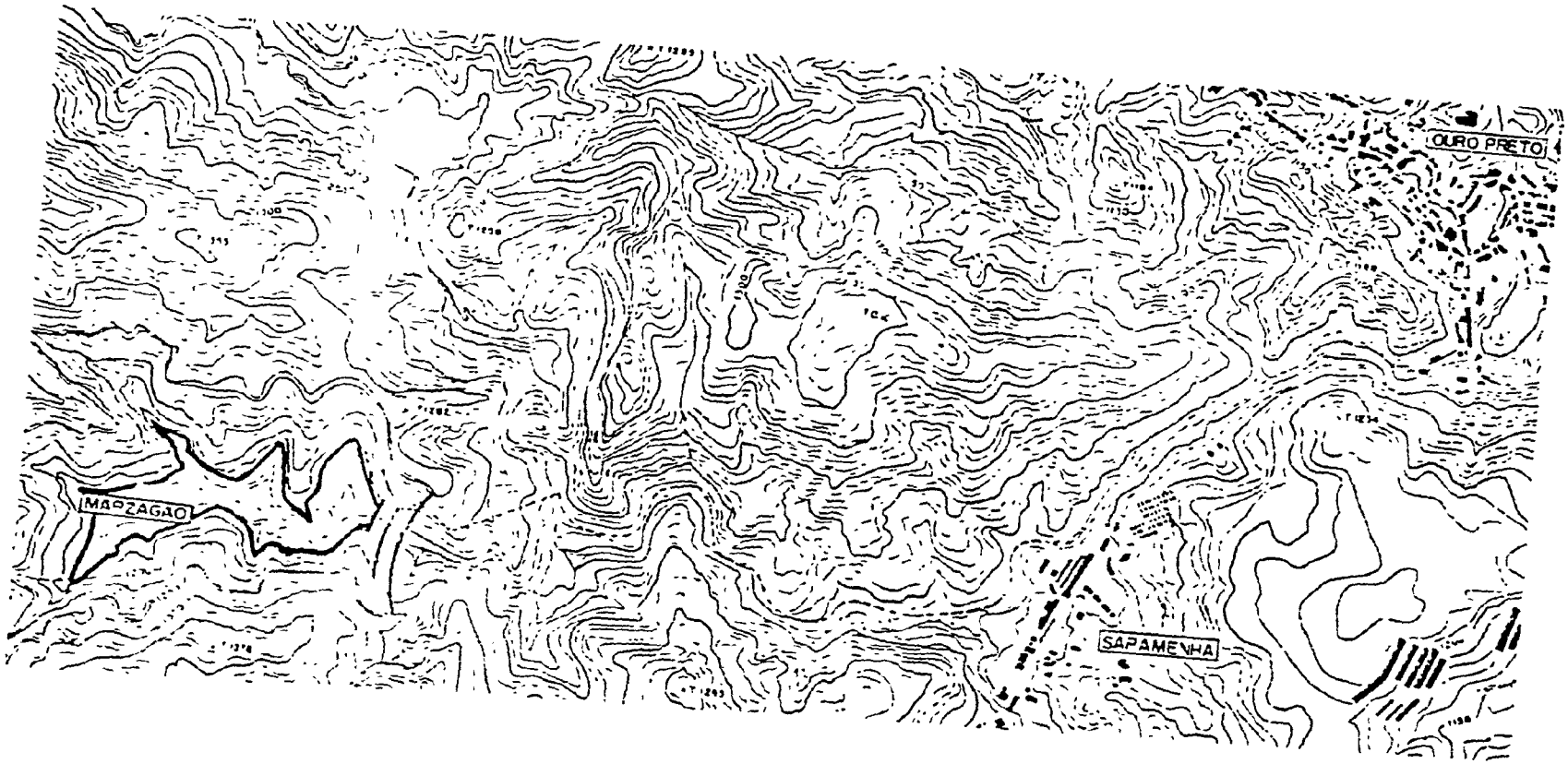

Figure 3.1 - View of the Region

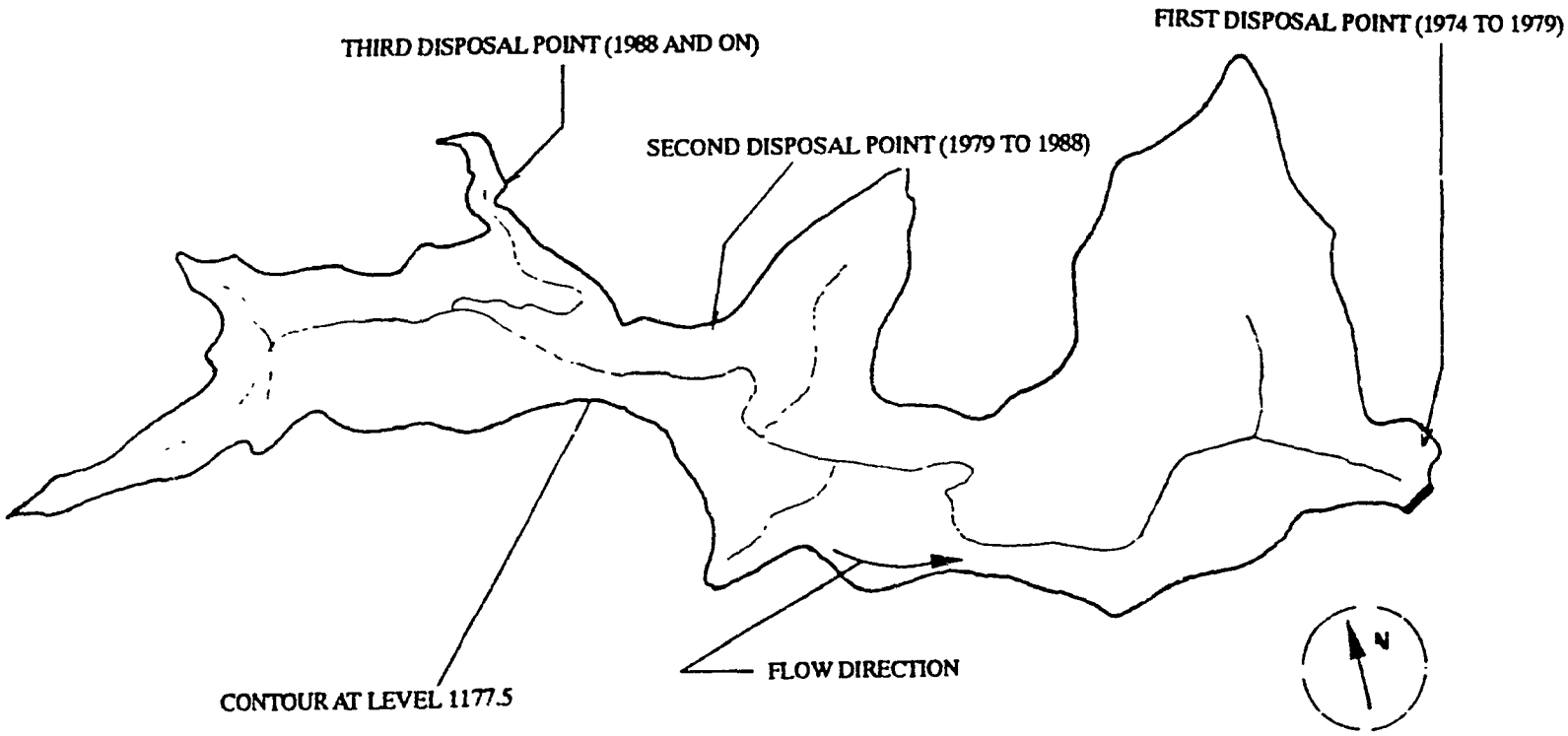

Figure 3.2 - Flow Direction and Waste Disposal Points

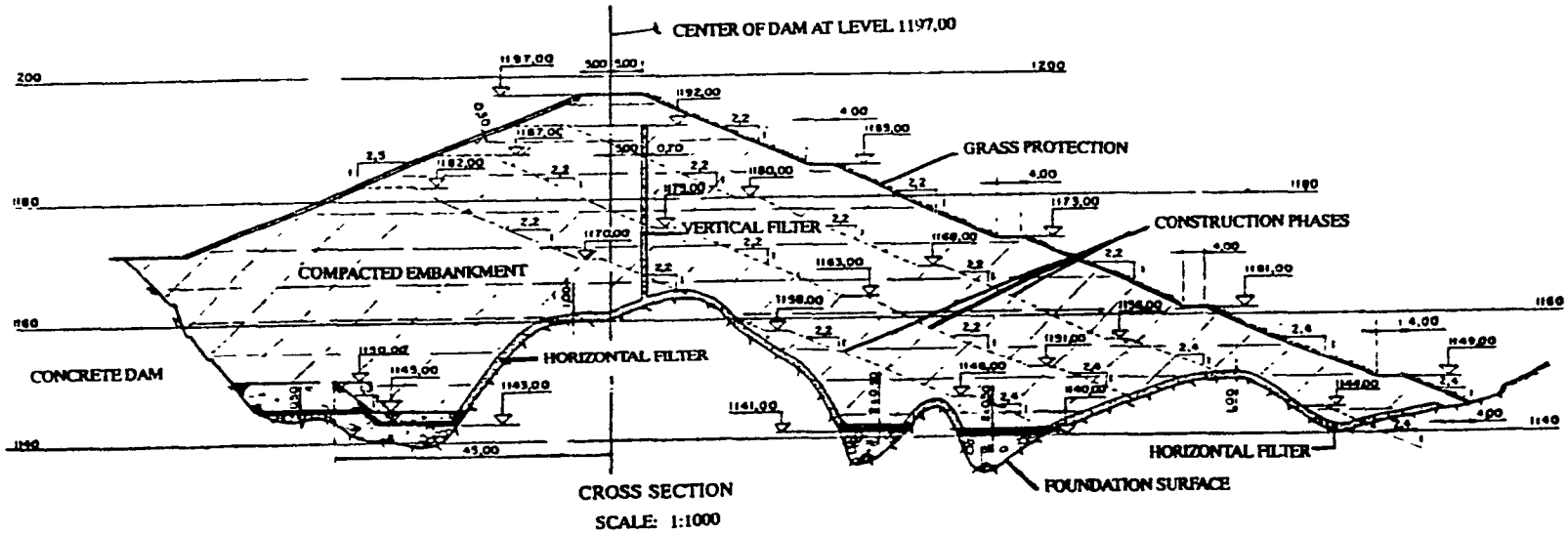

Figure 3.3 - Dam Cross Section

- Third Disposal Point (August/1988 to present), with a yearly average of 189000 tons of solid waste.

The water level has also changed during this period of time. It was at level 1173, from 1974 to November/1984. Then it rose to the level 1175. This level was maintained until October/1987, when it was once again raised, now to the level 1176. Since June/1988 it has been raised to the level 1177.5, its current level.

The transportation of the waste from the production unit to the disposal place is made by pumping of the material through metal pipes each 15 centimeters in diameter.

3.2. Previous Studies

In the development of a research plan at the Catholic University of Rio de Janeiro, the study of behavior of the bauxite waste from the ALCAN plant in Brazil started with the experimental study made by Abreu (1989) of vertical sedimentation of the material. The laboratory data thus obtained was compared with analytical data obtained using the model developed by Pane (1984). After that, Villar (1990) obtained field data recording the filling of the reservoir with time. This data consists of several cross section profiles of deposition and void ratio profiles and stresses developed in several depths at pre-specified locations. Further research at Catholic University of Rio de Janeiro consists of laboratory instrumentation of columns of sediments, with the objective of measuring the degree of sedimentation at several depths, as well as stress controlled unidimensional consolidation tests.

3.3. Geotechnical Characteristics

The bauxite waste, usually called "red slime", is a subproduct derived from the bauxite processing by the Bayer Method, in which by lixiviation of the mineral with a solution of sulfur acid the aluminum oxide is removed. By the chemical

analysis made by ALCAN technicians the main components are iron oxide (49.5%) and aluminum (17.5%). In Table 3.1 all the chemical components are presented with their percentage in weight.

Components	Fe_2O_3	Al_2O_3	TiO_3	CaO	Na_2O	SiO
% in Weight	49.5	17.5	5.0	3.0	2.7	9.5

Table 3.1 - Chemical Components of the Bauxite Waste

The mineral analysis does not detect any clay minerals.

The bauxite tailings have a unit weight of the solid particles (γ_s) in the range between 28.0 and 32.0 kN/m^3.

The initial concentration of solids (C) in the water at the point of disposal in the reservoir is approximately C=0.000396 for the First Disposal Point, C=0.00056 for the Second Disposal Point and C=0.00060 for the Third Disposal Point, according to data obtained from ALCAN DO BRASIL LIMITED (1989).

The grain size distribution is shown in Figure 3.4. The uniformity of the material and the relative absence of clay size particles are noteworthy.

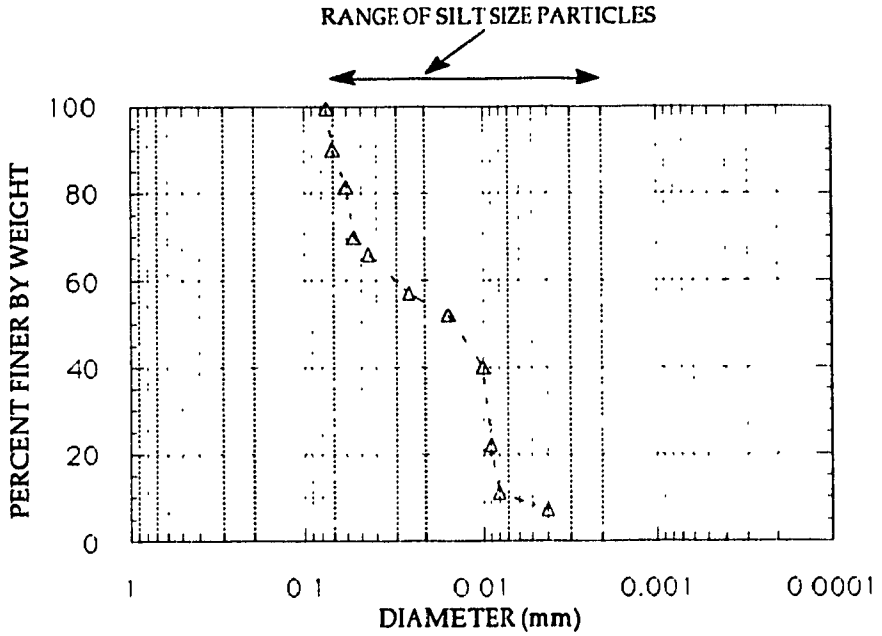

Figure 3.4 - Tailings Grain Size Distribution

The void ratio (e) separating the two distinct phases of the process (sedimentation and consolidation) is approximately e=5.0, according to field measurements (Villar, 1990). Within the context of this thesis, this void ratio (e=5.0) will be used to separate the two processes (Tan et al., 1990).

3.4. Special Laboratory Tests

Azevedo (1990) has reported unidimensional consolidation tests (Appendix F) with constant rate of deformation in which the permeability coefficient (k) is related to the void ratio (e) throughout the test (figure 3.5), as well as the relation between the vertical effective stress ($\sigma_{v'}$) and the void ratio (figure 3.6). The exponential relation between the permeability coefficient (k) and void ratio (e) is given by

$$k\,(m/s) = Exp[-26.54 + 2.99\,e] \qquad (3.1)$$

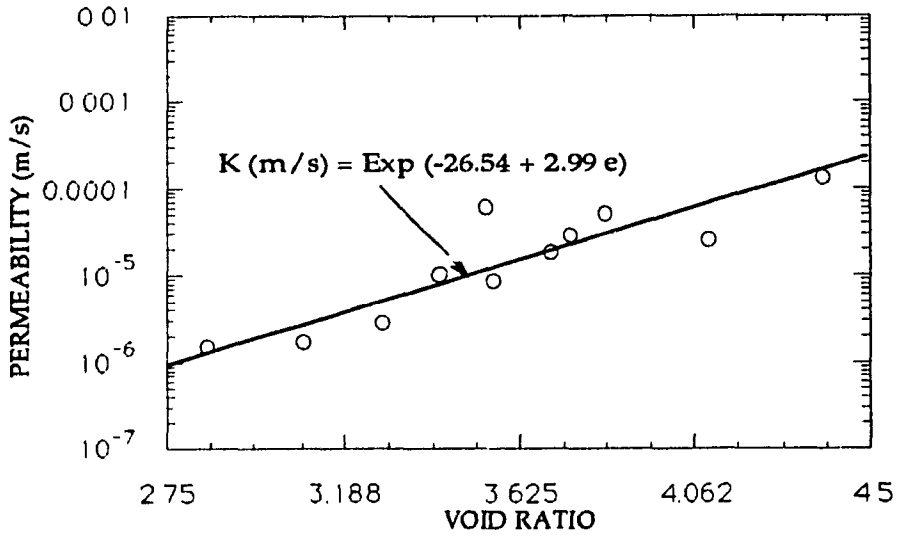

Figure 3.5 - Permeability Coefficient (k) Versus Void Ratio (e) for Special Consolidation Test

The average value of the fall velocity (ω) taken in this study is ω=0.00009 m/s, following conclusions reported by Abreu (1989), who experimented on the Saramenha Bauxite Tailings and obtained a relation between the fall velocity of the particles and the void ratio.

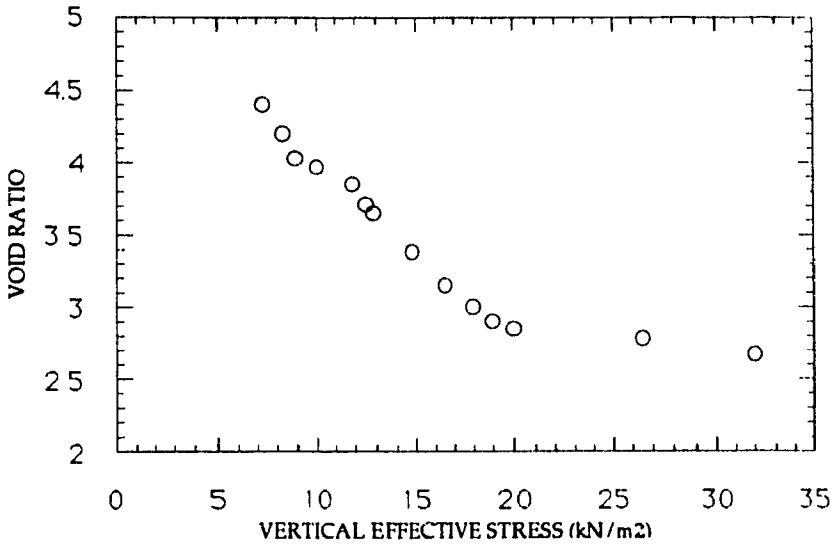

Figure 3.6 - Vertical Effective Stress ($\sigma_{v'}$) Versus Void Ratio (e) for Special Consolidation Test

3.5. Field Instrumentation

Before the end of 1984, only sporadic measurements of the elevation of the "red slime" had been made. After 1984, periodical measurements were made in detail in two cross sections of the reservoir, whose positions are shown in Figure 3.7, as well as, at the longitudinal section of the reservoir. In Figures 3.8, 3.9 and 3.10, are shown respectively the first and the second cross sections and the longitudinal section (Villar, 1990), with profiles of deposition in 1974, 1979, 1984 and 1988.

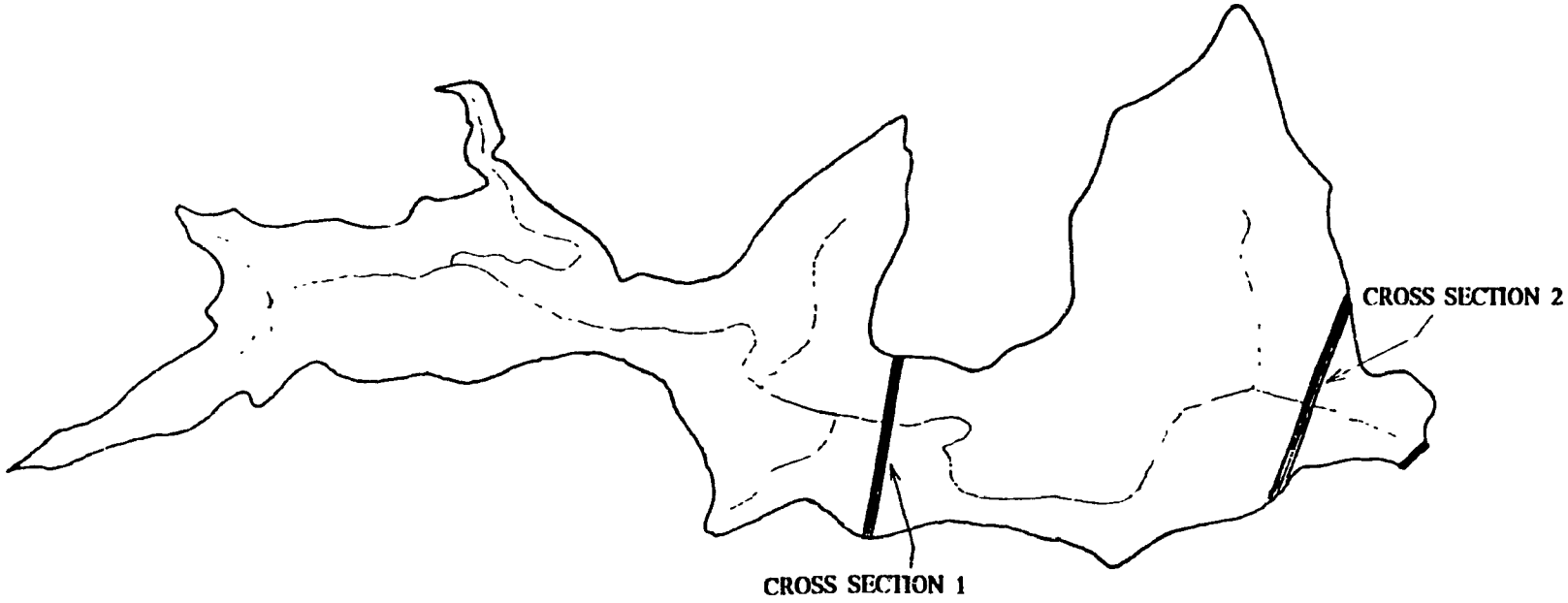

Figure 3.7 - Positions of Cross Sections of the Reservoir where Deposition Profiles were Measured Function of Time

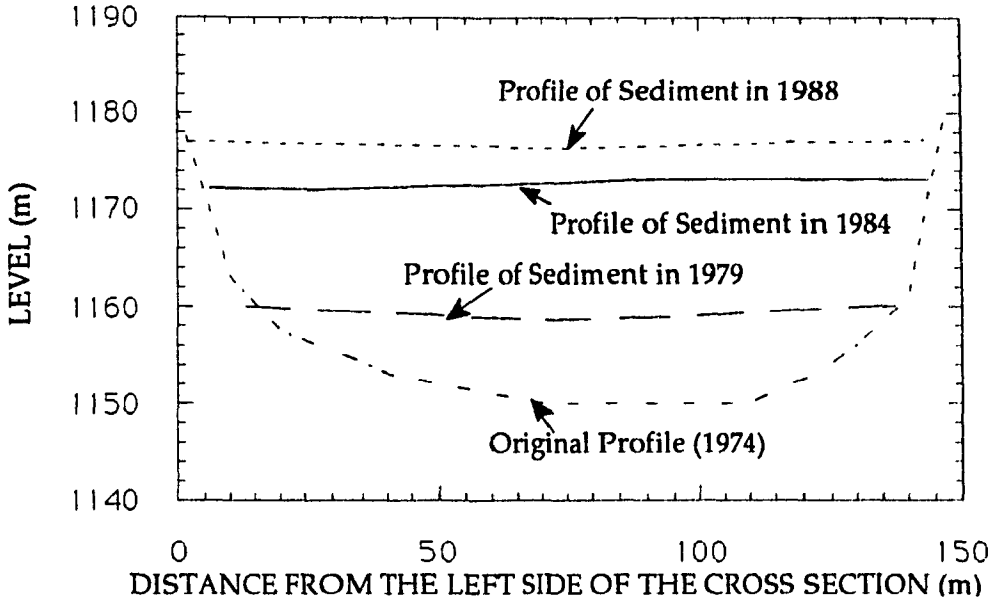

Figure 3.8 - First Cross Section and Profiles of Deposited Material

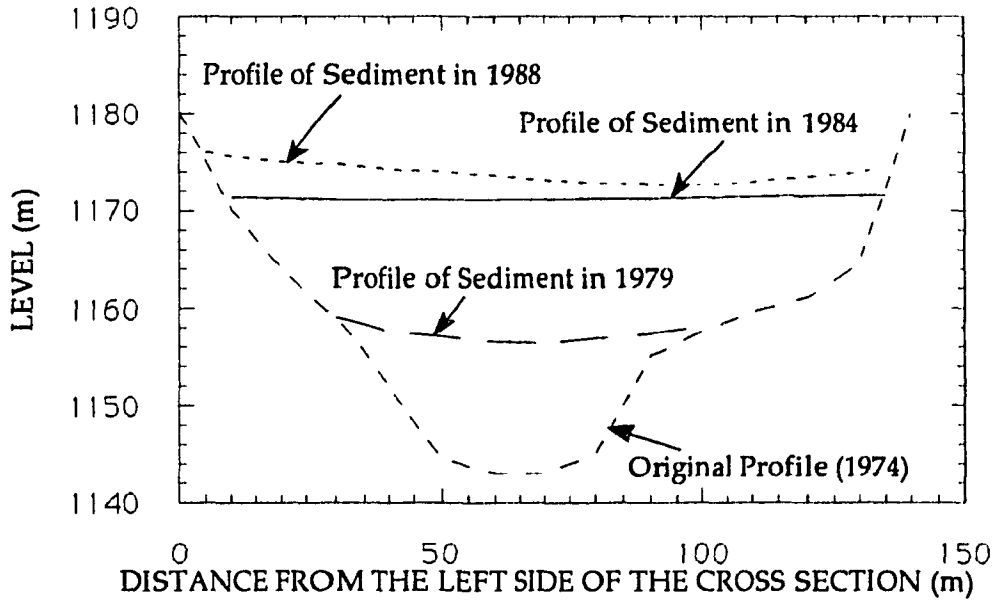

Figure 3.9 - Second Cross Section and Profiles of Deposited Material

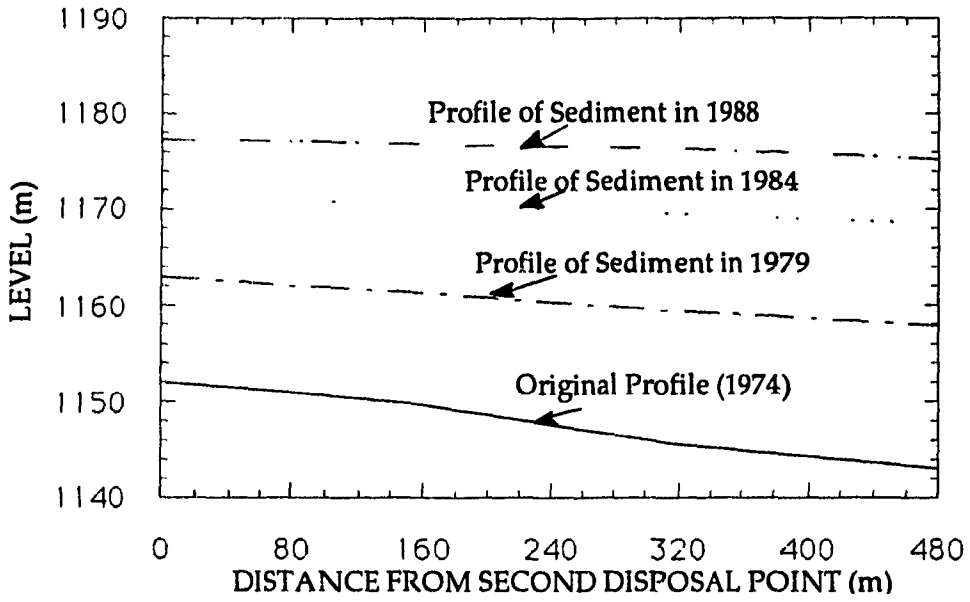

Figure 3.10 - Field Longitudinal Profile of Deposited Material with Time

At the center line of the second cross section, samples were taken at several depths to obtain in the laboratory, the values of the void ratio with depth. A profile of variation of void ratio with depth is shown in Figure 3.11.

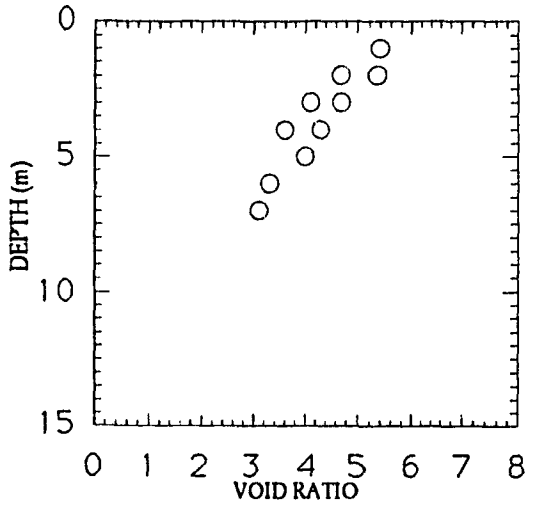

Figure 3.11 - Profile of Variation of Void Ratio (e) with Depth

At the same points the values of total stresses and effective stresses were obtained at various depths. These results are presented in Figure 3.12.

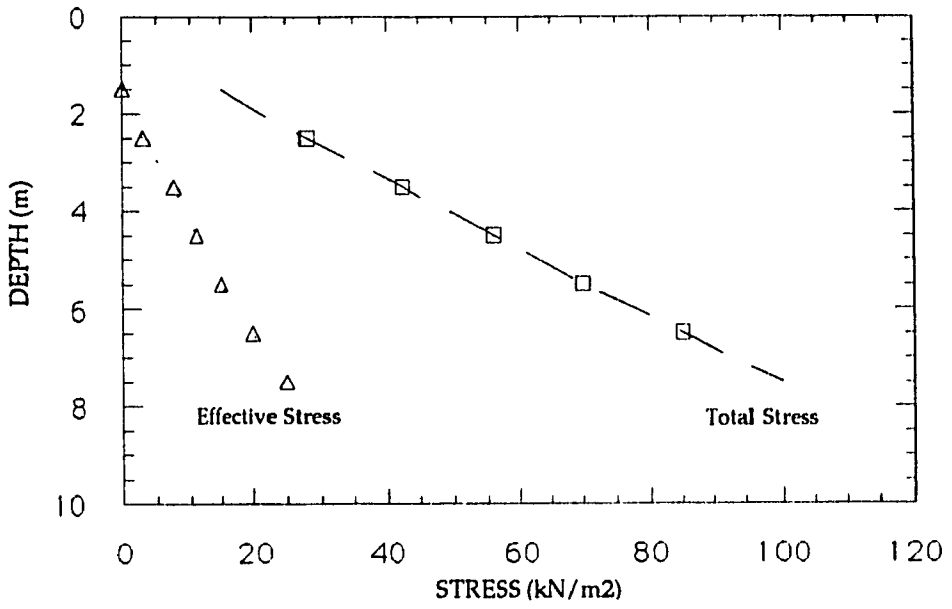

Figure 3.12 - Profiles of Total Stress and Effective Stress versus Depth

All the longitudinal distances (Figure 3.10) are measured between points in the middle of the cross sections.

CHAPTER 4

SEDIMENTATION MODELLING

4.1. Introduction

For a given fluid inflow at the disposal point of waste in the reservoir, and a given amount of tailings sediment dispersed in it, a model is proposed to give the pattern of sediment deposition along the length of the reservoir, for defined initial and boundary conditions. A set of three equations, which are the continuity equation of the mixture, the unsteady gradually varied flow equation and the equation for continuity of the sediments, form the system of governing equations which describe mathematically the behavior of the sediments and sediment-laden fluid flow.

4.2. Development of the Governing Equations

Considering a free surface flow of sediment-laden fluid problem, a stream is treated as a wide channel with mean flow in one main-direction. Generally speaking this is a three-dimensional problem, whose unknowns are functions of space and time (Iwagaki, 1956). The solution of this set of coupled partial differential equations is difficult to achieve and simplifications are needed. The main simplification for the solution of the equations for the flow of sediment-water mixture concerns the assumption of homogeneity of conditions in the stream cross-section. This allows a one-dimensional mathematical formulation of the problem. The stream is also idealized as a wide channel having rectangular cross section and an expression is introduced for the concentration of suspended sediments as a function of other physical variables. Thus an extra relationship among the variables may be established which allows the incorporation of the bottom boundary condition into the continuity equations. Other assumptions are still necessary, such as uniformity of velocity of flow over the cross section, and

homogeneity of the sediment-laden mixture so that the concentration of suspended sediment over a cross section can be expressed as the average concentration of the equivalent uniform flow.

The governing equations are formulated with respect to a finite control volume taken as a vertical slice of the stream (Figure 4.1).

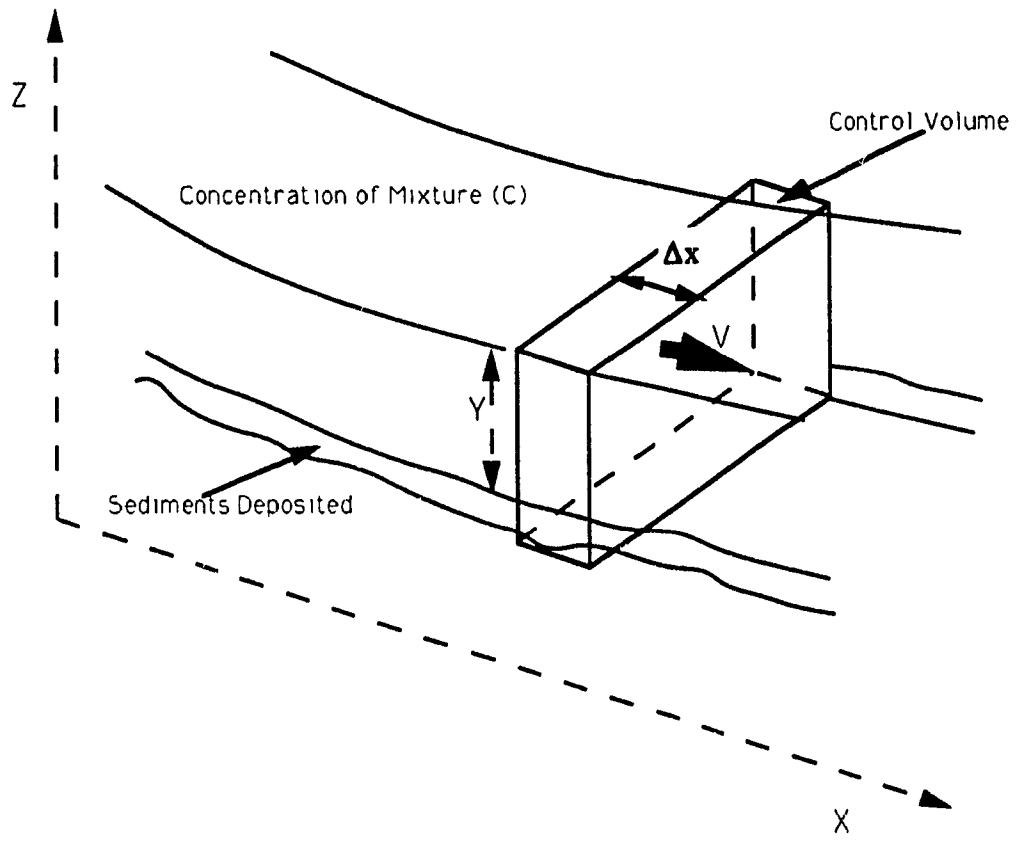

Figure 4.1 - Schematization of Stream

The total flow of mass out of the control volume is given by the net contribution

$$\frac{\partial(\rho VA)}{\partial x}\Delta x \qquad (4.1)$$

from the flow through the vertical section, where A is the cross sectional area of the sediment-fluid mixture (Figure 4.2) and ρ is the density of this mixture. The contribution

$$\rho_c \frac{\partial(A_c)}{\partial t} \Delta x \tag{4.2}$$

is the mass deposited on the bottom, where A_c is the cross sectional area of the sediment deposited layer (Figure 4.2) and ρ_c is the density of the top of this layer. Finally the time rate of increase of mass within the control volume is

$$\frac{\partial(\rho A)}{\partial t} \Delta x \tag{4.3}$$

The continuity is therefore expressed as

$$\frac{\partial(\rho V A)}{\partial x} + \rho_c \frac{\partial(A_c)}{\partial t} + \frac{\partial(\rho A)}{\partial t} = 0 \tag{4.4}$$

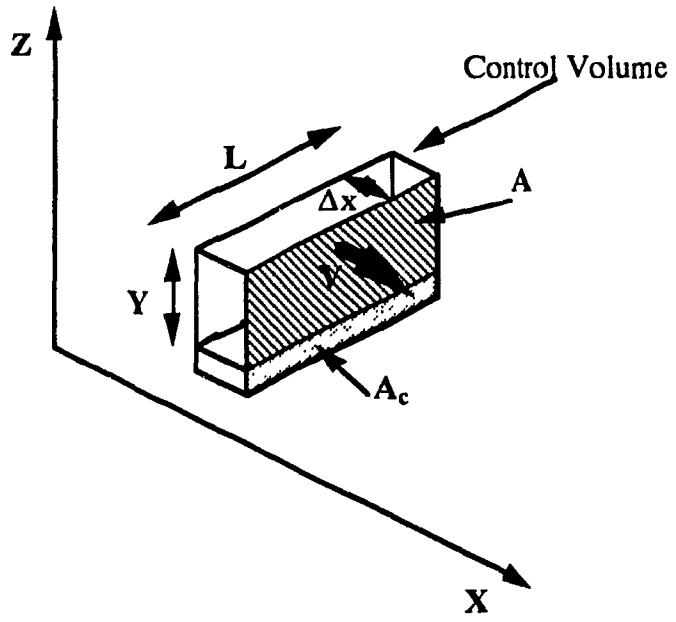

Figure 4.2 - Cross Sectional Area of Sediment-Fluid Mixture (A) and Cross Section Area of the Sediment Deposited (A_c)

The density of the sediment-laden fluid ρ and the density of the deposited matter ρ_c in the top, may be expressed as

$$\rho = \rho_s C + (1\text{-}C)\rho_w \tag{4.5}$$

and

$$\rho_c = \rho_s C_c + (1-C_c)\rho_w \tag{4.6}$$

with ρ_s and ρ_w the density of sediment and fluid and C and C_c are the material concentration in the fluid and in the top layer of the deposited sediments, respectively.

Substituting into Equation 4.4 the relations 4.5 and 4.6 one obtains

$$\rho_s\left\langle\frac{\partial(CA)}{\partial t}+\frac{\partial(CVA)}{\partial x}+C_c\frac{\partial A_c}{\partial t}\right\rangle+\rho_w\left\langle\frac{\partial([1-C]A)}{\partial t}+\frac{\partial([1-C]VA)}{\partial x}+(1-C_c)\frac{\partial A_c}{\partial t}\right\rangle=0 \tag{4.7}$$

If no lateral inflow of sediments and fluid are included, the equation of continuity of fluid and the equation of continuity of solid sediment written for the control volume under consideration, based on Equation 4.7 are respectively

$$\left\langle\frac{\partial([1-C]A)}{\partial t}+\frac{\partial([1-C]VA)}{\partial x}+(1-C_c)\frac{\partial A_c}{\partial t}\right\rangle=0 \tag{4.8}$$

and

$$\left\langle\frac{\partial(CA)}{\partial t}+\frac{\partial(CVA)}{\partial x}+C_c\frac{\partial A_c}{\partial t}\right\rangle=0 \tag{4.9}$$

as previously suggested by Iwagaki (1956) and Chang and Richards (1971).

The physical problem here studied deals with unsteady gradually varied flow which is characterized by slow changes of fluid level and flow rate with time.

By the energy principle and considering the change in the total head through a distance dx of the control volume accounting for the effects of friction (S_f dx), where S_f (friction slope) is given by (Chow, 1959):

$$S_f = \frac{n^2 V^2}{\left(\frac{A}{L+2Y}\right)^{\frac{4}{3}}} \tag{4.10}$$

and acceleration , $(1/g)(\partial V/\partial t)dx$, the following may be written

$$d\left(Z + Y + \alpha \frac{V^2}{2g}\right) = - S_f\, dx - \frac{1}{g}\frac{\partial V}{\partial t} dx \qquad (4.11)$$

where α is the Energy coefficient or Coriolis coefficient. This constant coefficient is used due to experimental findings that the true velocity head of an open channel flow is generally greater than the value computed according to the expression $V^2/2g$. The value of the coefficient α varies between 1.0 and 1.3, respectively for large streams and small channels.

Dividing Equation 4.11 by dx and utilizing partial differentials, the general dynamic equation for gradually varied unsteady flow is given by

$$\frac{\partial Y}{\partial x} + \alpha\frac{V\partial V}{g\,\partial x} + \frac{1}{g}\frac{\partial V}{\partial t} + \frac{\partial Z}{\partial x} + S_f = 0 \qquad (4.12)$$

as previously shown by Chen (1959).

The continuity and motion equations contain four unknowns, which are the depth of the flow Y(x,t), the mean cross-sectional velocity V(x,t), the coordinate at the bottom of the channel Z(x,t) and the average concentration of sediments in the water over a cross section C(x,t).

The rate of sediment transport is a function of variables such as discharge, average flow velocity, depth of flow, particle size, etc.

There are different theories to represent the concentration of sediment in flow as a function of the above mentioned variables. Following the approach given by Lane and Kalinske (1942), the average concentration of suspended sediment (ST) is a direct function of the mean velocity (V), the depth of the flow (Y), the sediment fall velocity (w), the slope of the channel bed ($I_c=\partial Z/\partial x$), the concentration of solids at the top level bed (C_c), the Manning Coefficient (n) . the acceleration of gravity (g), the Von Karman Constant (κ) and $\chi = h/Y$, where h varies between zero and Y, as stated in Equation (4.13) below

$$ST = \frac{C_c\, n\, V}{(I_c)^{1/2}\, Y^{2/3}} \left\langle \frac{\left(1+\frac{n}{\kappa}\frac{g^{1/2}}{Y^{1/6}}\right)\left(1-e^{\left(-\frac{6}{\kappa}\frac{\omega\, Y^{1/6}}{n\, V\, g^{1/2}}\right)}\right)}{\frac{6}{\kappa}\frac{\omega\, Y^{1/6}}{n\, V\, g^{1/2}}} + \frac{n}{\kappa}\frac{g^{1/2}}{Y^{1/6}} \int_0^1 \ln(\chi)\, e^{\left(-\chi\frac{6}{\kappa}\frac{\omega\, Y^{1/6}}{n\, V\, g^{1/2}}\right)} d\chi \right\rangle \tag{4.13}$$

There is, however, the necessity to account for the concentration of the suspended sediments at the disposal point of the waste (C). This is a function of external factors, and probably has a different value from that of the average concentration expressed by Lane and Kalinske (1942).

To deal with this problem, first assume that the concentration of the suspended sediments at the disposal point is higher than the concentration that the flow is capable of transporting. Considering the variation of the sediment concentration in a control volume (Figure 4.3),

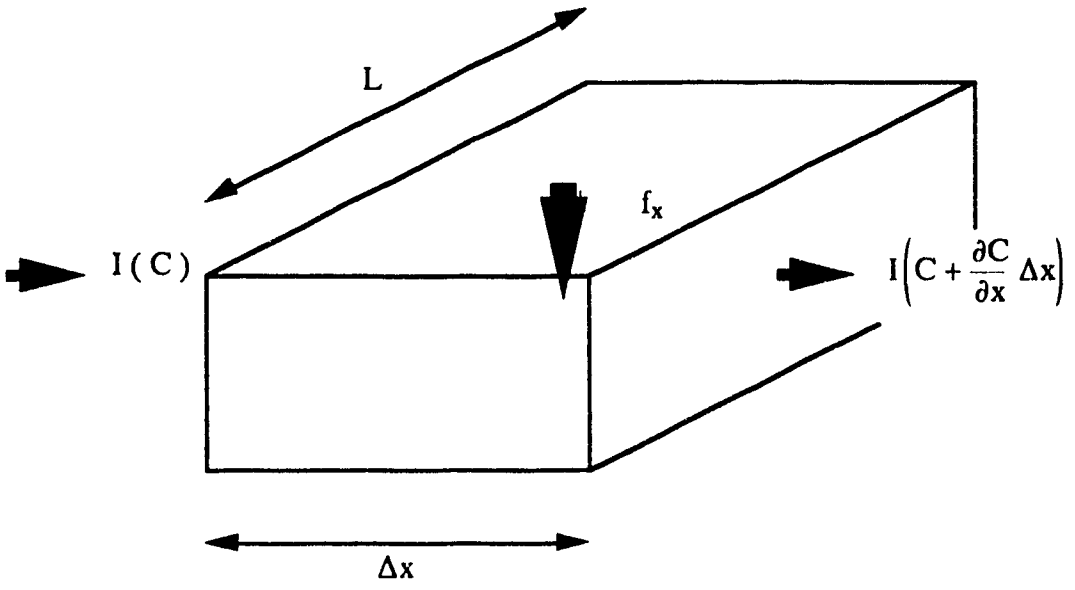

Figure 4.3 - Variation of Sediment Concentration in a Control Volume

the balance of sediments is expressed as

$$I\frac{\partial C}{\partial x}\Delta x = (-f_x)\, L\, \Delta x \tag{4.14}$$

where I is the inflow, f_x is the deposition flux and L is the width of the control volume.

As the flow is able to carry the concentration ST, the rate of deposition is given by

$$f_x = \omega (C - ST) \tag{4.15}$$

which upon substitution in Equation 4.14, results in

$$\frac{\partial C}{\partial x} + \frac{\omega (C - ST)}{V Y} = 0 \tag{4.16}$$

The solution of this linear differential equation between sections j and j+1 of the control volume, is given by Kaplan (1959);

$$C_{j+1} = ST_{j+1} + (C_j - ST_{j+1}) e^{\left(-\frac{\omega \Delta x}{V Y}\right)} \tag{4.17}$$

To summarize, the governing equations for the sedimentation process are Equations 4.8, 4.9 and 4.12.

4.3. Numerical Method for the Solution of the Sedimentation Problem

The amount of sediment trapped in a reservoir during a certain period of time is the difference between the sediment released at the disposal point and the sediment released with the outflow.

4.3.1. Preissmann Implicit Finite Difference Scheme

In order to obtain a numerical solution to the problem, the partial derivative in time ($\partial A_c / \partial t$) is eliminated from Equations 4.8 and 4.9 through the combination of the continuity equation of the sediments (Equation 4.9) and the continuity equation of the fluid (Equation 4.8), yielding

$$\frac{\partial A}{\partial t} - \frac{A}{(C_c - C)}\frac{\partial C}{\partial t} + \frac{\partial (V\,A)}{\partial x} - \frac{A\,V}{(C_c - C)}\frac{\partial C}{\partial x} = 0 \qquad (4.18)$$

Assuming $\partial C/\partial t \approx 0$ in Equation 4.18 and linking it with the general dynamic equation for gradually varied unsteady flow given by Equation 4.12, a system of equations is formed, where the Preissmann Implicit Four Point Finite Difference Scheme is applied to obtain the values of Y and V at the time t^{n+1}. The scheme replaces the continuous function f, its time derivative and its space derivative by the difference formulae

$$f = \Theta\left[\Omega\, f_{j+1}^{n+1} + (1 - \Omega) f_j^{n+1}\right] + (1 - \Theta)\left[\Omega\, f_{j+1}^{n} + (1 - \Omega) f_j^{n}\right] \qquad (4.19)$$

$$\frac{\partial f}{\partial t} = \frac{1}{\Delta t}\left[\Omega\left(f_{j+1}^{n+1} - f_{j+1}^{n}\right) + (1 - \Omega)\left(f_j^{n+1} - f_j^{n}\right)\right] \qquad (4.20)$$

$$\frac{\partial f}{\partial x} = \frac{1}{\Delta x}\left[\Theta\left(f_{j+1}^{n+1} - f_j^{n+1}\right) + (1 - \Theta)\left(f_{j+1}^{n} - f_j^{n}\right)\right] \qquad (4.21)$$

where f_j^n is the value of f at the point (x,t), Δt and Δx being the time step and mesh size of the grid (constant). The weighting factors, Ω for space and θ for time, range in value from zero to unity, and define the point about which the discretization is made. These may significantly affect the stability and convergence of the scheme. It has become standard to choose a scheme centered in space, $\Omega = 0.5$, since it yields second-order accuracy in time (Lyn, 1987). Lyn (1987) also studied the stability of the Preissmann Scheme and concluded that the stability is unconditional for $\theta = 1.0$, the value adopted in this work. All the other values in the development of the formulation are taken as the average value between two sections.

Applying the Preissmann Scheme, Equations 4.19, 4.20 and 4.21 to the System of equations formed by Equations 4.12 and 4.18 and rearranging them, the following finite difference equations are obtained

$$\hat{C}_j\,\Delta Y_j + \hat{D}_j\,\Delta V_j + \hat{A}_j\,\Delta Y_{j+1} + \hat{B}_j\,\Delta V_{j+1} + \hat{G}_j = 0 \qquad (4.22)$$

$$\widehat{C''}_j \Delta Y_j + \widehat{D''}_j \Delta V_j + \widehat{A''}_j \Delta Y_{j+1} + \widehat{B''}_j \Delta V_{j+1} + \widehat{G''}_j = 0 \tag{4.23}$$

where

$$\Delta f_j = f_j^{n+1} - f_j^n \tag{4.24}$$

$$\widehat{C}_j = \left\langle \overline{L} - \overline{V}\,\overline{L}\,\frac{\Delta t}{\Delta x} + \left(- \frac{V\,L}{C_c - C} \frac{\partial C}{\partial x} \right)_j \Delta t \right\rangle \tag{4.25}$$

$$\widehat{D}_j = \left\langle - \overline{A}\,\frac{\Delta t}{\Delta x} + \left(- \frac{A}{C_c - C} \frac{\partial C}{\partial x} \right)_j \Delta t \right\rangle \tag{4.26}$$

$$\widehat{A}_j = \left\langle \overline{L} + \overline{V}\,\overline{L}\,\frac{\Delta t}{\Delta x} + \left(- \frac{V\,L}{C_c - C} \frac{\partial C}{\partial x} \right)_{j+1} \Delta t \right\rangle \tag{4.27}$$

$$\widehat{B}_j = \left\langle \overline{A}\,\frac{\Delta t}{\Delta x} + \left(- \frac{A}{C_c - C} \frac{\partial C}{\partial x} \right)_{j+1} \Delta t \right\rangle \tag{4.28}$$

$$\widehat{G}_j = \left\langle \left[\overline{V}\,\overline{L} \left(Y_{j+1}^n - Y_j^n \right) \frac{\Delta t}{\Delta x} + \overline{A} \left(V_{j+1}^n - V_j^n \right) \frac{\Delta t}{\Delta x} \right] + \left(- \frac{A\,V}{C_c - C} \frac{\partial C}{\partial x} \right)_{j+1} \Delta t + \left(- \frac{A\,V}{C_c - C} \frac{\partial C}{\partial x} \right)_j \Delta t \right\rangle \tag{4.29}$$

$$\widehat{C''}_j = \left\langle - g\,\frac{\Delta t}{\Delta x} + \left(- \frac{4}{3}\, g\, S_f \left(\frac{1}{Y} - \frac{2}{2\,Y + L} \right) \right)_j \Delta t \right\rangle \tag{4.30}$$

$$\widehat{D''}_j = \left\langle 1 - \overline{V}\,\frac{\Delta t}{\Delta x} + \left(2\, g\, \frac{S_f}{V} \right)_j \Delta t \right\rangle \tag{4.31}$$

$$\widehat{A''}_j = \left\langle g\,\frac{\Delta t}{\Delta x} + \left(- \frac{4}{3}\, g\, S_f \left(\frac{1}{Y} - \frac{2}{2\,Y + L} \right) \right)_{j+1} \Delta t \right\rangle \tag{4.32}$$

$$\widehat{B''}_j = \left\langle 1 + \overline{V}\,\frac{\Delta t}{\Delta x} + \left(2\, g\, \frac{S_f}{V} \right)_{j+1} \Delta t \right\rangle \tag{4.33}$$

$$\widehat{G''}_j = \left\langle \left[g \left(Y_{j+1}^n - Y_j^n \right) \frac{\Delta t}{\Delta x} + \overline{V} \left(V_{j+1}^n - V_j^n \right) \frac{\Delta t}{\Delta x} \right] + \left(g \left(- \frac{\partial Z}{\partial x} + S_f \right) \right)_{j+1} \Delta t + \left(g \left(- \frac{\partial Z}{\partial x} + S_f \right) \right)_j \Delta t \right\rangle \tag{4.34}$$

and where the updating of Z is made step by step and the bar on the top of the variables means the average value of this variable between two sections j and j+1.

4.3.2. Double Sweep System Solver Method

Equations 4.22 and 4.23 may be written for any pair of computational points (j, j+1). They are not sufficient to find the values of ΔV_j, ΔY_j, ΔV_{j+1} and ΔY_{j+1} because for these four unknowns only two equations are available. But if there are N computational points in the model (j=1,2,.....,N-1,N), one can write 2(N-1) of such equations for 2N unknowns (ΔV_j , ΔY_j). As two boundary conditions must be available there are actually a system of 2N algebraic equations for 2N unknowns. Now this system may be solved for any time step Δt.

The solution of the system of Equations 4.22 and 4.23 must be solved for all computational points for every time step Δt. They form a system of linear algebraic equations and linearizing the boundary conditions in terms of ΔV and ΔY, the Double Sweep Solution Method applies. Assuming a linear relationship of the type

$$\Delta V_j = E_j \Delta Y_j + F_j \tag{4.35}$$

for a point j, substituting Equation 4.35 into Equations 4.22 and 4.23 and equating the function of ΔY_j , as follows

$$\Delta Y_j = \left\langle -\frac{\hat{A}_j}{(\hat{C}_j + \hat{D}_j E_j)} \right\rangle \Delta Y_{j+1} + \left\langle -\frac{\hat{B}_j}{(\hat{C}_j + \hat{D}_j E_j)} \right\rangle \Delta V_{j+1} + \left\langle -\frac{(\hat{D}_j F_j + \hat{G}_j)}{(\hat{C}_j + \hat{D}_j E_j)} \right\rangle \tag{4.36}$$

and

$$\Delta Y_j = \left\langle -\frac{\hat{A}''_j}{(\hat{C}''_j + \hat{D}''_j E_j)} \right\rangle \Delta Y_{j+1} + \left\langle -\frac{\hat{B}''_j}{(\hat{C}''_j + \hat{D}''_j E_j)} \right\rangle \Delta V_{j+1} + \left\langle -\frac{(\hat{D}''_j F_j + \hat{G}''_j)}{(\hat{C}''_j + \hat{D}''_j E_j)} \right\rangle \tag{4.37}$$

Then elimininating ΔYj between Equations 4.36 and 4.37 and expressing $\Delta Vj+1$ as a function of $\Delta Yj+1$ there results

$$\Delta V_{j+1} = \frac{\left[\left\langle \frac{\widehat{A''}_j}{\left(\widehat{C''}_j + \widehat{D''}_j E_j\right)}\right\rangle - \left\langle \frac{\hat{A}_j}{\left(\hat{C}_j+\hat{D}_j E_j\right)}\right\rangle\right]}{\left[\left\langle \frac{\hat{B}_j}{\left(\hat{C}_j+\hat{D}_j E_j\right)}\right\rangle - \left\langle \frac{\widehat{B''}_j}{\left(\widehat{C''}_j + \widehat{D''}_j E_j\right)}\right\rangle\right]} \Delta Y_{j+1} + \frac{\left[\left\langle \frac{\left(\widehat{D''}_j F_j + \widehat{G''}_j\right)}{\left(\widehat{C''}_j + \widehat{D''}_j E_j\right)}\right\rangle - \left\langle \frac{\left(\hat{D}_j F_j + \hat{G}_j\right)}{\left(\hat{C}_j+\hat{D}_j E_j\right)}\right\rangle\right]}{\left[\left\langle \frac{\hat{B}_j}{\left(\hat{C}_j+\hat{D}_j E_j\right)}\right\rangle - \left\langle \frac{\widehat{B''}_j}{\left(\widehat{C''}_j + \widehat{D''}_j E_j\right)}\right\rangle\right]} \tag{4.38}$$

which is a linear relationship of the same format as that of Equation 4.35 and consequently

$$E_{j+1} = \frac{\left[\left\langle \frac{\widehat{A''}_j}{\left(\widehat{C''}_j + \widehat{D''}_j E_j\right)}\right\rangle - \left\langle \frac{\hat{A}_j}{\left(\hat{C}_j+\hat{D}_j E_j\right)}\right\rangle\right]}{\left[\left\langle \frac{\hat{B}_j}{\left(\hat{C}_j+\hat{D}_j E_j\right)}\right\rangle - \left\langle \frac{\widehat{B''}_j}{\left(\widehat{C''}_j + \widehat{D''}_j E_j\right)}\right\rangle\right]} \tag{4.39}$$

and

$$F_{j+1} = \frac{\left[\left\langle \frac{\left(\widehat{D''}_j F_j + \widehat{G''}_j\right)}{\left(\widehat{C''}_j + \widehat{D''}_j E_j\right)}\right\rangle - \left\langle \frac{\left(\hat{D}_j F_j + \hat{G}_j\right)}{\left(\hat{C}_j+\hat{D}_j E_j\right)}\right\rangle\right]}{\left[\left\langle \frac{\hat{B}_j}{\left(\hat{C}_j+\hat{D}_j E_j\right)}\right\rangle - \left\langle \frac{\widehat{B''}_j}{\left(\widehat{C''}_j + \widehat{D''}_j E_j\right)}\right\rangle\right]} \tag{4.40}$$

Thus, if the linearized boundary condition (E1,F1) are known at the first point, a forward sweep can be carried on and all coefficients (Ej,Fj), j= 2, 3,....., N may be computed. At the last point j=N, the second boundary condition is used and then ΔY_N is explicitly expressed. Next a return sweep is made using Equation 4.38, where ΔV_N is obtained, then substituting both values in Equation 4.36 or 4.37 ΔY_{N-1} is obtained. The procedure is successively applied to all grid points.

The coefficients A_j, B_j, etc, can then be updated and the linear system can be solved again, furnishing the second iteration. The significant feature of this system is that in most cases the first iteration is good enough and there is no need for further iterations (Cunge et al, 1980).

4.3.3. Initial and Boundary Conditions for the Preissmann Scheme

The initial conditions for this problem are first the initial values of the slope of the bottom of the reservoir, obtained from direct consideration of topography. After that the values of V and Y, for all sections are needed and for this purpose the energy principle is recalled again, as it was for Equation 4.11. Thus for a steady state where $\partial V / \partial t = 0$, Equation 4.11 reduces to

$$d\left(Z+Y+\alpha\frac{V^2}{2g}\right) = -S_f dx \tag{4.41}$$

Now the computation is carried out by steps from station to station where the hydraulic characteristics have been determined. Such a procedure is usually carried backward and by trial and error. This procedure has already been introduced in the code developed and the initial values of Y and V are automatically calculated. Some other important data like initial concentration of sediments in the mixture are initially calculated as the values that the flow can transport by Equation 4.13 and then the waste sediment concentration is imposed in the disposal area.

As noted before, a linearized boundary condition is needed to furnish (E_1,F_1) at the first point. In this case Inflow (I) is given as function of time, then for the time step n to n+1 the linearized boundary condition (Cunge and Liggett, 1975) is

$$\Delta V_1^n = \left(-\frac{V_1^n}{Y_1^n}\right)\Delta Y_1^n + \left(\frac{(I^{n+1} - I^n)}{Y_1^n}\right) \tag{4.42}$$

where

$$E_1 = \left(-\frac{V_1^n}{Y_1^n}\right) \tag{4.43}$$

and

$$F_1 = \left(\frac{\left(I^{n+1} - I^n \right)}{Y_1^n} \right) \tag{4.44}$$

In the case of a reservoir with a constant maximum fluid level at the dam site due to the level of the spillway and constant inflow of fluid, the boundary condition at the dam position is given considering ΔY_N (variation of depth of the flow) equal to the thickness of the sediments deposited during the previous time step in section N. This is explained in more detail in Section 4.3.4 .

4.3.4. Sediment Deposited During Time Step

The procedure outlined in Sections 4.3.1 , 4.3.2 and 4.3.3, yields the values of V_j^{n+1} and Y_j^{n+1}. These values are required for the computation of C_j^{n+1} using Equations 4.13 and 4.17. Knowing these values, the Preissmann Implicit Difference Scheme is used once again, now to solve Equation 4.10, which is the equation of continuity of sediments. At this time a backward configuration with sections j-1 and j is used, starting with j=2, where Ω=0.0 and θ=1.0.

The variation of sedimented area is then given by

$$\left(\Delta A_c \right)_j = - \frac{\left[\left\langle \left(C_{j-1}^{n+1} A_{j-1}^{n+1} \right) - \left(C_{j-1}^{n} A_{j-1}^{n} \right) \right\rangle + \left\langle \left(C_j^{n+1} V_j^{n+1} A_j^{n+1} \right) - \left(C_{j-1}^{n+1} V_{j-1}^{n+1} A_{j-1}^{n+1} \right) \right\rangle \frac{\Delta t}{\Delta x} \right]}{C_c} \tag{4.45}$$

Considering the same thickness of sediments over all of the cross section, the value of the thickness of sediment increment is given by

$$\left(T_s \right)_j = \frac{\left(\Delta A_c \right)_j}{\left(L \right)_j} \tag{4.46}$$

and $\Delta Y_N = -\ (Ts)_N$ is used as the boundary condition for the next step, as proposed in Section 4.3.3.

4.4. Convergence Analysis Of The Developed Theory

A program named CONSED was developed, to codify the procedure developed above. In order to verify the convergence of the numerical scheme, a fixed grid was defined with Δx=100 meters and several computations with increasing values of Δt, from 15 minutes to 10 days were compared (Figure 4.4). From this test it was concluded that adopting Δt=1 hour is an appropriate approximation. The parameters used to characterize the problem were ω=0.00009, C_c=0.50, C=0.00112, initial slope of the bottom equal to 0.5%, constant width equal to 100 meters, fluid inflow of 10 m^3/s, n=0.015 and α=1.0.

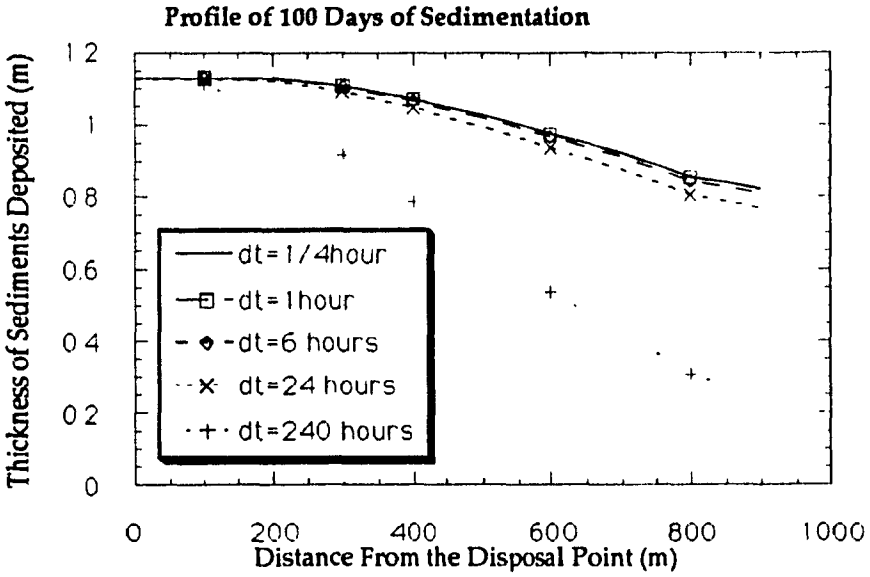

Figure 4.4 - Convergence Test for Several Δt and 100 Days of Sedimentation

A second convergence test was run, now with a constant Δt=1 hour with increasing values of Δx, from 50 to 450 meters (Figure 4.5). It was concluded that adopting an average value Δx=100 meters was an adequate approximation.

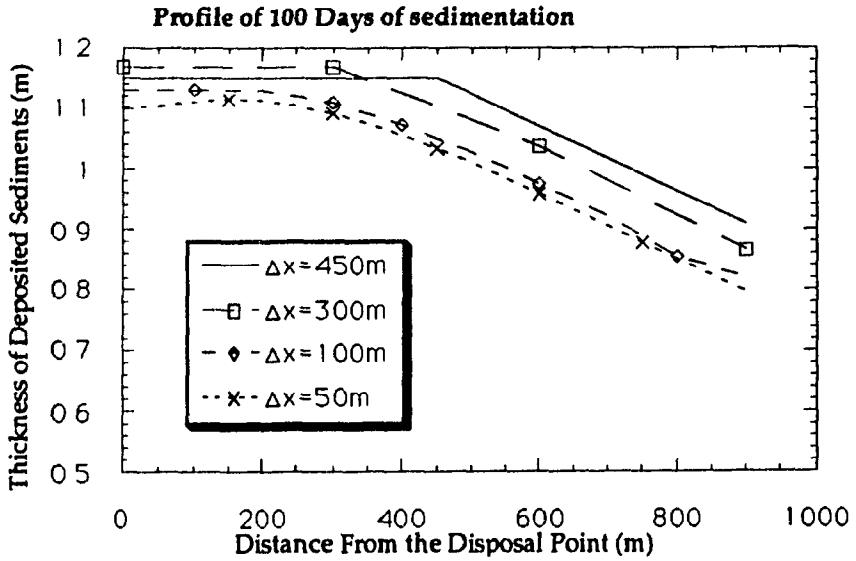

Figure 4.5 - Convergence Test for Several Δx and 100 Days of Sedimentation

Finally to test the efficiency of the numerical method in modelling the influence of the concentration of the sediments at the disposal point, a test was run with the same field characteristics of the previous examples, (Δx=100 meters, Δt=1 hour) and three different concentrations(C=0.00056, C=0.0112 and C=0.0028). The divergence of the sedimentation profiles shown in Figure 4.6, demonstrates the importance of the modelling of the sediments concentration at the disposal point.

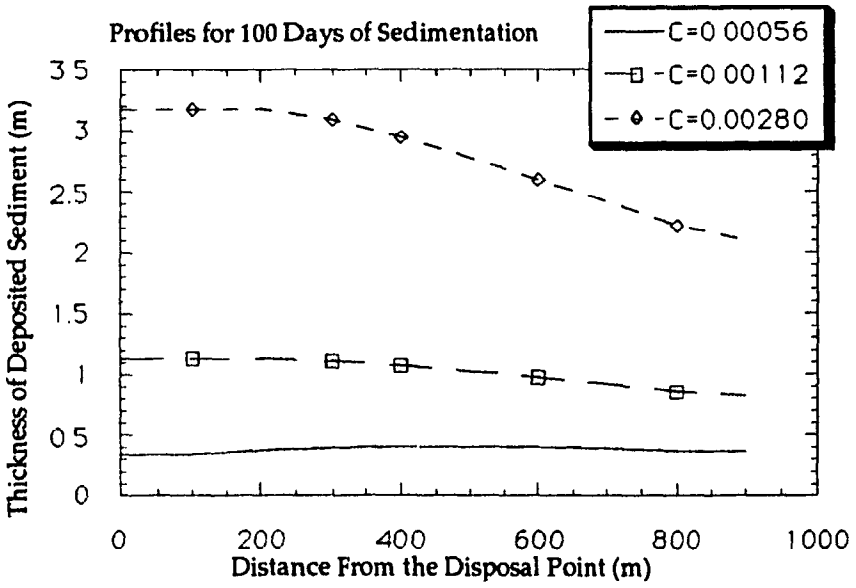

Figure 4.6 - Influence of the Concentration of Sediments at the Disposal Point

CHAPTER 5

CONSTITUTIVE MODELLING FOR SOIL FORMATION BASED ON STATE PARAMETERS

5.1. Introduction

To simulate the behavior of soil during the process of its formation, it is necessary to account for several changes of characteristics which occur during the process.

It is one the objectives of the work presented here to provide a new constitutive model that is able to take into consideration the changes that take place in the soil characteristics. This is required in order to better characterize its behavior throughout all phases, from the occurrence of the contact among grains and consequently appearance of effective stresses, through changes in stresses, void ratio and so on. To reach this point, concepts of state of a sample and changes of state of a sample (Poorooshasb, 1961) are introduced and a model able to satisfy most of the characteristics of soil formation as well as the normal behavior of soil under monotonic and cyclic loading is proposed. Thus not only the process of soil formation can be accounted for, but also once formed, its response to external loadings may be evaluated.

5.2. General Description

Making use of the concepts of "State" and "State Parameters", presented by Poorooshasb (1961) and Consoli and Poorooshasb (1991), and the idea of non-associated flow rule to explain the plastic flow of cohesionless granular media (Poorooshasb et al., 1966 and 1967), a new constitutive model is developed. Postulating the existence of the State Boundary Surface and an Ultimate State Surface, a number of experimental observations (e.g. curvature of the yield

surfaces) can be accounted for. This model is applicable to virgin loading, as well as other more complicated types of loading, e.g. elasto-plastic behavior during stress reversal. Here the concept of generalized plasticity is introduced and extended to the State Space.

5.2.1 Basic Definitions

Before discussing the constitutive modelling itself, some definitions and concepts must be stated.

The state of a sample is defined by the complete set of the pertinent state parameters. A state parameter is a quantity that is associated with the sample and can directly be measured at the moment of examination.

A pertinent state parameter is a state parameter that is judged to influence, in some way, the behavior of the sample during the particular process to which it is subjected.

Assuming homogeneity and isotropy of the sample, the void ratio (e) is considered a pertinent state parameter, as well as the effective state of stress (σ'_{ij}). Then the state of the sample in terms of the mechanical behavior is defined by the set of quantities (σ'_{ij}, e).

Recalling the symmetrical form of the effective stress tensor, the state of the sample can be represented by a point in a seven dimensional space. Representing the stress tensor by its invariants (three) or variables derived from it, the space can be reduced to only four dimensions. This space is called the state space.

From the first invariant of the stress tensor I_1 and the second and third invariants of the stress deviation tensor J_2 and J_3, the quantities p, q and θ may be defined as follows :

$$p = \frac{I_1}{\sqrt{3}} \qquad (5.1)$$

$$q = \sqrt{2}\,\sqrt{J_2} \tag{5.2}$$

and

$$\theta = \frac{1}{3}\sin^{-1}\left(\frac{-3\sqrt{3}\,J_3}{2\,\sqrt[3]{J_2}}\right) \tag{5.3}$$

where

$$I_1 = \sigma'_{ii} \tag{5.4}$$

$$J_2 = \frac{1}{2}(S_{ij}\,S_{ij}) \tag{5.5}$$

and

$$J_3 = \frac{1}{3}(S_{ki}\,S_{jk}\,S_{ij}) \tag{5.6}$$

S_{ij} is the stress deviation tensor expressed as

$$S_{ij} = \sigma'_{ij} - \left(\frac{I_1}{3}\right)\delta_{ij} \tag{5.7}$$

In Figure 5.1 the meaning of variables p (hydrostatic component) and q (deviator component) are shown, as well as variable θ, which has a similar meaning to the Lode's angle and its range is from $-\pi/6$ to $\pi/6$.

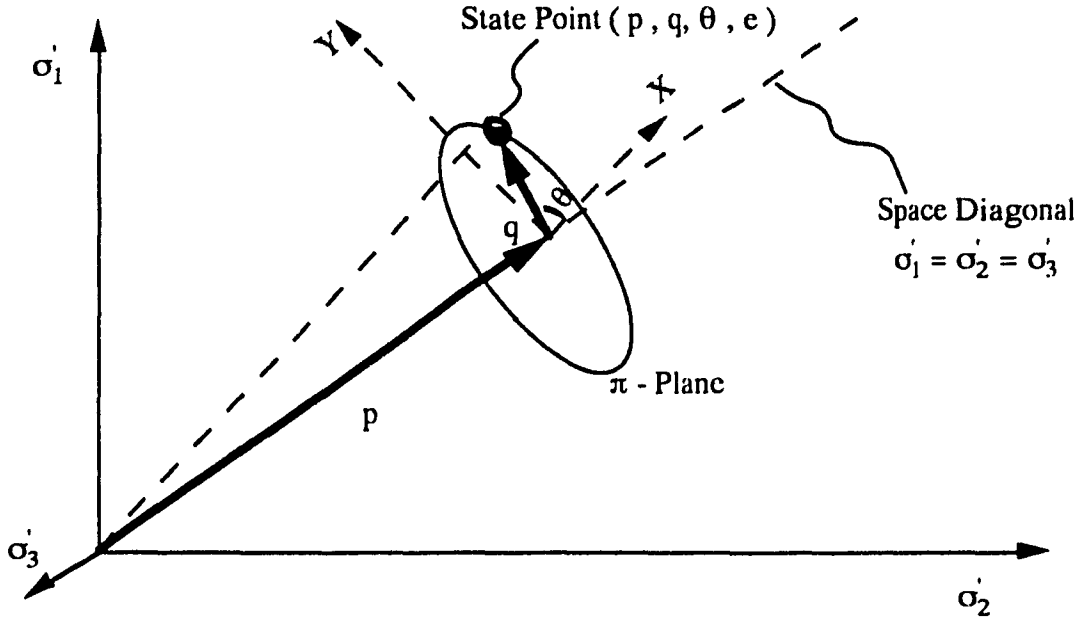

Figure 5.1 - State Point in the State Space

5.2.1.1. The Concept of State Boundary Surface

It is postulated that there exists a surface, in the state space, which encloses all the possible states a sample of a cohesionless medium may assume. This surface is called State Boundary Surface (Poorooshasb, 1961). It may be represented by the equation:

$$q - p\, g(\theta)\left[\mu - e'\,\delta\right] = 0 \tag{5.12}$$

The function $g(\theta)$ defines the cross sectional shape of the State Boundary Surface in the π -Plane. The soil parameters μ and δ define respectively the slope of the Ultimate State Surface in the p - q subspace under the triaxial compression testing condition and the angle of the dilatation of the medium. The formulation proposed by William and Warnke (1975) is used to quantify the function $g(\theta)$ and its value is chosen to be unity under the stress conditions of the triaxial compression test and equal to a value satisfying the Mohr-Coulomb Failure criterion under the triaxial extension test

$$g(\theta = \text{extension triaxial}) = \frac{\left[3 - \sin\phi\right]}{\left[3 + \sin\phi\right]} \tag{5.13}$$

and ϕ is the Mohr-Coulomb angle of friction.

Function $g(\theta)$ can be expressed by [William and Warnke (1975)]:

$$g(\theta) = \left\{ \frac{\left[2\left(W^2 - 1\right)\cos\left(\theta - \frac{\pi}{6}\right) + \left((2 - W)^2\left(4(W^2 - 1)\cos^2\left(\theta - \frac{\pi}{6}\right) + (5 - 4W)\right)^{1/2}\right]}{\left[\left(4(W^2 - 1)\cos^2\left(\theta - \frac{\pi}{6}\right)\right) + (2 - W)^2\right]} \right\} \tag{5.14}$$

where

$$W = \frac{g(\text{compression triaxial})}{g(\text{extension triaxial})} \tag{5.15}$$

and in the π - Plane it is seen as

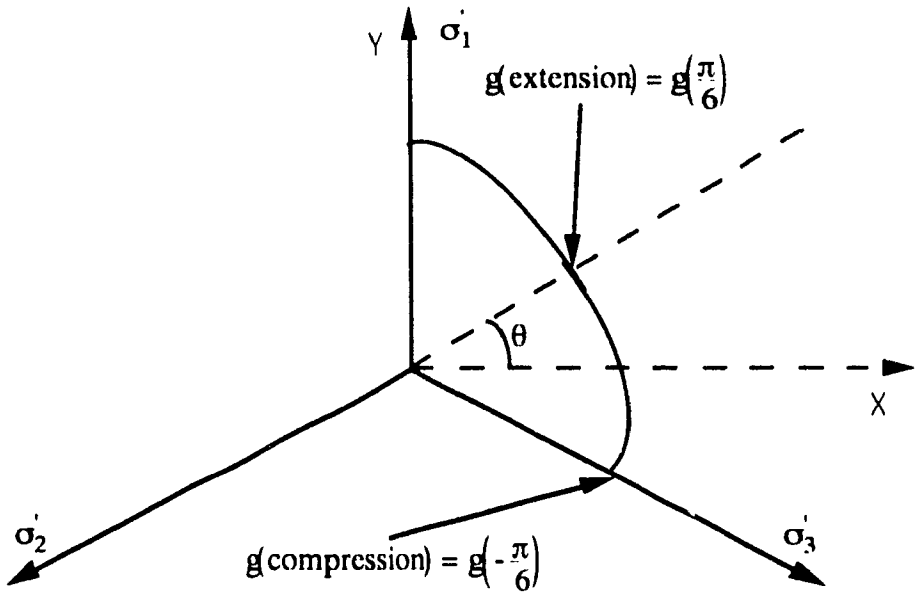

Figure 5.2 - Function g(θ) in the π - Plane

Figure 5.3 shows the State Boundary Surface for two different void ratios

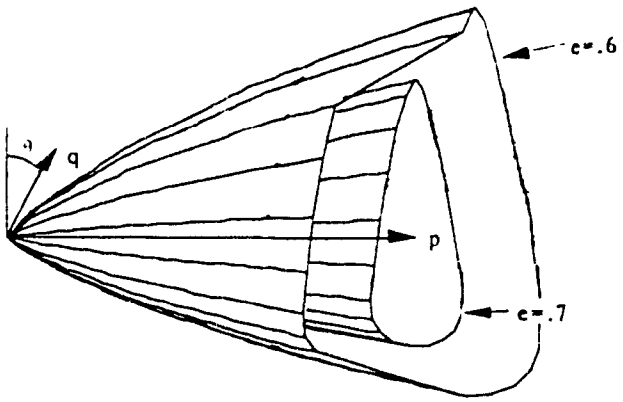

Figure 5.3 - State Boundary Surface for Two Different Void Ratios

5.2.1.2 The Concept of the Ultimate State

It is postulated that there exists a surface in the state space for which

$$\frac{\partial p}{\partial \varepsilon} = \frac{\partial q}{\partial \varepsilon} = \frac{\partial \theta}{\partial \varepsilon} = \frac{\partial e}{\partial \varepsilon} = 0 \qquad (5.8)$$

where ε is a measure of sample distortion and is derived from the second invariant of the strain deviator tensor. This set of points defines a surface in the state space that is known as the Ultimate State Surface. For this condition, the shear deformation continues, without further volume change and the void ratio at this stage is independent of the initial void ratio. It is important to mention that the Ultimate State Surface is an extension of the concept of Critical State Line (Poorooshasb, 1961), which was an extension of the concept of the Critical Void Ratio Line (same that Casagrande's Line). It is also considered to be equivalent to the Steady State Line concept developed by Castro and Poulos (1977), as referenced by Poorooshasb and Consoli (1991).

Postulating a unique relation between two of the state parameters at the Ultimate State, a three dimensional space may be used to represent the surface. Through the use of the equation of Casagrande's Line

$$e_{Casagrande} = e_0 - L \ln\left(\frac{I_1}{3}\right) \qquad (5.9)$$

a relation between state parameters p and e is obtained, where e_0 and L are soil parameters.

In the context of the Casagrande's Line a new state parameter e' is created to define the effective density of the granular material. This new variable is named effective void ratio and is defined by the equation

$$e' = e - e_{Casagrande} \qquad (5.10)$$

which after substitution of Equation 5.9 in Equation 5.10 yields

$$e' = e - e_0 + L \ln\left(\frac{I_1}{3}\right) \tag{5.11}$$

Figure 5.4 shows a three-dimensional view of the Ultimate State Surface in the Space (q, θ, e).

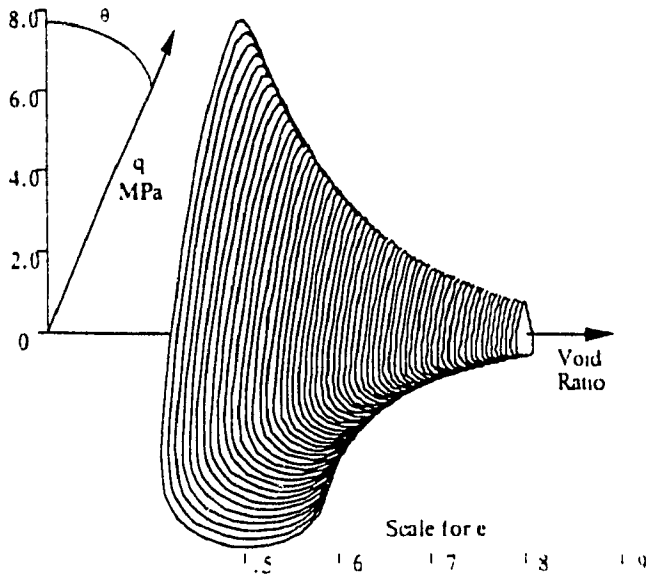

Figure 5.4 - Ultimate State Surface in the Space (q, θ, e)

5.2.2 Formulation of the Model

The complete modelling of the elasto plastic behavior of a soil begins with the definition of the surface which is able to define the point where plastic deformation due to virgin loading starts. This response is given by the yield surface, the form of which is usually established experimentally.

The Yield Surface must be enclosed by the State Boundary Surface, hence it must also conform to the same curvature of this surface. One way of achieving this is to postulate that the yield surfaces are similar in shape to the State Boundary Surface except that their relative position is controlled by the current state of the sample assuming the loading to be in its virgin phase.

Representing the Yield Function by F and following the similarity in shape, the Yield Surface may be expressed by

$$F = q - p\,\Psi(e^p)\,g(\theta)\left[\mu - e'\,\delta\right] = 0 \tag{5.16}$$

The soil parameters μ and δ are the same previously defined and represent respectively the slope of the Ultimate State Surface in the p-q space under the triaxial compression condition and the angle of the dilatation of the medium.

The function $\Psi(e^p)$ records the history of the plastic flow, it has a range between zero (no plastic flow) and unity (continuous plastic flow) and is given by the following hyperbolic format

$$\Psi(e^p) = \frac{e^p}{K + e^p} \tag{5.17}$$

where

$$e^p = \int de^p \tag{5.18}$$

$$de^p = \left[d\bar{\varepsilon}^p_{ij}\, d\bar{\varepsilon}^p_{ij}\right]^{1/2} \tag{5.19}$$

and

$$d\bar{\varepsilon}^p_{ij} = d\varepsilon^p_{ij} - \frac{d\varepsilon^p_{nn}\,\delta_{ij}}{3} \tag{5.20}$$

The variable K is function of the state parameters p and e and of three parameters of the soil R, S and T. p_a is the atmospheric pressure (constant used for obtaining a dimensionless parameter K) and e^p is the plastic distortion.

$$K = (R + S\,e)\left(\frac{p}{p_a}\right)^T \tag{5.21}$$

Adopting the idea of non-associated flow rule to explain the plastic flow of cohesionless granular media (Poorooshasb et al., 1966 and 1967), the increments of the plastic strain ($d\varepsilon^p_{ij}$) are given by the following equation

$$d\varepsilon^p_{ij} = d\Gamma \frac{\partial \Lambda}{\partial \sigma'_{ij}} \tag{5.22}$$

where $d\Gamma$ is a scalar value which is responsible for the magnitude of the plastic strain increment and $\partial\Lambda/\partial\sigma'_{ij}$ is responsible for the direction of the strain increment and Λ is the Plastic Potential Function. In terms of the state parameters p, q and θ the function Λ has the form;

$$\Lambda = p \,.\, Exp\left[\frac{\left\langle \frac{q}{p\, g(\theta)} \right\rangle}{\mu}\right] = Constant \tag{5.23}$$

The non-associated flow rule comes from the fact that Λ is not the same function as the yield function (F). This has been proven experimentally (Poorooshasb et al., 1966 and 1967).

5.2.2.1 Virgin Loading

Making use of the consistency condition, which states that during loading each stress increment leading from one plastic state to another, the condition F=0 must hold, it may be shown that;

$$dF = \left(\frac{\partial F}{\partial \sigma'_{ij}}\right) d\sigma'_{ij} + \left(\frac{\partial F}{\partial c'}\right) dc' + \left(\frac{\partial F}{\partial \Psi}\right)\left(\frac{\partial \Psi}{\partial e^p}\right) de^p = 0 \tag{5.24}$$

where

$$\frac{\partial F}{\partial \sigma'_{ij}} = \frac{\partial F}{\partial p}\frac{\partial p}{\partial \sigma'_{ij}} + \frac{\partial F}{\partial (\sqrt{J_2})}\frac{\partial (\sqrt{J_2})}{\partial \sigma'_{ij}} + \frac{\partial F}{\partial J_3}\frac{\partial J_3}{\partial \sigma'_{ij}} \tag{5.25}$$

$$dc' = dc + L\left(\frac{dI_1}{I_1}\right) \tag{5.26}$$

$$de = -(1 + e)\, d\varepsilon_{ii} \tag{5.27}$$

$$d\varepsilon_{ij} = \left[C_{ijkl}\, \sigma'_{kl} + d\Gamma \left(\frac{\partial \Lambda}{\partial \sigma'_{ij}} \right) \right] \tag{5.28}$$

$d\varepsilon_{ij}$ is the sum of elastic and plastic incremental deformations.

C_{ijkl} is the elastic constitutive matrix. For linear isotropic elastic material there are only two constants, Young's Modulus (E) and Poisson' s Ratio (ν). As non-linear isotropic elasticity is considered, the parameter E changes and is calculated by the following equation (Consoli, 1987)

$$E = E_0 + \frac{I_1}{A}(1 - 2\nu)(1 + e) \tag{5.29}$$

where E_0 and A are soil parameters.

$$de^p = d\Gamma \left[dev\left(\frac{\partial \Lambda}{\partial \sigma'_{ij}} \right) dev\left(\frac{\partial \Lambda}{\partial \sigma'_{ij}} \right) \right]^{1/2} \tag{5.30}$$

de^p is the plastic distortion increment.

$$\frac{\partial \Lambda}{\partial \sigma'_{ij}} = \frac{\partial \Lambda}{\partial p} \frac{\partial p}{\partial \sigma'_{ij}} + \frac{\partial \Lambda}{\partial (\sqrt{J_2})} \frac{\partial (\sqrt{J_2})}{\partial \sigma'_{ij}} + \frac{\partial \Lambda}{\partial J_3} \frac{\partial J_3}{\partial \sigma'_{ij}} \tag{5.31}$$

$$dev \frac{\partial \Lambda}{\partial \sigma'_{ij}} = \frac{\partial \Lambda}{\partial (\sqrt{J_2})} \frac{\partial (\sqrt{J_2})}{\partial \sigma'_{ij}} + \frac{\partial \Lambda}{\partial J_3} \frac{\partial J_3}{\partial \sigma'_{ij}} \tag{5.32}$$

$$\frac{\partial \Lambda}{\partial \sigma'_{ii}} = \frac{\partial \Lambda}{\partial p} \frac{\partial p}{\partial \sigma'_{ii}} \tag{5.33}$$

Substituting the appropriate terms in the consistency equation (5.24) and rearranging in terms of $d\Gamma$

$$d\Gamma = -\frac{\left[\frac{\partial F}{\partial \sigma_{ij}} d\sigma_{ij} - \frac{\partial F}{\partial e'}(1+e) C_{iikl}\, d\sigma_{kl} + \frac{\partial F}{\partial c'} L \frac{dI_1}{I_1}\right]}{\left[-\frac{\partial F}{\partial e'}(1+e)\frac{\partial \Lambda}{\partial \sigma_{ii}} + \frac{\partial F}{\partial \Psi}\frac{\partial \Psi}{\partial e^p}\left(dev\frac{\partial \Lambda}{\partial \sigma_{ij}}\ dev\frac{\partial \Lambda}{\partial \sigma_{ij}}\right)^{1/2}\right]} \qquad (5.34)$$

where the denominator is commonly called plastic hardening (H_p), i.e.

$$H_p = \left[-\frac{\partial F}{\partial e'}(1+e)\frac{\partial \Lambda}{\partial \sigma_{ii}} + \frac{\partial F}{\partial \Psi}\frac{\partial \Psi}{\partial e^p}\left(dev\frac{\partial \Lambda}{\partial \sigma_{ij}}\ dev\frac{\partial \Lambda}{\partial \sigma_{ij}}\right)^{1/2}\right] \qquad (5.35)$$

Then the elasto-plastic relation for virgin loading between the increment of strain tensor and the increment of the stress tensor is

$$d\varepsilon_{ij} = d\varepsilon_{ij}^{elastic} + d\varepsilon_{ij}^{plastic} = \left[C_{ijkl} + \left(\frac{\lambda_{kl}}{H_p}\right)\left(\frac{\partial \Lambda}{\partial \sigma'_{ij}}\right)\right] d\sigma'_{kl} \qquad (5.36)$$

where

$$\lambda_{kl} = -\left[\frac{\partial F}{\partial \sigma_{kl}} - \frac{\partial F}{\partial e'}(1+e) C_{iikl} + \frac{\partial F}{\partial c'} L \frac{\delta_{kl}}{I_1}\right] \qquad (5.37)$$

and δ_{kl} is the Kronecker Delta.

The inverse of the constitutive relation previously obtained is the relation between the increment of the stress tensor and the increment of the strain tensor. It is obtained as follows :

Multiplying both sides of Equation 5.36 by D_{ijkl}, which is the inverse of the elastic matrix C_{ijkl}, yields

$$D_{ijkl}\, d\varepsilon_{ij} = \left\{1 - \frac{\left[D_{ijkl}\frac{\partial F}{\partial \sigma'_{kl}}\frac{\partial \Lambda}{\partial \sigma'_{ij}} - \frac{\partial F}{\partial e'}(1+e) D_{ijkl}\, C_{nnkl}\frac{\partial \Lambda}{\partial \sigma'_{ij}} + \frac{\partial F}{\partial e'} L \frac{\delta_{kl}}{I_1} D_{ijkl}\frac{\partial \Lambda}{\partial \sigma'_{ij}}\right]}{H_p}\right\} d\sigma'_{kl}$$

(5.38)

Thus the inverse of Equation 5.38 is obtained in the following form

$$d\sigma'_{ij} = \left\{ D_{ijkl} - \frac{\left[-D_{ijpq} \frac{\partial F}{\partial \sigma'_{pq}} \frac{\partial \Lambda}{\partial \sigma'_{rs}} D_{rskl} + \frac{\partial F}{\partial e'} (1+e) D_{ijpq} C_{nnpq} \frac{\partial \Lambda}{\partial \sigma'_{rs}} D_{rskl} - \frac{\partial F}{\partial e'} \frac{L}{I_1} D_{ijpq} \delta_{pq} \frac{\partial \Lambda}{\partial \sigma'_{rs}} D_{rskl} \right]}{\left[H_p - \frac{\partial F}{\partial \sigma'_{pq}} D_{pqrs} \frac{\partial \Lambda}{\partial \sigma'_{rs}} + \frac{\partial F}{\partial e'} (1+e) C_{nnpq} D_{pqrs} \frac{\partial \Lambda}{\partial \sigma'_{rs}} - \frac{\partial F}{\partial e'} \frac{L}{I_1} \delta_{pq} D_{pqrs} \frac{\partial \Lambda}{\partial \sigma'_{rs}} \right]} \right\} d\varepsilon_{kl} \tag{5.39}$$

This completes the incremental elasto-plastic stress-strain relation for virgin loading.

5.2.2.2 Unloading-Reloading Stress-Strain Relations

So far, the concepts have been applied only to virgin loading. In the classical theory of plasticity, cases of unloading/reloading conditions were treated as if the material were elastic. This is an unreasonable assumption for granular media such as soils.

To model the incremental stress-strain relations of elasto-plastic materials under unloading/reloading conditions realistically, the concept of generalized plasticity (Zienkiewicz and Mroz, 1984) is introduced. Generalized plasticity concept states that the plastic material behavior is fully described anywhere inside the virgin yield surface after characterization of a unit tensor normal to the yield function passing through the actual stress point. The definition of a unit tensor to characterize the direction of the plastic deformation is also needed, as well as the obtainance of the hardening parameter scalar, which is defined after an interpolation rule in the π - Plane from the corresponding values on the virgin yield surface.

Extending the above mentioned concepts from the Stress Space to the State Space, the behavior of the material may be formulated with the aid of a yield surface f and a unit tensor normal to this surface (v^f_{kl}).

The consistency condition is f=0, and consequently df=0 leads to

$$\Omega_{kl} = -\left[\frac{\partial f}{\partial \sigma'_{kl}} - \frac{\partial f}{\partial \varepsilon'}(1+e)C_{iikl} + \frac{\partial f}{\partial \varepsilon'}\gamma\frac{\delta_{kl}}{I_1}\right] \tag{5.40}$$

where Ω_{kl} is similar to λ_{kl} (Equation 5.37), except that all values in the present configuration are obtained with reference to the current yield surface f.

The unit tensor (v^f_{kl}), normal to this internal yield function f has the form

$$v^f_{kl} = \frac{\Omega_{kl}}{[\Omega_{kl}\,\Omega_{kl}]^{1/2}} \tag{5.41}$$

To formulate the flow law, recent studies by Yang (1990) were extended. This author, proposed that the directions of the plastic deformation could be obtained in a simplified way if numerical studies based on the two-surface model with reflecting plastic potential, were analyzed.

The conclusions of Yang (1990), now extended for the State Space are that for the case of reloading, the direction of the plastic deformation is the same as that for loading, except that the plastic potential surface (Λ^f) passes through the actual stress point, located inside the virgin yield surface. For unloading, two cases are distinguished, where the hydrostatic component of the direction (same direction of space diagonal shown in Figure 5.1, represented by p) of the plastic deformation has opposite sign that the reloading case when the state point is positioned below the Ultimate State Surface and the same sign when it is above that surface. The deviator component (direction in the π - plane, represented by J_2 and J_3) keeps the same direction as of the reloading.

The above discussions may be formulated as follows

Reloading and Unloading (Above Ultimate State Surface)

$$\frac{\partial \Lambda^f}{\partial \sigma'_{ij}} = \frac{\partial \Lambda^f}{\partial p}\frac{\partial p}{\partial \sigma'_{ij}} + \frac{\partial \Lambda^f}{\partial (\sqrt{J_2})}\frac{\partial (\sqrt{J_2})}{\partial \sigma'_{ij}} + \frac{\partial \Lambda^f}{\partial J_3}\frac{\partial J_3}{\partial \sigma'_{ij}} \tag{5.42}$$

Unloading (Below Ultimate State Surface)

$$\frac{\partial \Lambda^f}{\partial \sigma'_{ij}} = -\frac{\partial \Lambda^f}{\partial p}\frac{\partial p}{\partial \sigma'_{ij}} + \frac{\partial \Lambda^f}{\partial (\sqrt{J_2})}\frac{\partial (\sqrt{J_2})}{\partial \sigma'_{ij}} + \frac{\partial \Lambda^f}{\partial J_3}\frac{\partial J_3}{\partial \sigma'_{ij}} \tag{5.43}$$

The unit tensor v_{Pij} normal to the plastic potential surface Λ^f may be expressed as

$$v^p_{ij} = \frac{\dfrac{\partial \Lambda^f}{\partial \sigma'_{ij}}}{\left[\dfrac{\partial \Lambda^f}{\partial \sigma'_{ij}}\dfrac{\partial \Lambda^f}{\partial \sigma'_{ij}}\right]^{1/2}} \tag{5.44}$$

Finally the magnitude of the Hardening Parameter for reloading/unloading ($H_{r/u}$) is assumed to depend of the position of the actual stress point within the virgin yield surface. For this purpose it is convenient to define an Associate State Point $(\sigma_{ij},e)^a$ in the π-plane. This is defined by the intersection of a straight line passing through the present state point and the origin of the π - Plane, and the virgin yield surface. The same angle θ of the actual state point is used in the case of reloading and $\theta=\theta+180^0$ in the case of unloading. A Datum State Point $(\sigma_{ij},e)^d$ is also defined in the intersection of the same straight line of the Associate State Point, in the intersection with the virgin yield surface, but 180^0 apart in the π-plane. If the spatial angle between the actual state point and its associate is ϑ and the corresponding angle between the datum and associate is ϑ_0, then (Poorooshasb and Pietruszczak, 1986);

$$\vartheta = \cos^{-1}\left\{\frac{\left(\sigma'_{ij}\,\sigma^a_{ij}\right)}{\left[\left(\sigma'_{kl}\,\sigma'_{kl}\right)\left(\sigma^a_{pq}\,\sigma^a_{pq}\right)\right]^{1/2}}\right\} \tag{5.45}$$

$$\vartheta_0 = \cos^{-1}\left\{\frac{\left(\sigma^d_{ij}\,\sigma^a_{ij}\right)}{\left[\left(\sigma^d_{kl}\,\sigma^d_{kl}\right)\left(\sigma^a_{pq}\,\sigma^a_{pq}\right)\right]^{1/2}}\right\} \tag{5.46}$$

and

$$\frac{1}{H_{r/u}} = \frac{\left[(\Omega_{ij})^{*}(\Omega_{ij})^{*}\right]^{1/2}\left[\left(\frac{\partial\Lambda}{\partial\sigma'_{kl}}\right)^{*}\left(\frac{\partial\Lambda}{\partial\sigma'_{kl}}\right)^{*}\right]^{1/2}}{(H_p)^{*}}\left(1-\frac{\vartheta}{\vartheta_0}\right)^{\xi} \qquad (5.47)$$

where (*) signifies quantities evaluated in the Associated State Point in the Virgin Yield Surface of the State Space and ξ is a soil constant.

The incremental elasto-plastic strain tensor for reloading/unloading conditions may now be stated as

$$d\varepsilon_{ij} = d\varepsilon_{ij}^{elastic} + d\varepsilon_{ij}^{plastic} = \left[C_{ijkl} + \left(\frac{v_{kl}^{f}}{H_{r/u}}\right)\left(v_{ij}^{p}\right)\right] d\sigma'_{kl} \qquad (5.48)$$

The similarity of this equation with that of 5.36 is noteworthy.

The inverse of the previous relation may be obtained following the same procedure used for deriving Equation 5.39 for virgin loading, with the result:

$$d\sigma'_{ij} = \left\{ D_{ijkl} - \frac{\left[-D_{ijpq}\frac{\partial f}{\partial\sigma'_{pq}}\frac{\partial\Lambda^{f}}{\partial\sigma'_{rs}}D_{rskl} + \frac{\partial f}{\partial e'}(1+e)D_{ijpq}C_{nnpq}\frac{\partial\Lambda^{f}}{\partial\sigma'_{rs}}D_{rskl} - \frac{\partial f}{\partial e'}\frac{L}{I_1}D_{ijpq}\delta_{pq}\frac{\partial\Lambda^{f}}{\partial\sigma'_{rs}}D_{rskl}\right]}{\left[H_{i(r/u)} - \frac{\partial f}{\partial\sigma'_{pq}}D_{pqrs}\frac{\partial\Lambda^{f}}{\partial\sigma'_{rs}} + \frac{\partial f}{\partial e'}(1+e)C_{nnpq}D_{pqrs}\frac{\partial\Lambda^{f}}{\partial\sigma'_{rs}} - \frac{\partial f}{\partial e'}\frac{L}{I_1}\delta_{pq}D_{pqrs}\frac{\partial\Lambda^{f}}{\partial\sigma'_{rs}}\right]} \right\} d\varepsilon_{kl}$$

(5.49)

where

$$H_{i(r/u)} = \frac{\left[(\Omega_{ij})(\Omega_{ij})\right]^{1/2}\left[\left(\frac{\partial\Lambda^{f}}{\partial\sigma'_{kl}}\right)\left(\frac{\partial\Lambda^{f}}{\partial\sigma'_{kl}}\right)\right]^{1/2}}{\left[(\Omega_{ij})^{*}(\Omega_{ij})^{*}\right]^{1/2}\left[\left(\frac{\partial\Lambda}{\partial\sigma'_{kl}}\right)^{*}\left(\frac{\partial\Lambda}{\partial\sigma'_{kl}}\right)^{*}\right]^{1/2}}\left(1-\frac{\vartheta}{\vartheta_0}\right)^{\xi}(H_p)^{*} \qquad (5.50)$$

Note again that all quantities are evaluated at the present state point , except those with an asterisk (*), which are evaluated for the Associate State Point in the Virgin Yield Surface of the State Space.

5.3. Numerical Implementation

Two computer programs were developed to evaluate numerically the validity of the constitutive model proposed.

In the first one, named CONDIR, the stress controlled development was introduced, with equations 5.36 for virgin loading and 5.48 for the case of reloading and unloading. This Code is able to determinate the strain increment for a given effective stress increment with known initial state. After each step, the state variables are updated.

It is worth mentioning that during numerical simulation of the drained tests under monotonic loading, as soon as the stresses reach the State Boundary Surface they are directed to follow the surface until the Ultimate State is reached (Figure 5.5).

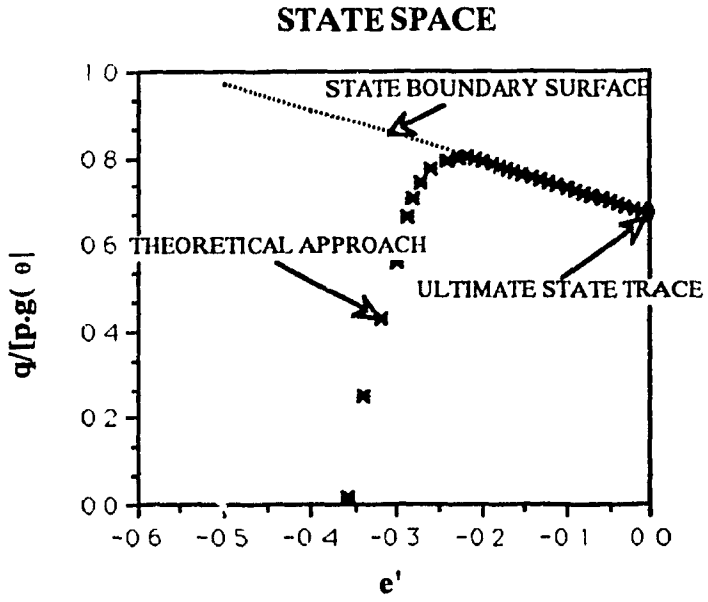

Figure 5.5 - Behavior of a Sample Until Reaching Ultimate State

In the second program, named CONINV, the strain controlled process was codified, incorporating Equation 5.39 for virgin loading and Equation 5.49 for strain paths inside the virgin yield surface. This Code is able to to determine the

effective stress increment due to a strain increment with a known initial state of strain and stress.

In the numerical method to be developed in Chapter 6 this strain controlled elasto-plastic stress-strain matrix will be introduzed to characterize the material behavior. This is considered to be one of the important factors for a reliable analysis.

Here the information available is the state of the element at the beginning of the loading step and the strain at the end of the step. What is required is to determine the state of the element at the end of the step. To this end first a test is performed using only the elastic matrix. Once the loading direction is determined, the numerical evaluation may proceed using the appropriate elasto-plastic formulation.

To correct any discrepancy in the consistency condition, (i. e., if $F \neq 0$) in the end of the step, p and θ are kept the same and the value of q which satisfies the consistency condition is found.

After that the state variables are updated for the next step. Small step increments are suggested for better results.

5.4. Evaluation of Parameters

As a check of this new model, reliable experimental data from monotonic and cyclic triaxial tests reported by Seed and Lee (1966) and Lee and Seed (1967) on Sacramento River Sand (Cohesionless Material) were used to calibrate the model and to obtain the required parameters.

From drained compression triaxial tests shown in Figure 5.6, the parameters μ, δ, e_0, L, R, S, T and W are evaluated, through calibration.

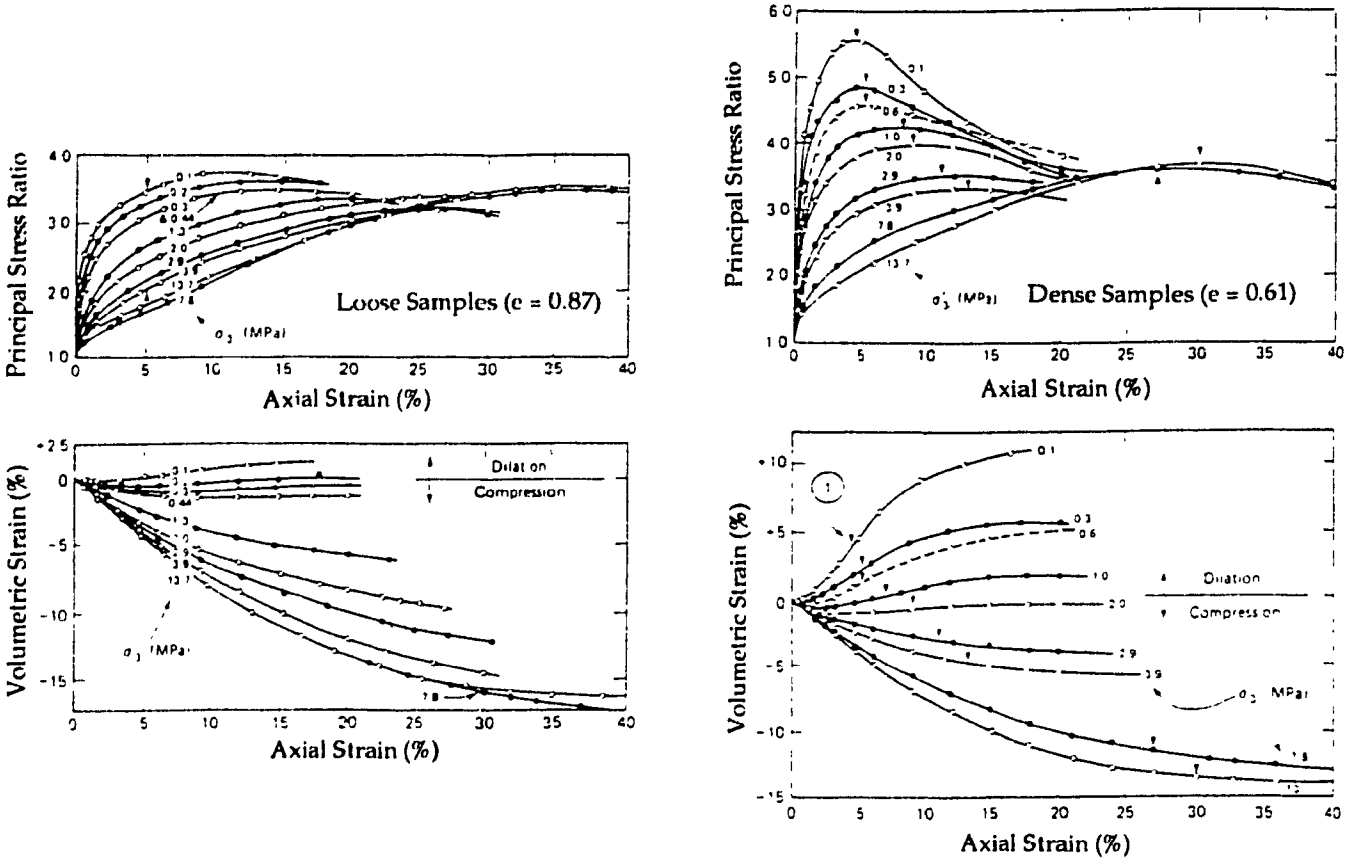

Figure 5.6 - Drained Triaxial Compression Tests For the Sacramento River Sand

First of all, in the subspace p x q under triaxial compression, using the stress obtained from points with more than 20% of deformation in the stress-strain curves (considered reaching the Ultimate State) for different confining pressures, the parameter μ is obtained, as can be seen in Figure 5.7, $\mu = 0.65$.

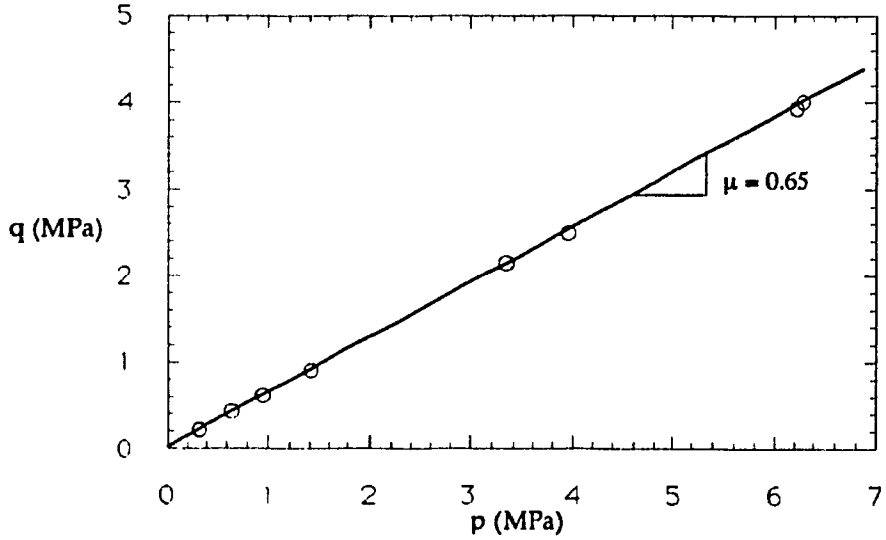

Figure 5.7 - Parameter μ for the Sacramento River Sand

In Figure 5.8 the parameter δ is obtained for several tests with different confining pressures and it can be seen that its value is constant and equal to δ=0.79

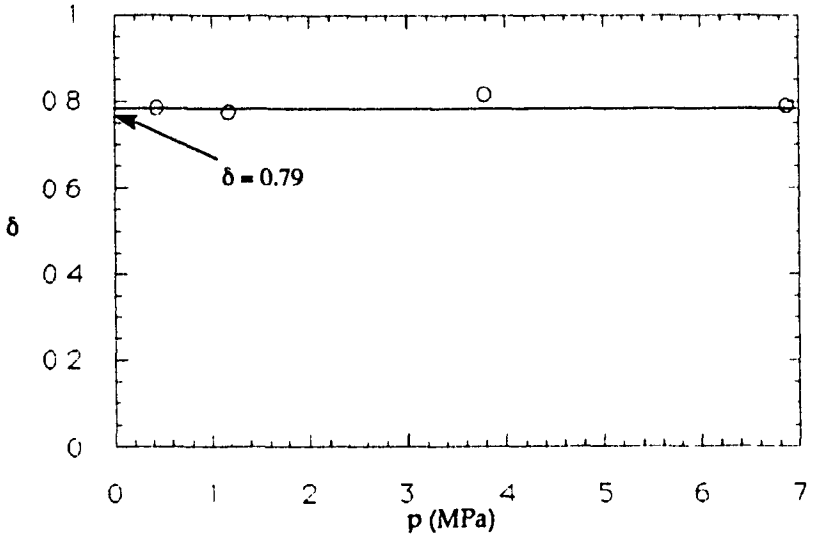

Figure 5.8 - Parameter δ for the Sacramento River Sand

The parameters e_0 and L of the Casagrande's Line are obtained in Figure 5.9

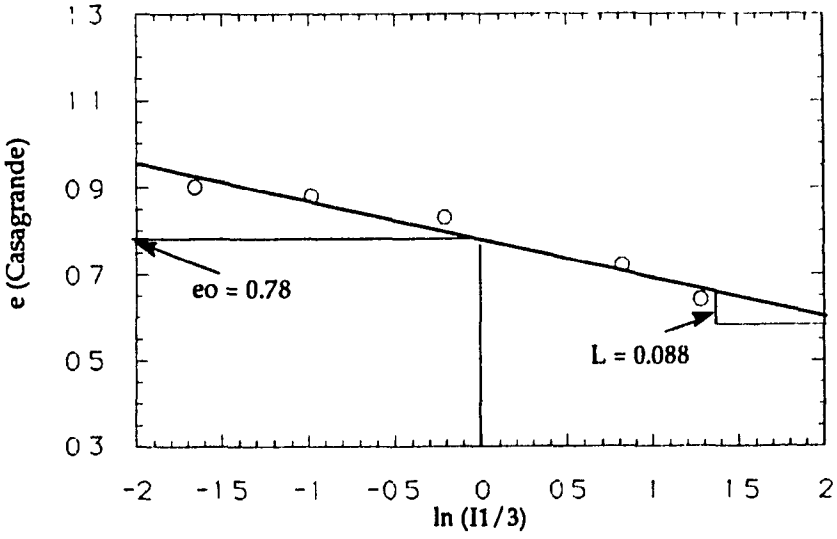

Figure 5.9 - Parameter e_0 and L for the Sacramento River Sand

The parameters R, S and T are obtained through the calibration of two different densities, a loose one (e=0.82) and a dense one (e=0.61) as can be seen in Figure 5.10,

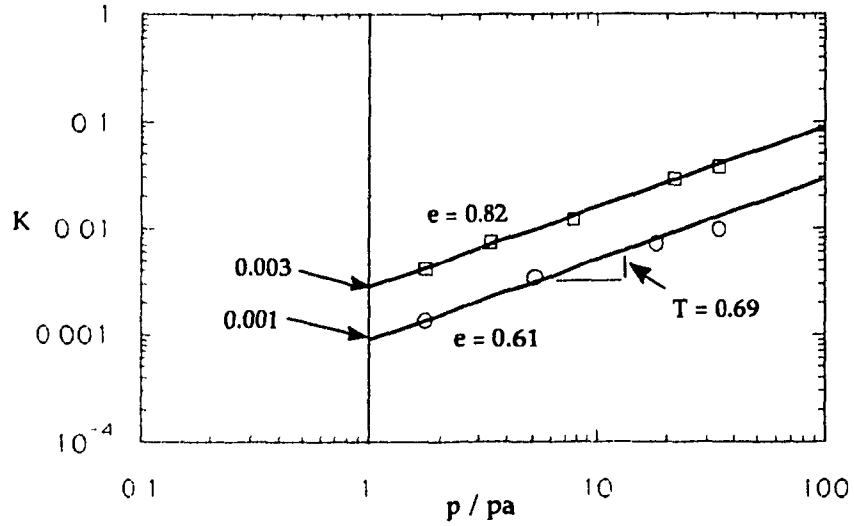

Figure 5.10 - Determination of Parameter T

then using the intersection of the two parallel lines with a vertical line passing through p/pa =1 the parameters which indicate the influence of the void ratio are obtained in Figure 5.11.

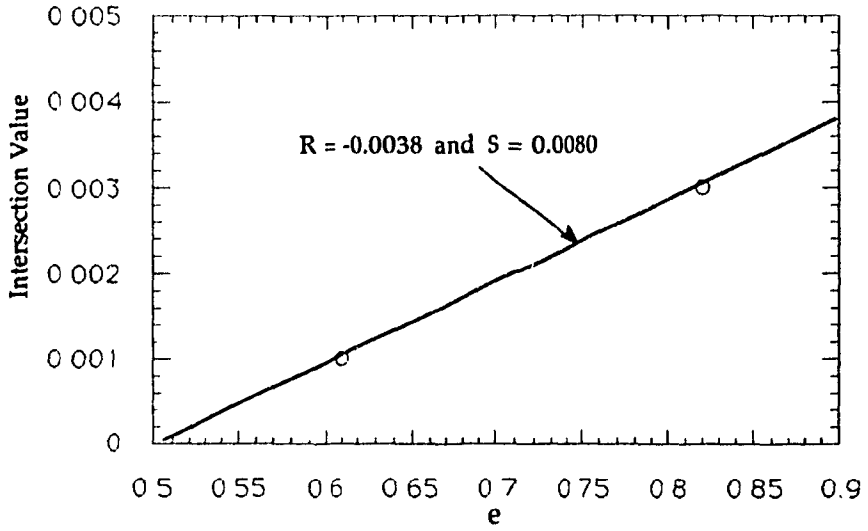

Figure 5.11 - Linear Influence of the Void Ratio (Parameters R and S)

The parameter W is obtained through the use of Equation 5.13 where $\phi=33^0$, then W=1.44.

The parameter ξ is obtained by trial and error using undrained cyclic triaxial tests during stress reversal as checking. The best value found was $\xi=6.0$.

The elastic parameters are Poisson's Coefficient $\nu=0.3$, a typical value for sand, $E_0=15$ MPa and A=2.0. These values yield results which agree well with the laboratory findings.

The complete set of parameters for the Sacramento River Sand are shown in Table 5.1.

E_0 = 15 MPa	A = 2.0	ν = 0.3	μ = 0.65
δ = 0.79	e_0 = 0.78	L = 0.088	R = - 0.0038
S = 0.008	T = 0.69	W = 1.44	ξ = 6.0

Table 5.1 - Parameters of the Constitutive Relation for the Sacramento River Sand

5.5. Modelling of Laboratory Tests

Using the above mentioned two programs, Stress Controlled and Strain Controlled tests were numerically reproduced and compared with the laboratory tests conducted by Seed and Lee (1966) and Lee and Seed (1967).

First the analytical reproduction of the triaxial drained tests was attempted with good results for several confining pressures (0.1 to 2.0 MPa) and different void ratio. In Figures 5.12, 5.13, 5.14 and 5.15 the comparison between analytical and laboratory stress controlled tests are shown.

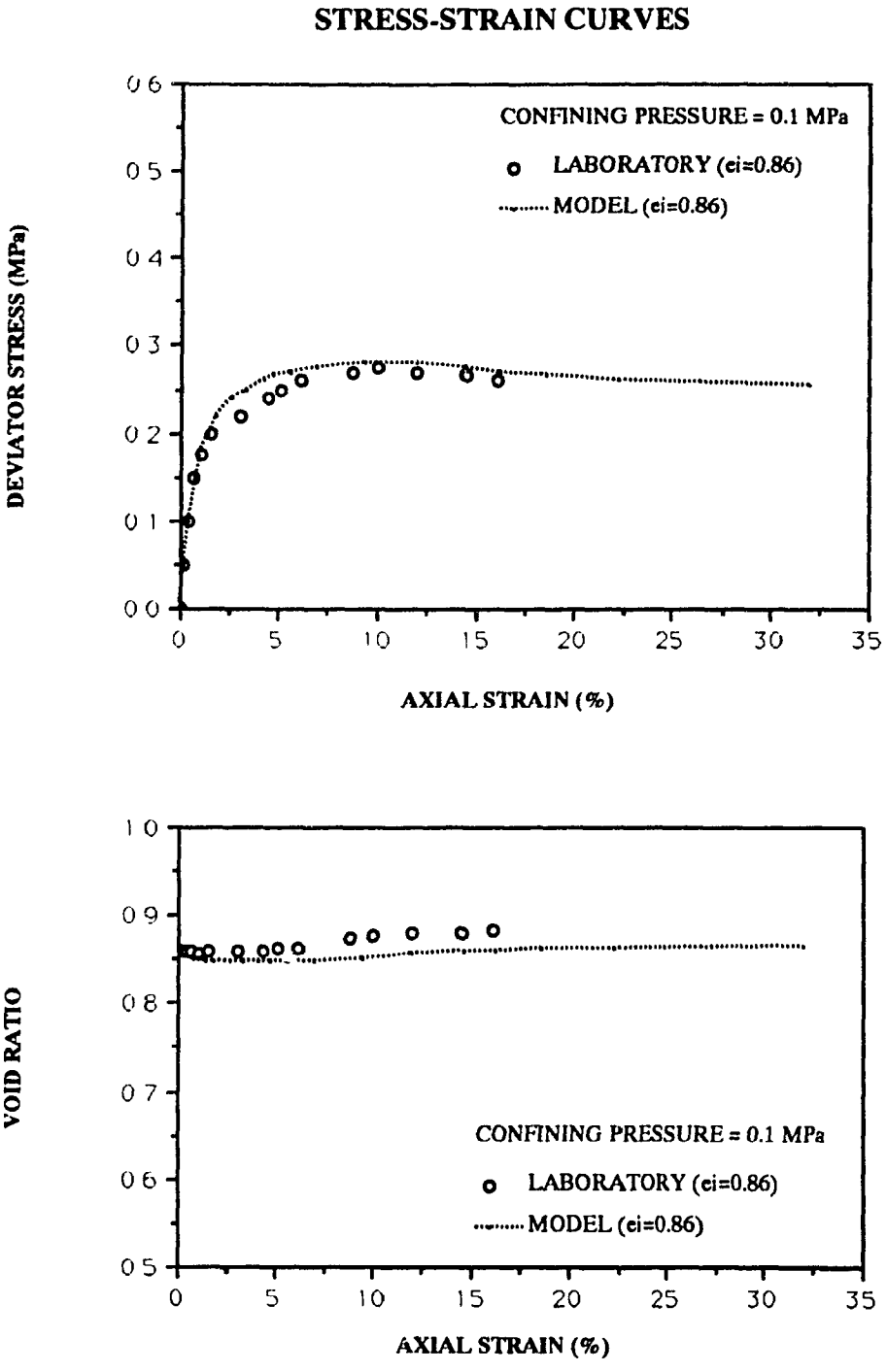

Figure 5.12 - Stress Control Analytical and Laboratory Tests for σ=0.1 MPa

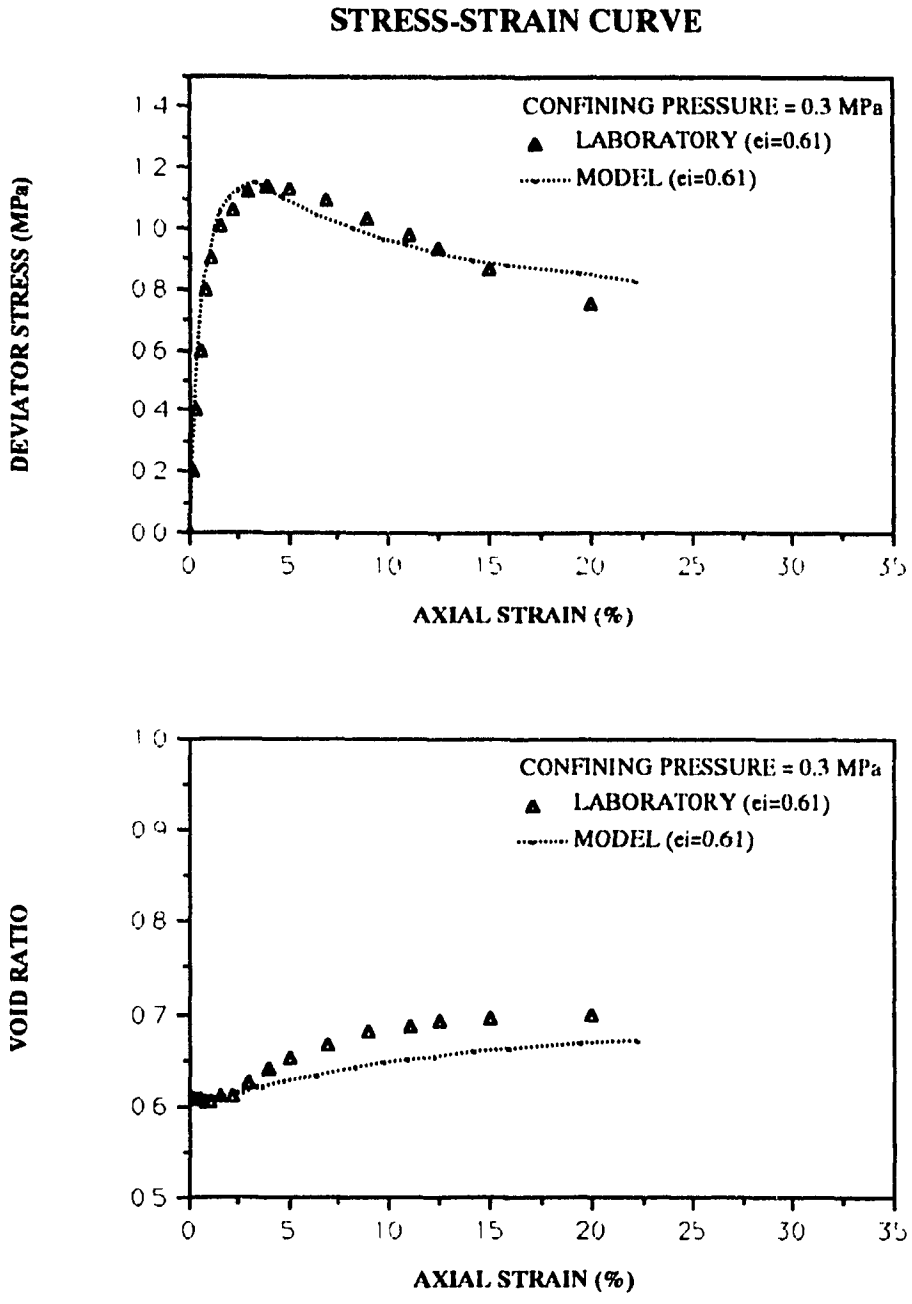

Figure 5.13 - Stress Control Analytical and Laboratory Tests for σ=0.3 MPa

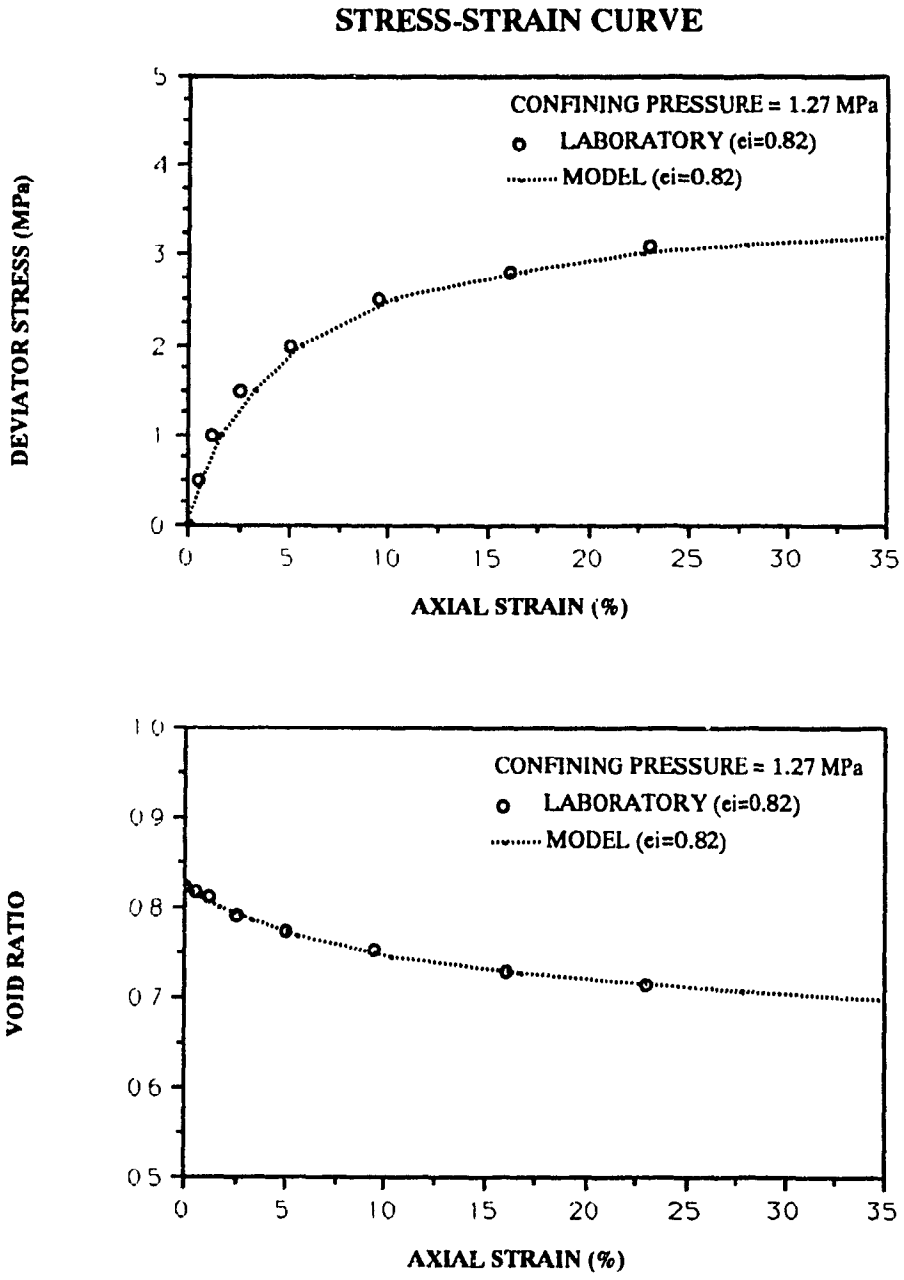

Figure 5.14 - Stress Control Analytical and Laboratory Tests for σ=1.27 MPa

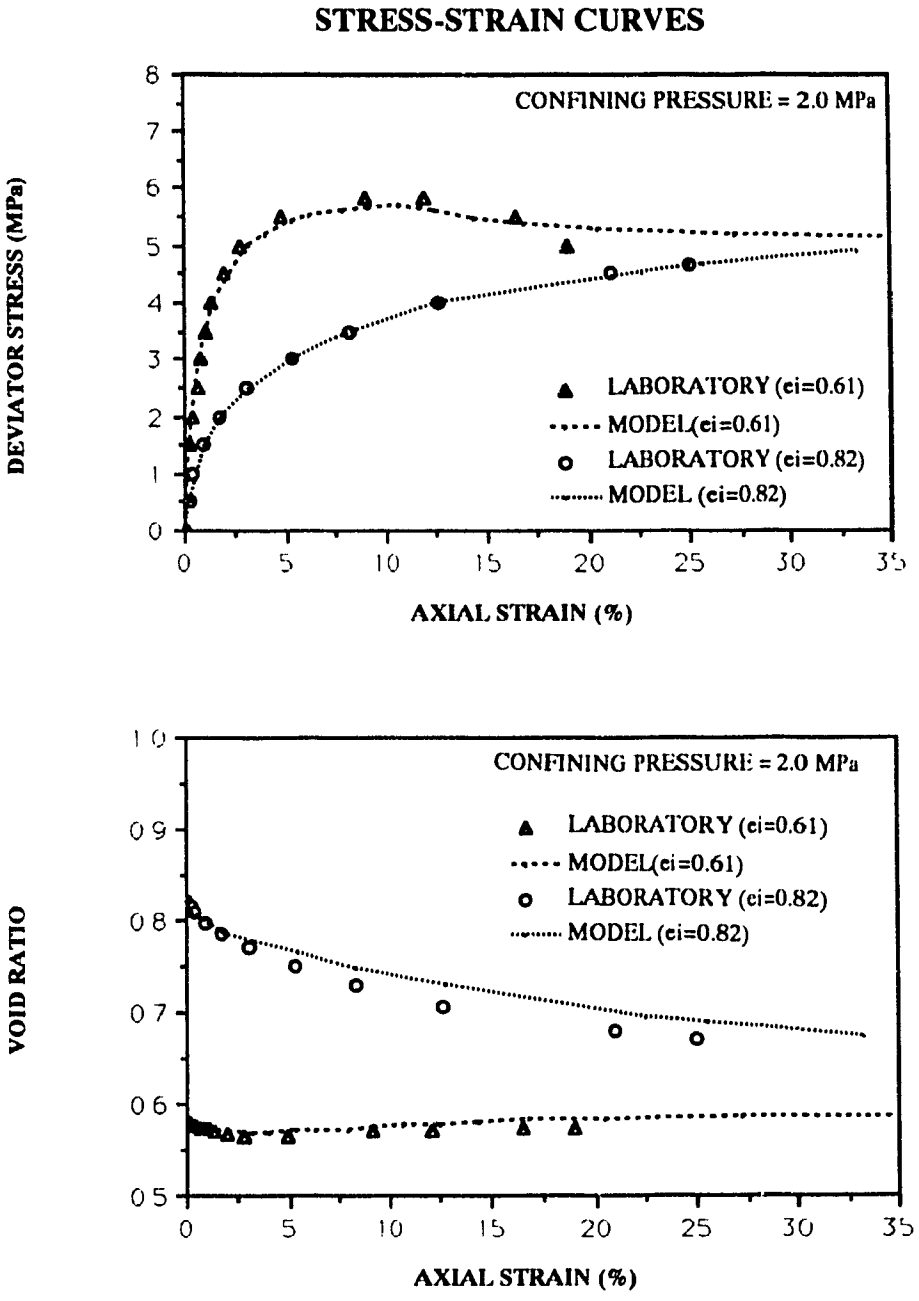

Figure 5.15 - Stress Control Analytical and Laboratory Tests for σ=2.0 MPa

In Figures 5.16 and 5.17, the stress path of four strain control undrained tests are shown, changing for each test the confining pressure and/or the void ratio. The behavior of samples with the same void ratio and different confining pressure shows that these samples reach the same final point, located on the Ultimate State Surface, confirming facts analytically obtained in laboratory by Seed and Lee (1966). In the case of higher void ratio (e=0.87) the stress path is completely different in the two cases. For the smaller pressure a slight decrease of p in the beginning is followed by a continuous increase until reaching the Ultimate State. In contrast with the higher confining pressure, the mean stress p decreases continually until reaching the same point as in the previous case. For the case of void ratio equal to e=0.74, both confining pressures behave in the same way, with a slight decrease of p in the beginning and then a continuous increase until stabilizing at the Ultimate State.

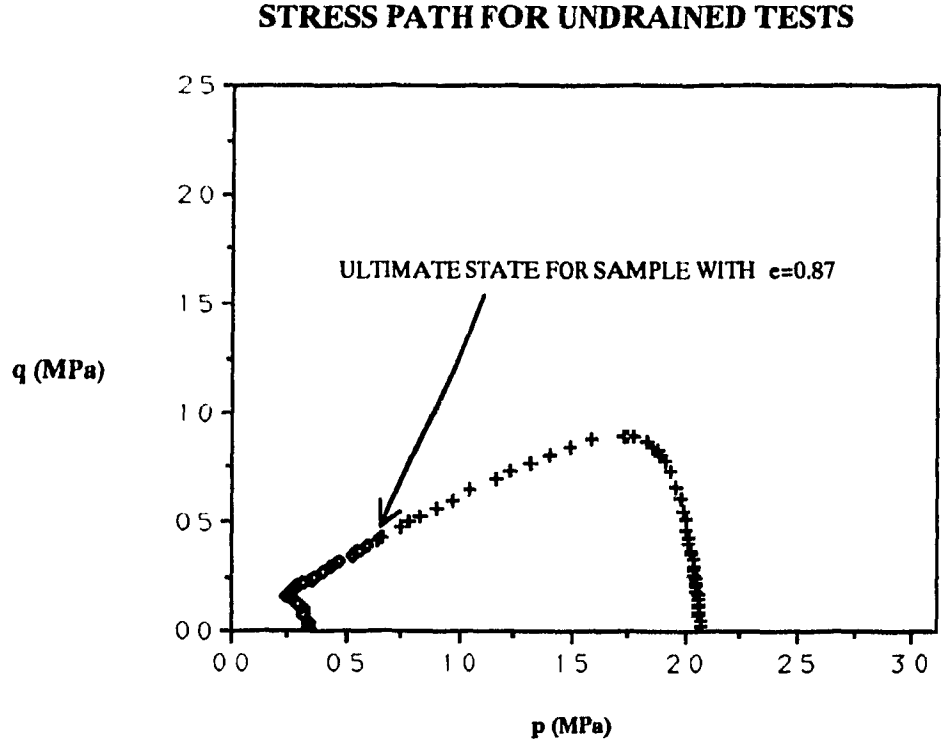

Figure 5.16 - Triaxial Undrained Tests for e=0.87 and Different Confining Stresses

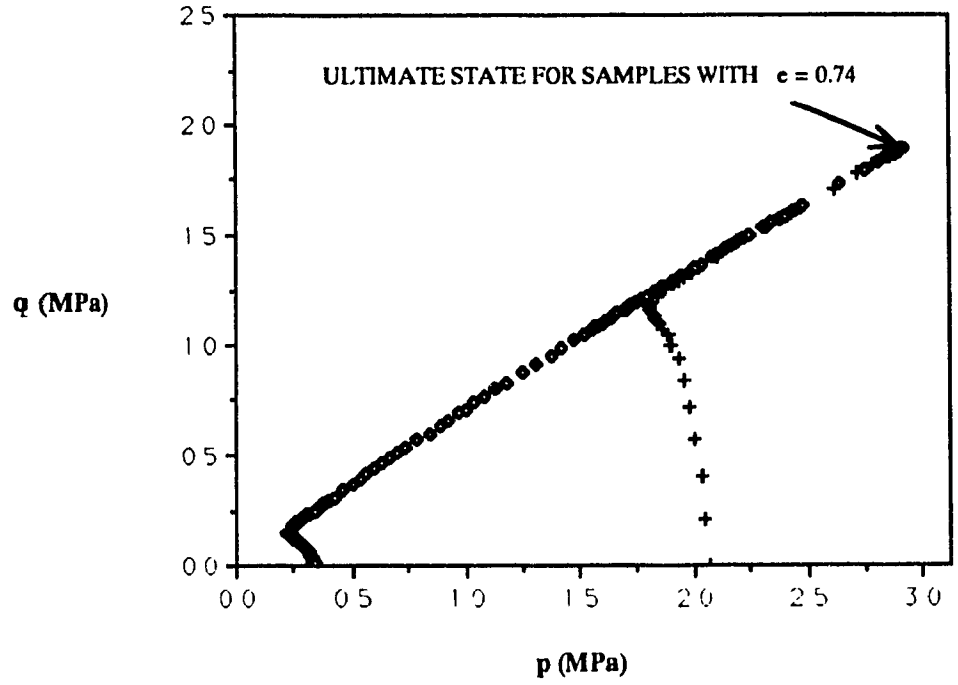

Figure 5.17 - Triaxial Undrained Tests for e=0.74 and Different Confining Stresses

In Figures 5.18 and 5.19 cyclic undrained strain control tests are numerically simulated for two void ratios (e=0.87 and e=0.71) and the same confining stress. The stress path and stress-strain relation are shown for both cases.

It is noted that many more cycles are required to approach liquefaction for the originally dense sample (e=0.71) compared to the number of cycles required for the loose sample.

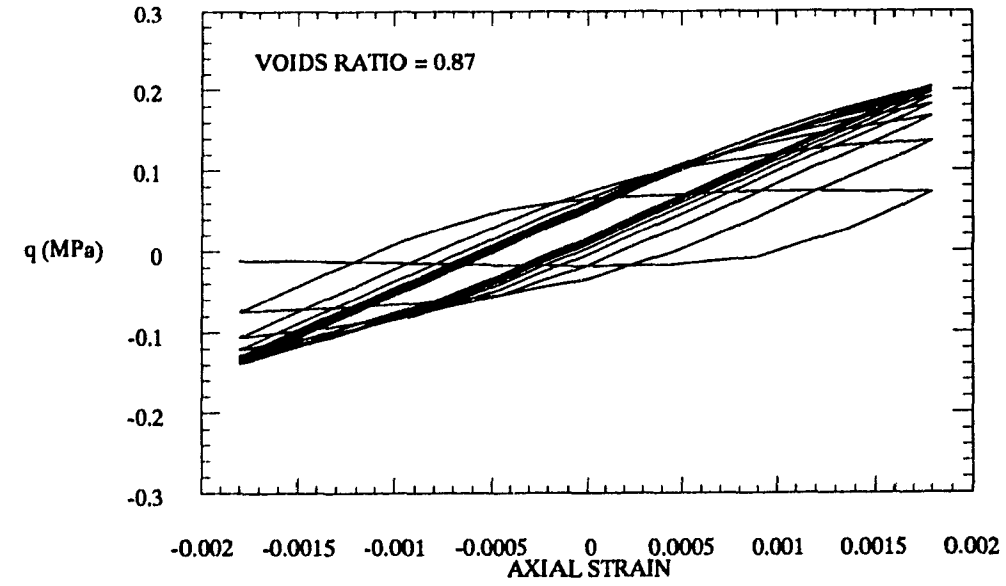

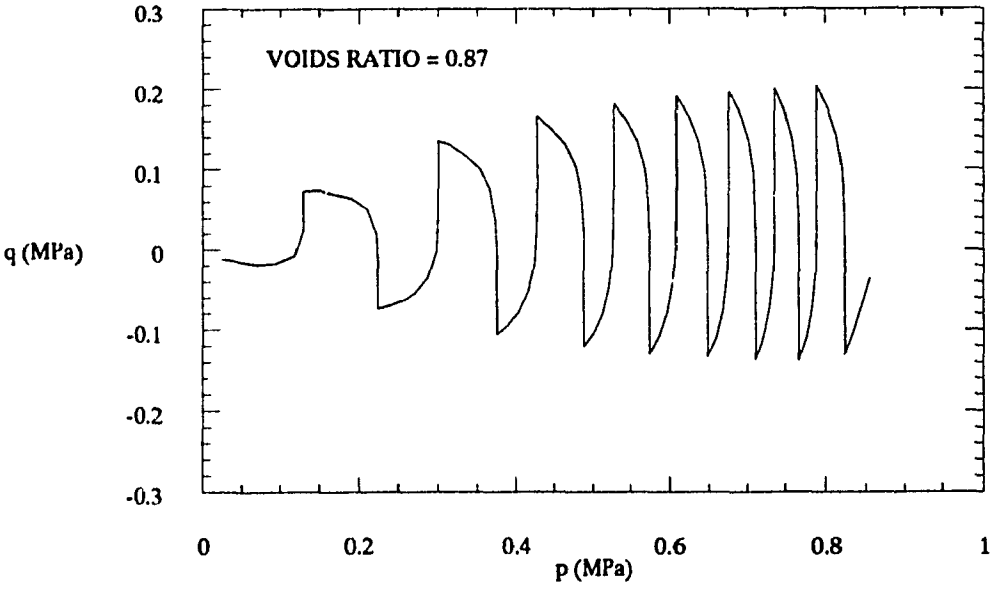

Figure 5.18 - Cyclic Undrained Strain Control Test with e=0.87

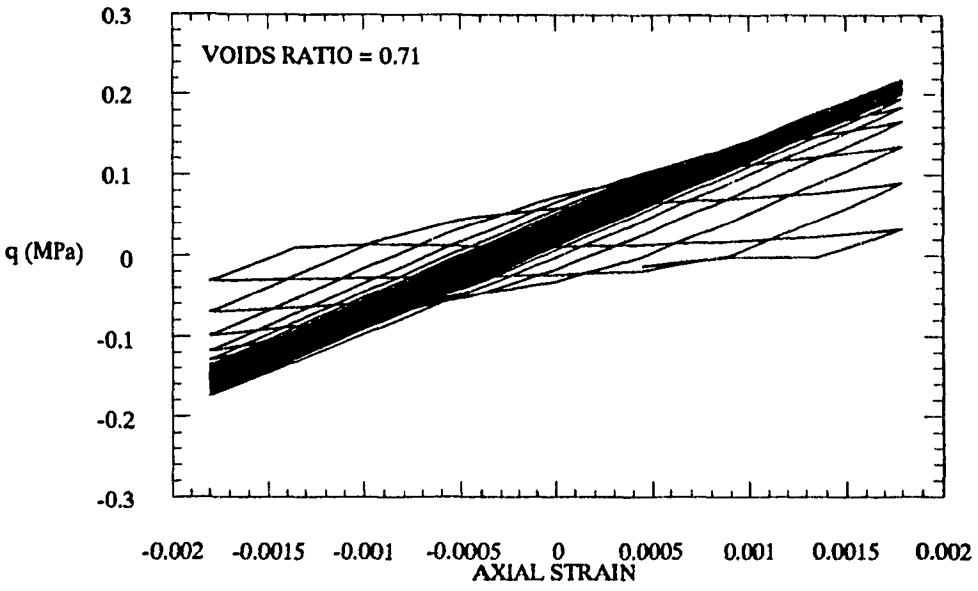

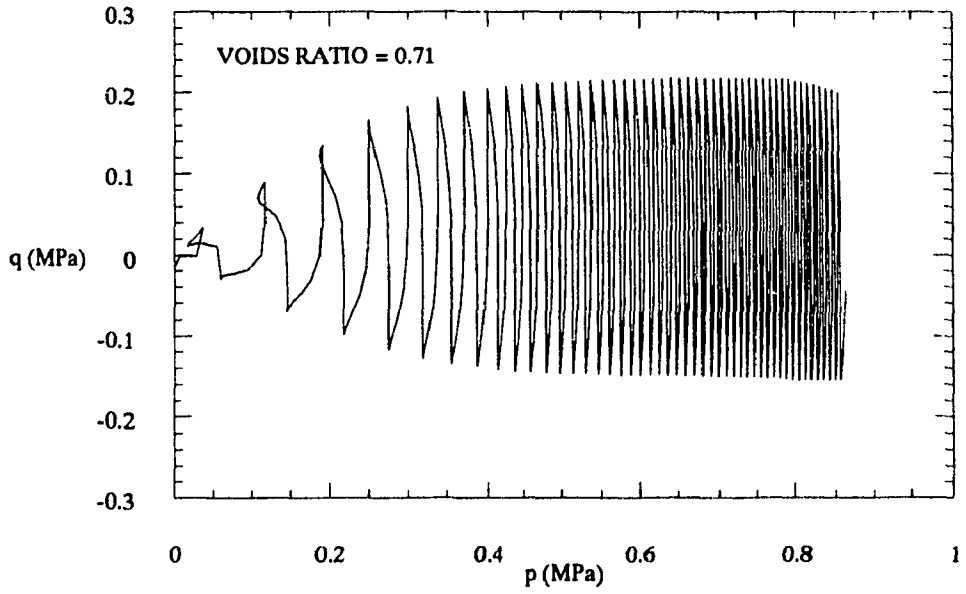

Figure 5.19 - Cyclic Undrained Strain Control Test with e=0.71

CHAPTER 6

MATERIAL AND GEOMETRICAL NON-LINEARITY FINITE ELEMENT IN THE SOLUTION OF COUPLED CONSOLIDATION PROBLEMS

6.1. Introduction

Most of the presently available formulations for analysis of inelastic finite deformation are primarily intended for analysis of plates and shells problems involving large displacements (rotation) but small strains (small strain large displacement analysis). Consequently these formulations are inappropriate for application to bulky geometries such as those encountered in soil mechanics.

The objective of this part of the study is to develop governing equations for the coupled consolidation behavior of an elasto-plastic soil skeleton. The analysis accounts for deformations of large magnitude, as well as nonlinearities due to material response. A second objective is to establish a numerical procedure to solve the governing equations.

The formulation is based upon equilibrium conditions, the continuity equation and the elasto-plastic constitutive formulation generalized from the one developed in Chapter 5 by the introduction of an Eulerian viewpoint of a frame invariant (objective) stress rate.

The incremental or rate form of the constitutive equations suggests that a rate approach be taken toward the entire problem so that flow is viewed as a history dependent process rather than an event. A direct consequence of the consistent adoption of the rate viewpoint in a spatial reference frame is that the problem is found to be governed by quasi-linear differential equations in time and space, hence the analysis requires solution of boundary value problems involving instantaneously linear equations, as suggested by Osias and Swedlow (1974).

Equations for the piecewise linear incremental finite element analysis are developed by the application of the Gauss Theorem to the instantaneously linear governing differential equation of equilibrium and the Galerkin Method to the continuity equation.

6.2. Basic Governing Equations for Elasto-Plastic Flow Without Restricting Deformation Magnitude

For a cubic element of soil, composed of a solid skeleton and an incompressible fluid, the basic equilibrium equations, containing the effective stress principle of Terzaghi, may be written directly as

$$\frac{\partial \sigma'_{ij}}{\partial x_j} + \delta_{ij} \frac{\partial p}{\partial x_j} + F_i = 0 \qquad (6.1)$$

where

σ'_{ij} = the components of Cauchy's Effective Stress Tensor

δ_{ij} = the Kronecker Delta

p = the pore pressure

F_i = the components of the body force

Considering that the fluid has an actual velocity v_i^f, then the apparent velocity of the fluid relative to the skeleton is $n(v_i^f - v_i)$, where n is the material porosity and v_i is the velocity of the material skeleton.

Assuming first that the movement of fluid through the soil is governed by Darcy's Law, which states that the apparent velocity is proportional to the hydraulic gradient, it follows that :

$$n\left(v_i^f - v_i\right) = - K_{ij} \frac{\partial\left(\frac{p}{\gamma^f}\right)}{\partial x_j} \qquad (6.2)$$

where

K_{ij} = the components of the permeability matrix

γ^f = the unit weight of the pore fluid

Under the hypothesis of complete saturation, incompressibility of the pore fluid and incompressibility of the solid grains, the continuity equation may be stated as follows:

The rate of change of volume of a cubic element is equal to the rate of change of the fluid volume and may be stated by the equation

$$\frac{\partial v_i}{\partial x_i} = \frac{\partial\left[n\left(v_i^f - v_i\right)\right]}{\partial x_i} = \frac{\partial\left\{-K_{ij}\left[\frac{\partial\left(\frac{p}{\gamma^f}\right)}{\partial x_j}\right]\right\}}{\partial x_i} \qquad (6.3)$$

Special attention must be paid to the way the strain tensor is expressed. In the infinitesimal theory of elasto-plastic deformations, it is possible to define strain in a unique way. This is not true in finite deformation theory, since a variety of coordinate systems may be used to describe the translation, straining and rotation motions and these tend to give rise to different descriptions of the movement.

Consider a body subjected to large displacements as shown in Figure 6.1.

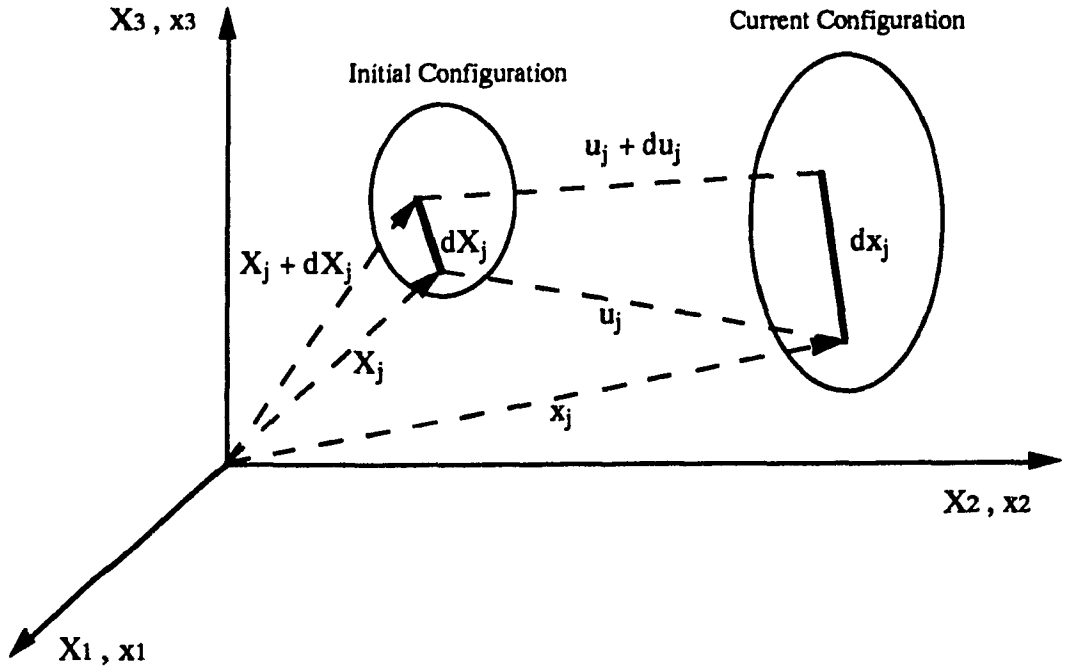

Figure 6.1 - Initial (Undeformed) and Current Configurations of a Body

Two separate approaches, termed Lagrangian and Eulerian, may be used to describe the kinematics of deformation of the body.

When a continuum undergoes deformation (flow), the particles of the continuum move along various paths in space. This motion may be expressed by equations of the form

$$x_j = x_j(X_j , t) \tag{6.4}$$

which give the present location x_j of the particle that occupied the point X_j at time t_0. Also, Equation 6.4 may be interpreted as a mapping of the initial configuration into the current configuration. It is assumed that such a mapping is one-to-one and continuous, with continuous partial derivatives to whatever order is required. The description of motion expressed by Equation 6.4 is known as the Lagrangian Formulation.

If, on the other hand, the motion is given through equations of the form

$$X_j = X_j(x_j , t) \tag{6.5}$$

in which the independent variables are the coordinates x_j and t, the description is known as the Eulerian formulation. This description may be viewed as one which provides a tracing to its original position of the particle that now occupies the location x_j.

Adopting the Eulerian coordinates system, the material strain rates are related to the instantaneous configuration, the deformation mapping is given as

$$x_j = X_j + u_j \tag{6.6}$$

where X_j and x_j are the coordinates of a specified material point of the material skeleton at times t_n and t_{n+1} respectively, and u_j represents the displacement of this solid particle during this time step, measured relative to the position of the body at time t_n.

The instantaneous rate of deformation may be described by the velocity gradient as follows

$$\frac{\partial v_i}{\partial x_j} = \frac{1}{2}\left(\frac{\partial v_i}{\partial x_j} + \frac{\partial v_j}{\partial x_i}\right) + \frac{1}{2}\left(\frac{\partial v_i}{\partial x_j} - \frac{\partial v_j}{\partial x_i}\right) \tag{6.7}$$

where the first and the second terms of the right side of the expression are respectively the symmetric deformation rate tensor ($\dot{\varepsilon}_{ij}$) and the skew symmetric spin tensor, and

$$v_i = \frac{\partial[u_i(x_k,t)]}{\partial t} \tag{6.8}$$

is the velocity of the material skeleton.

When considering finite deformations, it is necessary to employ a frame indifferent stress rate. The Jaumann Stress Rate (Prager, 1961) is chosen and the following expression is obtained

$$\frac{\partial \sigma_{ij}}{\partial t} = D^{ep}_{ijkl}\left[\frac{1}{2}\left(\frac{\partial v_k}{\partial x_l} + \frac{\partial v_l}{\partial x_k}\right)\right] + \sigma_{ip}\left[\frac{1}{2}\left(\frac{\partial v_p}{\partial x_j} - \frac{\partial v_j}{\partial x_p}\right)\right] + \sigma_{jp}\left[\frac{1}{2}\left(\frac{\partial v_p}{\partial x_i} - \frac{\partial v_i}{\partial x_p}\right)\right] + \delta_{ij}\frac{\partial p}{\partial t} \quad (6.9)$$

where D_{ijkl}^{ep} is the special elasto-plastic matrix that relates the effective stress rate tensor to the strain rate tensor derived in Chapter 5.

6.3. Materially and Geometrically Non-Linear Finite Element Formulation

The equilibrium equation relating the total stress (σ_{ij}) and the body forces (F_i) to the boundary condition (T_i) specified on the boundary S of the domain V (Figure 6.2)

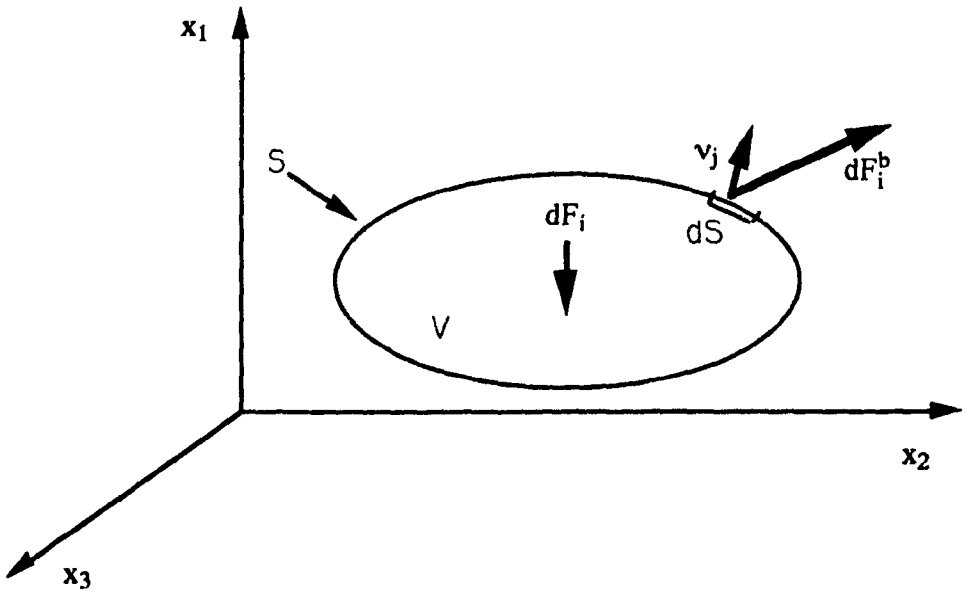

Figure 6.2 - Boundary (S) and Domain(V) of a Body

is formulated using the Gauss Theorem in the following scheme:

If v_j is the normal vector to dS and dF_i^b is a small boundary force in the small surface boundary dS (Figure 6.2) then

$$T_i = \frac{dF_i^b}{dS} \tag{6.10}$$

and

$$T_i = \sigma_{ij}\, \nu_j \tag{6.11}$$

and if dv_i is a fictitious incremental vector of the velocities of the material skeleton, then multiplying these fictitious velocities by the traction Ti and integrating over the whole surface, the following expression may be written

$$\int_s dv_i\, T_i\, dS = \int_s dv_i\, \sigma_{ij}\, \nu_j\, dS \tag{6.12}$$

and using the Gauss theorem, which express

$$\int_s A\, \nu_i\, dS = \int_v \frac{\partial A}{\partial x_i} dV \tag{6.13}$$

where A is a field function, then

$$\int_s dv_i\, \sigma_{ij}\, \nu_j\, dS = \int_v \frac{\partial (dv_i\, \sigma_{ij})}{\partial x_j} dV \tag{6.14}$$

After differentiation of the right hand side of Equation 6.14, this part of the equation becomes

$$\int_s dv_i\, \sigma_{ij}\, \nu_j\, dS = \int_v \left[\frac{\partial (dv_i)}{\partial x_j}\, \sigma_{ij} + \frac{\partial (\sigma_{ij})}{\partial x_j}\, dv_i \right] dV \tag{6.15}$$

substituting Equations 6.1 and 6.7 into Equation 6.15, follows

$$\int_s dv_i\, \sigma_{ij}\, \nu_j\, dS = \int_v \left[d\dot{\varepsilon}_{ij}\, \sigma_{ij} - dv_i\, F_i \right] dV \tag{6.16}$$

or

$$\int_s dv_i \, T_i \, dS = \int_v \left[d\dot{\varepsilon}_{ij} \, \sigma_{ij} - F_i \, dv_i \right] dV \tag{6.17}$$

where

$d\dot{\varepsilon}_{ij}$ is the fictitious deformation rate.

Introducing Equation 6.9 in Equation 6.17 , one obtains

$$\int_S dv_i \, T_i \, dS = \int_V \left[d\dot{\varepsilon}_{ij} \int_{t_n}^{t_{n+1}} \left[D^{ep}_{ijkl} \, \dot{\varepsilon}_{kl} + \sigma_{ip} \left(\frac{1}{2} \left(\frac{\partial v_p}{\partial x_j} - \frac{\partial v_j}{\partial x_p} \right) \right) + \sigma_{jp} \left(\frac{1}{2} \left(\frac{\partial v_p}{\partial x_i} - \frac{\partial v_i}{\partial x_p} \right) \right) + \frac{\partial p}{\partial t} \delta_{ij} \right] dt + d\dot{\varepsilon}_{ij} \, \sigma^0_{ij} - F_i \, dv_i \right] dV \tag{6.18}$$

In connection with the solution of the case history problem, due to the geometry of the case, plane strain conditions apply for the several cross sections to be studied.

Under plane strain conditions, the domain is divided into a finite number of elements, whose geometry is defined by the location of the nodal points. The displacements and pore-pressures are described by their respective values at the element nodes and defined inside each element in terms of the shape functions. Representing the values of the nodal displacements and nodal pore-pressures by u_i^N and p^N respectively and approximating the continuous field in terms of the nodal values , the following formulation is obtained:

$$v_i = N_d \left(\frac{\partial u_i^N}{\partial t} \right) = N_d \left(v_i^N \right) \tag{6.19}$$

and

$$p = N_p \left(p^N \right) \tag{6.20}$$

where Nd and Np are the shape functions for the displacement and pore-pressure fields respectively, and these functions are dependent on the particular type of the element used. In this work the triangle with six nodes (Figure 6.3) is the chosen one.

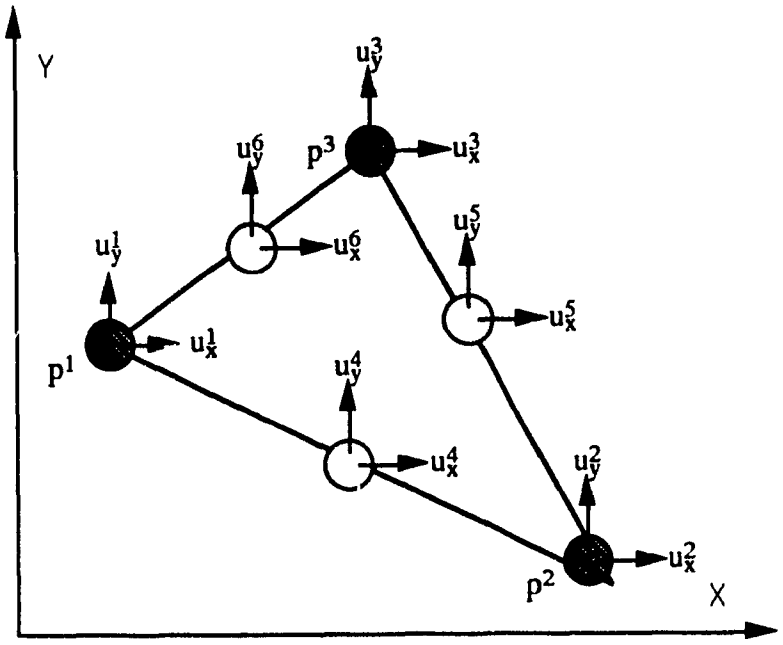

Figure 6.3 - Triangle with Six Nodes for Displacement and Corner Nodes for Pore-Pressure

Then in terms of the nodal quantities, Equation 6.18 can be approximated by

$$d\left(\frac{\partial u_i^N}{\partial t}\right)\{f_i\} = d\left(\frac{\partial u_i^N}{\partial t}\right)\int_V\left[\frac{\partial(N_d)}{\partial x_j}\left[\int_{t_n}^{t_{n+1}}\left(D_{ijkl}^{\varphi}\left[\frac{\partial(N_d)}{\partial x_k}\right]\left[\frac{\partial\left(u_l^N\right)}{\partial t}\right]+[R_{ij}]\right)dt\right]\right]dV + d\left(\frac{\partial u_i^N}{\partial t}\right)\Delta p^N\int_V\left[\delta_{ij}\left(\frac{\partial N_d}{\partial x_j}\right)N_p\right]dV \tag{6.21}$$

where

$$f_i = \int_S [N_d T_i dS] - \int_V\left[\frac{\partial N_d}{\partial x_j}\right]\sigma_{ij}^0\,dV + \int_V N_d\,F_i\,dV \tag{6.22}$$

and

$$R_{ij} = \sigma_{ip}\left\{\frac{1}{2}\left(\frac{\partial\left(N_d\frac{\partial\left(u_p^N\right)}{\partial t}\right)}{\partial x_j} - \frac{\partial\left(N_d\frac{\partial\left(u_j^N\right)}{\partial t}\right)}{\partial x_p}\right)\right\} + \sigma_{jp}\left\{\frac{1}{2}\left(\frac{\partial\left(N_d\frac{\partial\left(u_p^N\right)}{\partial t}\right)}{\partial x_i} - \frac{\partial\left(N_d\frac{\partial\left(u_i^N\right)}{\partial t}\right)}{\partial x_p}\right)\right\} \tag{6.23}$$

where R_{ij} is the part of the equation which deals with the rotation.

For an arbitrary $d\left(\frac{\partial u_i^N}{\partial t}\right)$, Equation 6.21 becomes,

$$\{f_i\} = \int_V \left[\left(\frac{\partial N_d}{\partial x_j}\right)\left[\int_{t_n}^{t_{n+1}}\left(D_{ijkl}^{ep}\left[\frac{\partial(N_d)}{\partial x_k}\right]\left[\frac{\partial\left(u_i^N\right)}{\partial t}\right] + [R_{ij}]\right)dt\right]\right]dV + \Delta(p^N)\int_V\left[\delta_{ij}\left(\frac{\partial N_d}{\partial x_j}\right)N_p\right]dV \tag{6.24}$$

After time integration, the last equation yields

$$\{f_i\} = \Delta\left(u_i^N\right)\int_V\left[\left(\frac{\partial N_d}{\partial x_j}\right)\left(D_{ijkl}^{ep}\left[\frac{\partial(N_d)}{\partial x_k}\right] + [W_{ij}]\right)\right]dV + \Delta(p^N)\int_V\left[\delta_{ij}\left(\frac{\partial N_d}{\partial x_j}\right)N_p\right]dV \tag{6.25}$$

where

$$W_{ij} = \sigma_{ip}\left\{\frac{1}{2}\left(\frac{\partial(N_d)}{\partial x_j} - \frac{\partial(N_d)}{\partial x_p}\right)\right\} + \sigma_{jp}\left\{\frac{1}{2}\left(\frac{\partial(N_d)}{\partial x_i} - \frac{\partial(N_d)}{\partial x_p}\right)\right\} \tag{6.26}$$

The Galerkin Method, which is a special case of the Weighted Residual Method, states that if an approximate solution is substituted into some differential equation, it does not satisfy the equation and an error term results. The integral of the product of the error term and a weighting function (the shape function itself) is required to be zero. (Segerlind, 1984).

Applying this concept for the governing equation expressed by Equation 6.3 and adding the prescribed flow boundary conditions, it follows that

$$\left(\frac{\partial u_i^N}{\partial t}\right)\left\{\int_V\left[\delta_{ij}\left(\frac{\partial N_d}{\partial x_j}\right)N_p\right]dV\right\}-\left\{\int_V \frac{\partial N_p}{\partial x_i}K_{ij}\frac{\partial N_p}{\partial x_j}dV\right\}p^N=-\int_S N_p\, n_i\, K_{ij}\frac{\partial p}{\partial x_j}dS \qquad (6.27)$$

where n_i is a unit vector normal to the boundary surface.

Integrating with respect to the interval t_n to t_{n+1}, Equation 6.27 yields the following approximation:

$$\Delta\left(u_i^N\right)\left\{\int_V\left[\delta_{ij}\left(\frac{\partial N_d}{\partial x_j}\right)N_p\right]dV\right\}-\alpha\,\Delta t\left\{\int_V \frac{\partial N_p}{\partial x_i}K_{ij}\frac{\partial N_p}{\partial x_j}dV\right\}\Delta(p^N)=-\Delta t\int_S N_p\, n_i\, K_{ij}\frac{\partial p}{\partial x_j}dS+\Delta t\left\{\int_V \frac{\partial N_p}{\partial x_i}K_{ij}\frac{\partial N_p}{\partial x_j}dV\right\}\left(p^N_{(t_r}\right.$$

(6.28)

where

$$\int_{t_n}^{t_{n+1}}\left\{\int_V \frac{\partial N_p}{\partial x_i}K_{ij}\frac{\partial N_p}{\partial x_j}dV\right\}(p^N)\,dt\sim\left\{\int_V \frac{\partial N_p}{\partial x_i}K_{ij}\frac{\partial N_p}{\partial x_j}dV\right\}\Delta t\left[\alpha\, p^N_{t_{n+1}}+(1-\alpha)p^N_{t_n}\right] \qquad (6.29)$$

and $p_{tn}{}^N$ is the nodal pore-pressure at the beginning of the time step.

To ensure stability of the step by step process it is necessary to choose $\alpha \geq 0.5$ (Booker and Small, 1975). In this work the chosen value is $\alpha = 0.5$, following the recommendation of Zienkiewicz (1977).

It is important to mention that all the values are average values in the time step and the numerical solution is made iteratively step by step.

6.4. Numerical Implementation of the Incremental Material and Geometrical Non-Linear Finite Element Formulation

The Eulerian formulation may be used in practical problems by dividing the loading into a large number of equilibrium states of the body.

The analysis for obtaining the increments of displacements and pore pressure at time t_{n+1} starting from the initial time state t_n may be developed as follows:

1 - Solution of the system of equations formed by Equations 6.25 and 6.28 gives as results the incremental nodal displacements and nodal pore-pressure. At the first approximation all the basic values (stresses, shape functions) are obtained at the beginning of the time step, in the other iterations average values of these values are used, based in the moving mesh during the time increment. It is important to mention that the original Newton-Raphson Method (Figure 6.4) is used to deal with the nonlinearity, changing the stiffness matrices corresponding to change of geometry and material properties within each iteration;

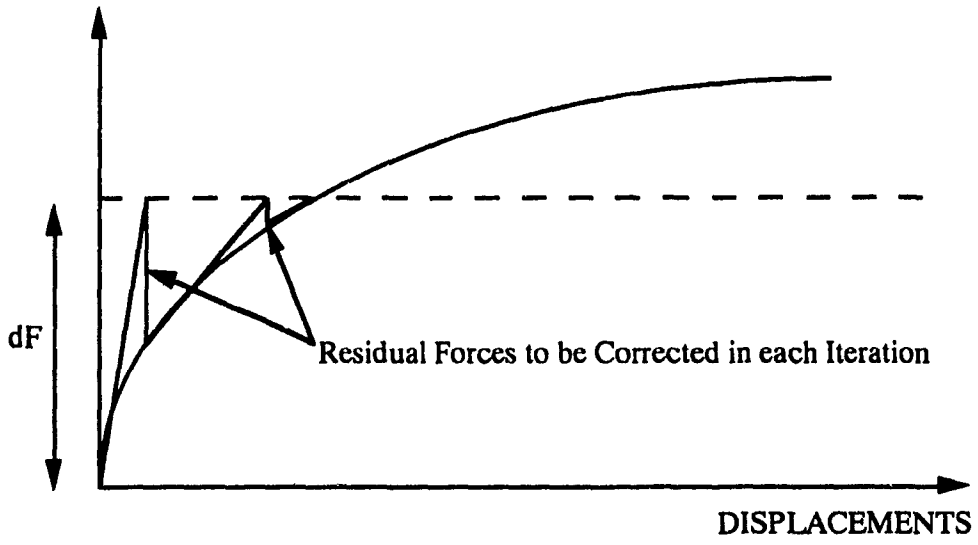

Figure 6.4 - Original Newton-Raphson Method

2 - Transform the Kirchoff stress (S_{ij}) at time t_{n+1} to Cauchy stresses (σ_{ij}) by using the relation

$$\sigma'_{ij} = \det\left|\frac{\partial X_l}{\partial x_m}\right|\left[\frac{\partial x_i}{\partial X_\alpha}\frac{\partial x_j}{\partial X_\beta}\right] S_{\alpha\beta} \qquad (6.30)$$

where Kirchoff stresses are the stresses based on the original mesh configuration at time t_n and the Cauchy stresses are based on the new mesh configuration. These assignments are needed once that the constitutive law is expressed in terms of stresses based on the current state of the sample;

3 - Go back to step 1 and repeat the the calculations so that average stress history is obtained in evaluating the constitutive tensor D_{ijkl}^{ep};

4 - Check that the consistency condition is satisfied with the new Cauchy stresses and correct it, if necessary;

5 - Update coordinates and stresses;

6 - Proceed to the next increment.

It is important to comment that the program incorporates an equilibrium check to ensure that equilibrium is satisfied at the end of each increment. This check is essential in any analysis using interactive methods. After reaching the convergence tolerance the residual forces are added to the load increment of the next time step.

A Finite Deformation Finite Element Code named CONFDEF was developed incorporating all the procedures developed in this chapter.

A brief review of the basic relations among the several stress tensors which might be used in analysis regarding finite deformation are presented in Appendix A.

CHAPTER 7

DISCUSSION OF THE FINITE ELEMENT CODE INCORPORATING MATERIAL AND GEOMETRICAL NON-LINEARITIES

7.1. Generalities

The analytical tool developed in Chapter 6 to deal with material behavior and geometrically non-linear routine of the problem must be checked before its application to simulate the problem under study, i.e. consolidation of tailings. Some special features, such as a subroutine that was developed to deal with layer construction and the dependence of the permeability coefficient on the void ratio are worth of examination in some detail.

A number of tests were run using the program CONFDEF, which uses the theory developed in Chapter 6. The results of the numerical solutions were compared with those from known exact solutions of unidimensional and bidimensional consolidation problems. Layer construction, as well as the implementation of the constitutive model developed in Chapter 5 were also tested. As a final test to give reliability to the developed program, a flexible shallow foundation loading was analytically tested. The two soil types [loose (e=0.87) and dense (e=0.58) cohesionless material] beneath the foundation were assumed to deform under undrained, partially drained and drained conditions. These conditions correspond, respectively, to rapid, relatively rapid and slow application of the surface load. The stress paths followed by both materials and the importance of the time of loading in final footing settlements are discussed.

7.2. One-Dimensional Finite and Infinitesimal Consolidation Analysis

Using the Linear Elastic Constitutive Relation, a comparison was made between the exact solution obtained by Terzaghi (Lambe and Whitman, 1979) for the one-

dimensional consolidation of a soil layer and the solution obtained using the program CONFDEF.

The finite element mesh used is presented in Figure 7.1

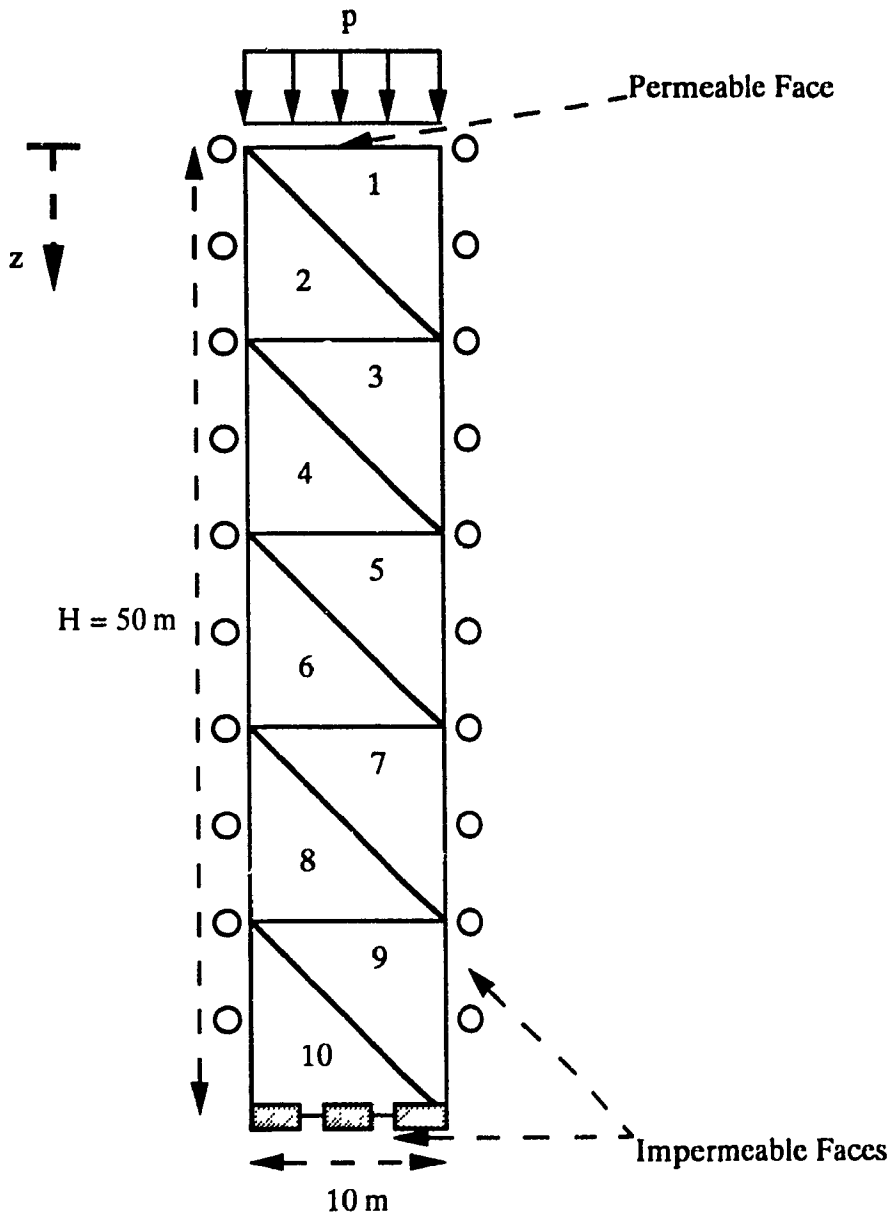

Figure 7.1 - Finite Element Mesh for One-Dimensional Consolidation Tests

The assumed high ratio for E/p (≥1000.0) made the geometrical non-linearity, in this particular case, negligible. Thus the above comparison was rational.

Two other one-dimensional tests were run, both with low values of Young's Modulus/Pressure ratio (E/p) = 1.0. In one of the tests the permeability coefficient was kept the same all the time and in the second an exponential function was used to relate the permeability coefficient as a function of the void ratio. This provided a check not only of the importance of the geometrical non-linearity, but also of the influence of the variation of the permeability due to changes in the void ratio, as experimentally demonstrated by Schiffman et al (1984).

Comparison between pore-pressure dissipation due to an instantaneous loading obtained by Terzaghi's exact solution and the numerical solution obtained with the approximate infinitesimal theory using a ratio E/p = 10000 are shown in Figure 7.2. The agreement is satisfactory.

The soil parameters used in this test are:

Young's Modulus = E = 20,000.0 kN/m^2

Poisson's Ratio = ν = 0.0

Permeability Coefficient = k = 0.00000015 m/s

Unit Weight of Water = γ^w = 10.0 kN/m^3

Total Unit Weight = γ^t = 20.0 kN/m^3

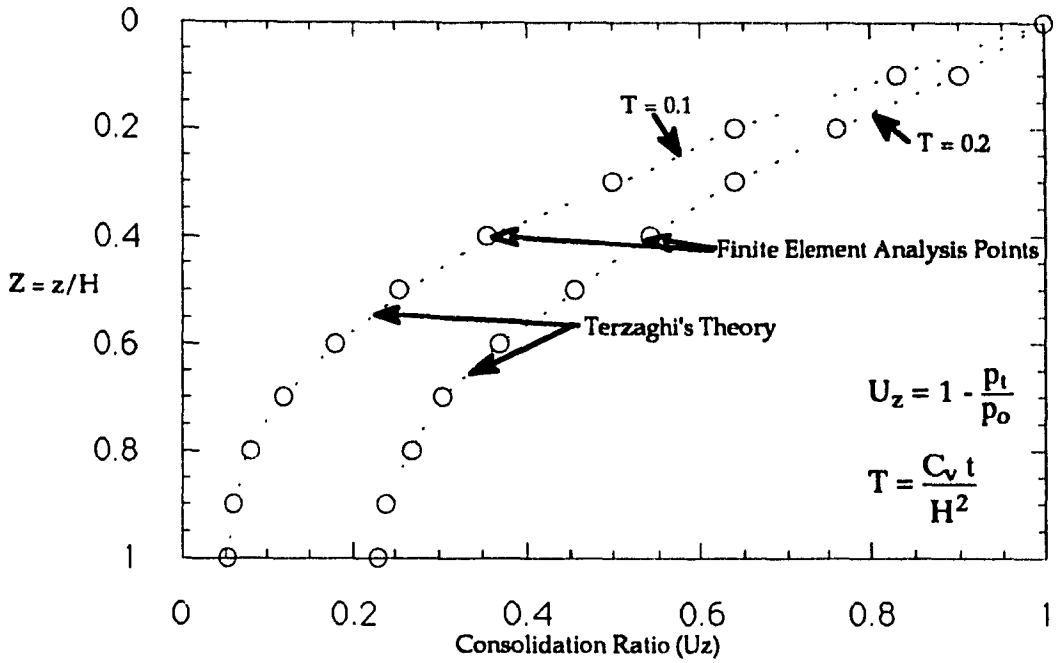

Figure 7.2 - Comparison of Terzaghi's Exact Solution and Numerical Solution

where p_o and p_t are respectively the pore pressure at the moment of instantaneous load application and at time t, after dissipation has started.

To better understand the influence of geometrical non-linearity, exact one-dimensional displacements and pore-pressure dissipation solutions of Terzaghi's Infinitesimal Strain Theory using E/p = 1.0 are compared to the solution of the same problem, with the same parameters, but under the assumption of finite deformation, considering in one case a constant permeability coefficient and also its variation with the void ratio through the relation

$$k(m/s) = Exp[-26.54 + 2.99\, e] \qquad (7.1)$$

In Figures 7.3 and 7.4 the comparisons are shown and it can be seen that the differences are substantial, proving the importance of incorporating the influence of finite deformation and the variation of permeability in highly deformable material.

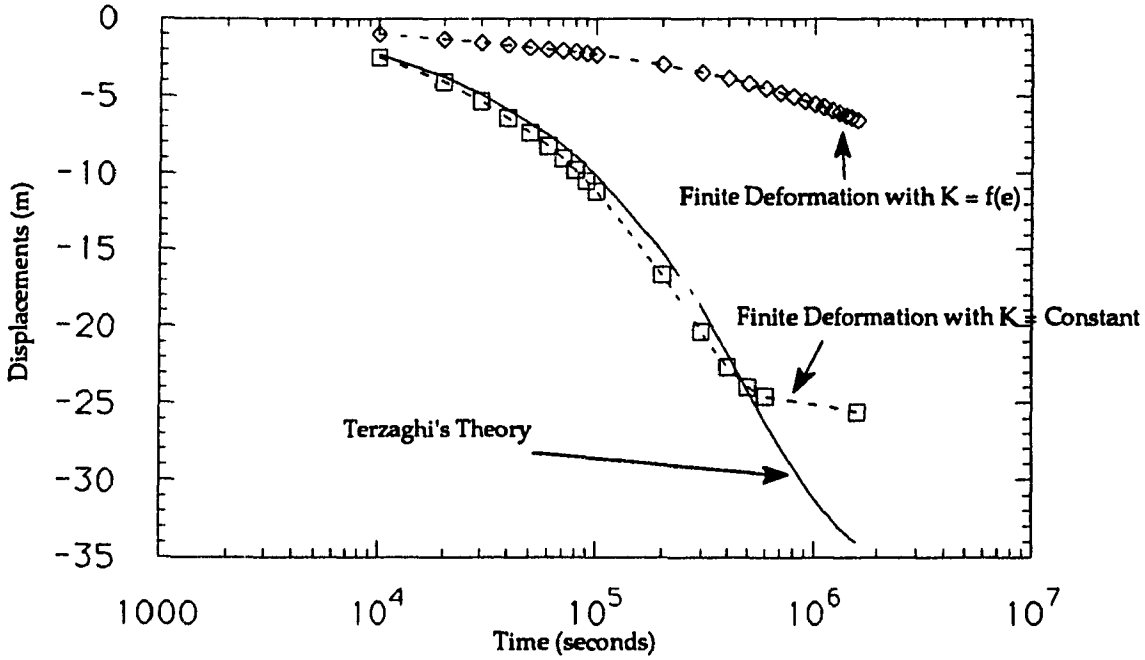

Figure 7.3 - Displacements Comparisons

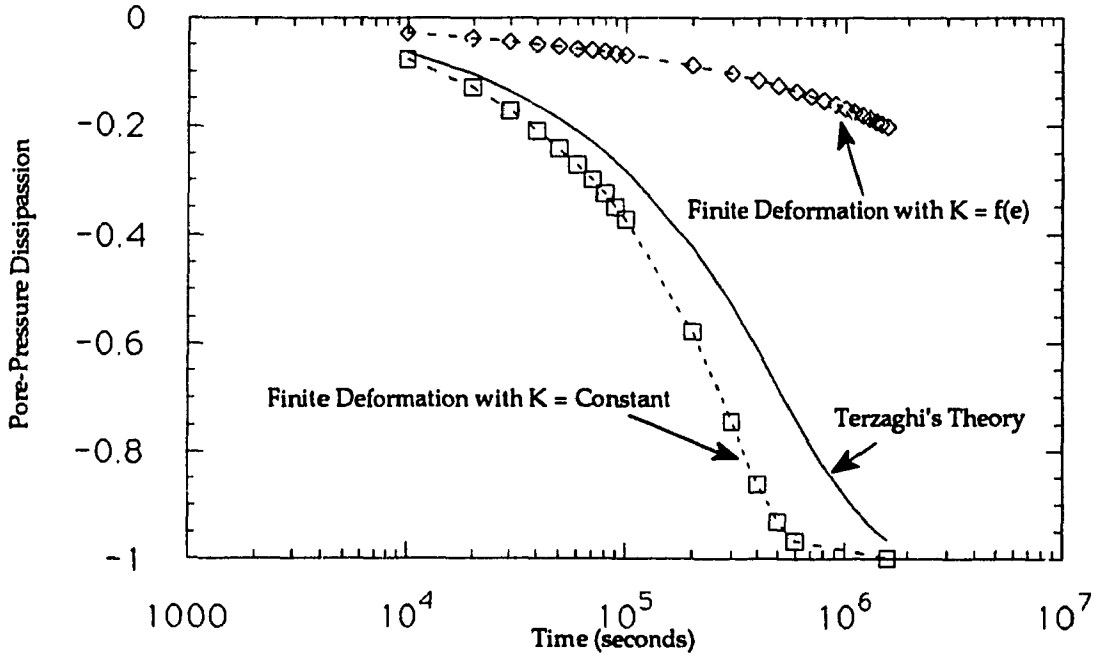

Figure 7.4 - Pore-Pressure Comparisons

7.3. Bi-Dimensional Half-Plane Loading (Mandel-Cryer Effect) Analysis

To be able to test the efficiency of the program CONFDEF in relation to bidimensional consolidation, the development of pore-pressure in the soil just beneath a distributed load in a half plane is studied.

Any realistic three-dimensional theory of consolidation couples the equilibrium of total stresses and the continuity of soil mass. Schiffman et al., (1969) have studied some special characteristics of the coupled consolidation equations, which manifest the variation of total stresses with time, resulting in an excess of pore pressure before it starts to dissipate. Such an increase in pore pressure during the early stages of consolidation (Mandel-Cryer Effect) has been noted in experiments and in theoretical solutions for several multidimensional problems. Such increases in pore pressure cannot be predicted by any solution that ignores the change in total stress.

In Figure 7.5 the mesh used to analyze numerically the same problem as that analytically studied by Schiffman et al., (1969) is presented.

In Figure 7.6 the result of the excess pore-pressure ratio (ratio between excess of pore-pressure at time t and the excess of pore pressure after instantaneous loading) versus time, at 0.5 meter below the center of the loaded area, obtained by Schiffman et al., (1969), is shown. Also shown in the same figure is the numerical solution obtained in this work. The same conditions (plane strain problem) and parameters (elastic behavior) as those used by Schiffman et al (1969) were employed in the present analysis.

Comparison of the two sets of results indicates the efficiency and accuracy of the numerical method developed here.

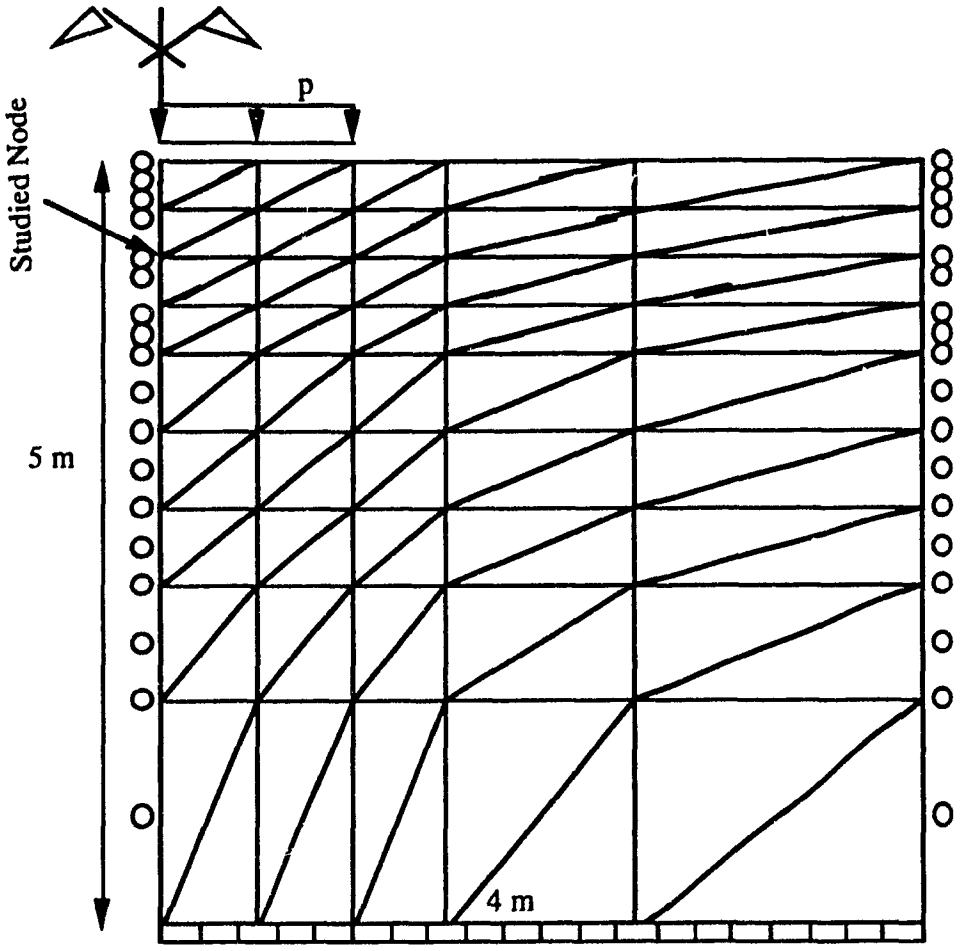

Figure 7.5 - Bi-Dimensional Consolidation Mesh

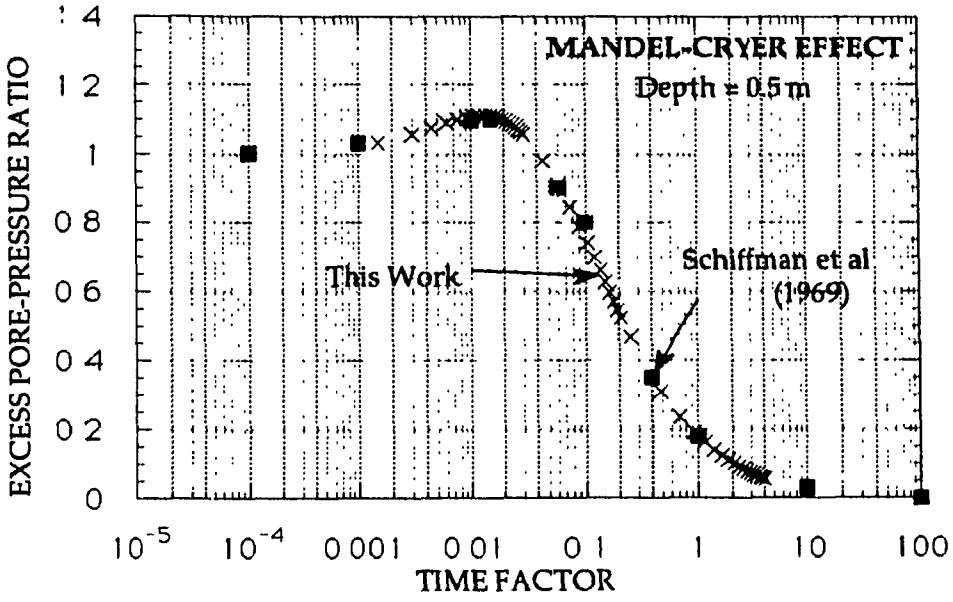

Figure 7.6 - Comparison Between Excess Pore-Pressure Obtained in this Work and Results of Schiffman et al., (1969) Under the Same Conditions

7.4. Construction Analysis

A special subroutine was developed and implemented in the program to deal with elements built in layers with time.

Following the principle established by King (1965), the finite element mesh is arranged so that the mobilization occurs in layers, as it does in the field. The layer being built is assumed to be placed in a liquid state where the material has weight but is incapable of carrying shear stresses. It is then possible to model the transition between the sedimentation and consolidation phases given that the layer is assumed to stiffen upon completion. The loading proceeds with the placement of the next layer.

Initially a complete undeformed mesh with a defined initial configuration is introduced as data in the Finite Deformation Finite Element Program, characterizing the initial conditions of existing portions of soil, as well as layers which would be raised in the future, but at that moment were inactive. Special attention was given to the movement of the the elements which were still inactive at certain point of time. In dealing with finite deformation, these elements must translate due to the displacements occurring in the already active elements, as the updating of the nodes was carried out. To deal with this problem, the mesh must be built in such a way that all the inactive elements have their corner nodal points located in vertical lines with the same X-coordinates as the top nodes of the top active layer. The nodal points of the inactive elements have a rigid body movement of the same magnitude as the displacements occurring in the top nodes of the top active layer.

To demonstrate the correct implementation of this subroutine, the mesh shown in Figure 7.1 were rebuilt in five steps. The vertical total stresses obtained were equal to the geostatic stresses (total unit weight of the soil multiplied by the depth), demonstrating the correct implementation of the theory.

7.5. Checking of the Constitutive Model Implemented in the CONFDEF Program

To test the correct implementation of the constitutive relation developed in Chapter 5 in the program CONFDEF, a plane strain test was run numerically, using the same parameters as the ones obtained in Section 5.4. The strains obtained in the plane strain test were then used as entrance data for the program CONINV and stresses were obtained. With these stresses as input data for program CONDIR, strains were obtained. The results of the three runs, in terms of stress-strain relation are compared in Figure 7.7. As may be noted, they are almost identical. This builds a further level of confidence in the applicability and the accuracy of the program CONFDEF.

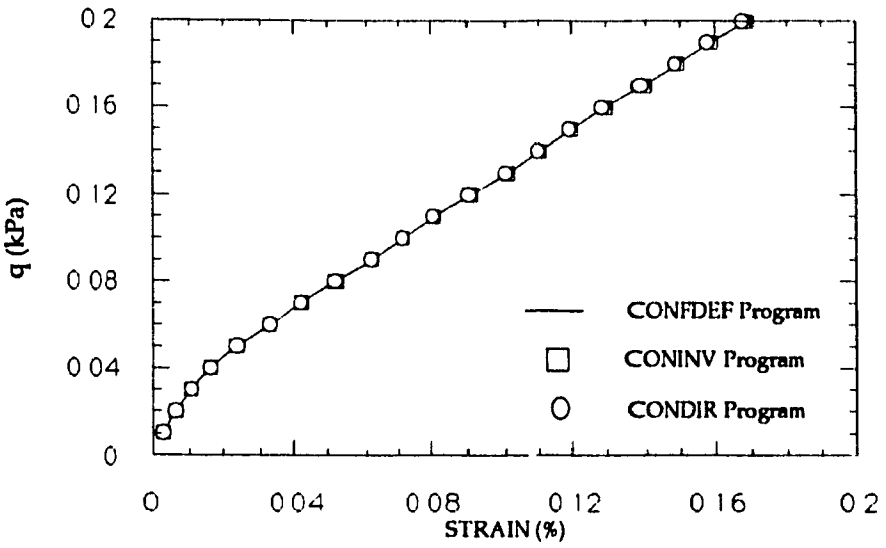

Figure 7.7 - Checking of Correct Implementation of Model in program CONFDEF

7.6. Influence of Time Loading and Drainage Conditions in a Shallow Foundation Analysis

As a final test, the mode of settlement of a surface footing supported by a layer of loose sand (e = 0.87) was examined. In particular the effect of the rate of the loading of the footing and its performance are examined. The same test was performed on a denser material (e = 0.58).

The finite element mesh used in both cases (Void Ratios = 0.58 and 0.87) is shown in Figure 7.8.

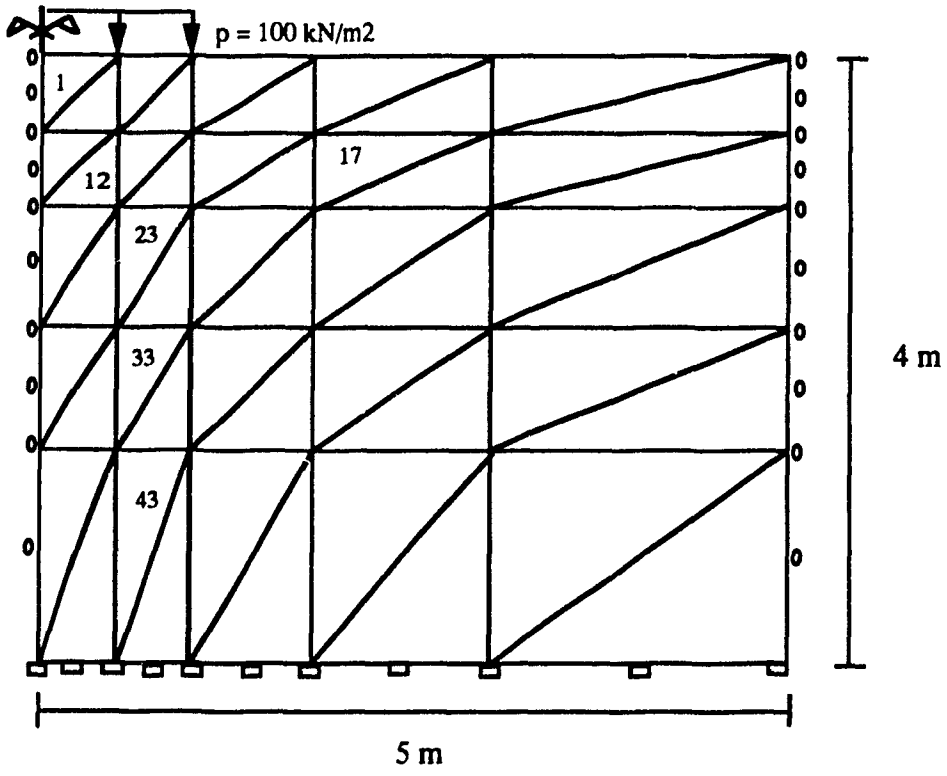

Figure 7.8 - Finite Element Mesh for Strip Loading Test

The material parameters used in this study are the same as those calibrated previously in Section 5.4. The other material properties are:

$\gamma^t = 20\ kN/m^3$

$\gamma^f = 10\ kN/m^3$

$k = 0.00000015\ m/s$

and

$K_o = 0.65$

The rate of loading was zero for Drained solution and infinite for Undrained solution. For the Partly Drained case the rate of loading was 0.002 kN/m2/s.

Figure 7.9 presents the surface displacement versus duration of loading for the loose deposit. As may be seen the final settlement is somewhat sensitive to the rate of loading of the footing.

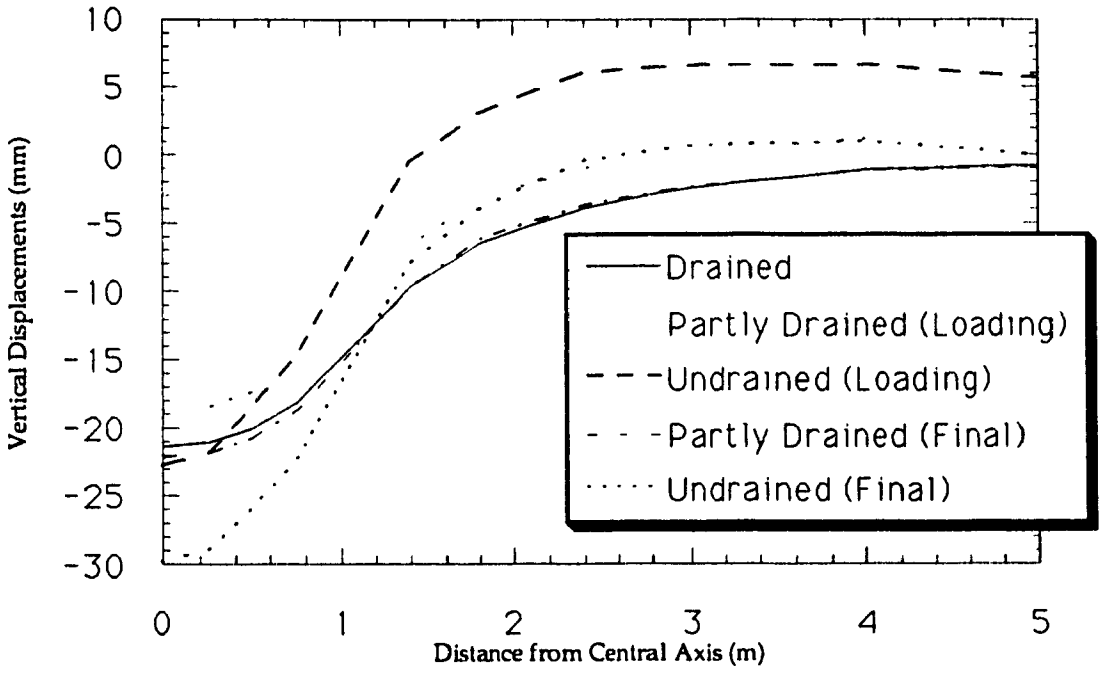

Figure 7.9 - Surface Displacements for Void Ratio=0.87

In Figure 7.10, which presents the surface displacement versus duration of loading for the dense material, almost no differences are found in the final displacements.

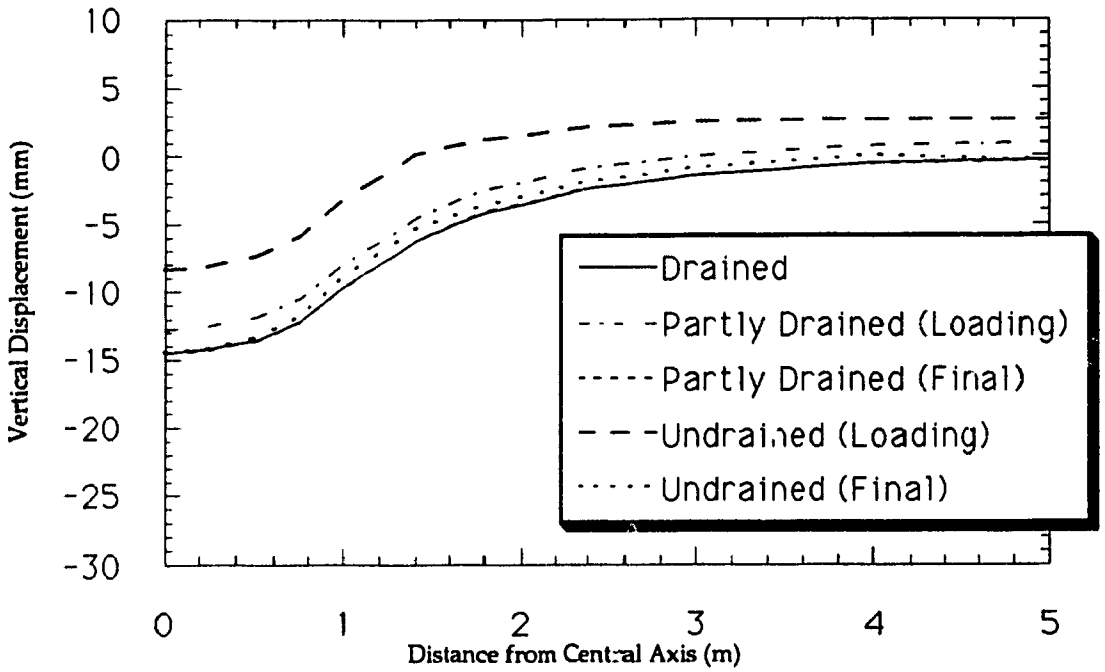

Figure 7.10 - Surface Displacements for Void Ratio=0.58

From Figures 7.9 and 7.10 it can be concluded that the final superficial settlement of a strip foundation supported by a cohesionless granular medium is dependent on the loading rate for loose material and independent for dense material. However even in the case of loose material the discrepancy among the final displacements is not large. This is of great practical significance as it clearly demonstrates the relative lack of importance of the loading history of the foundation; a view held generally in the past, but without any proof.

Certain stress paths followed by specific elements are shown in Figures 7.11 and 7.12, respectively for undrained behavior of loose and dense material, starting in both cases from Ko-Line.

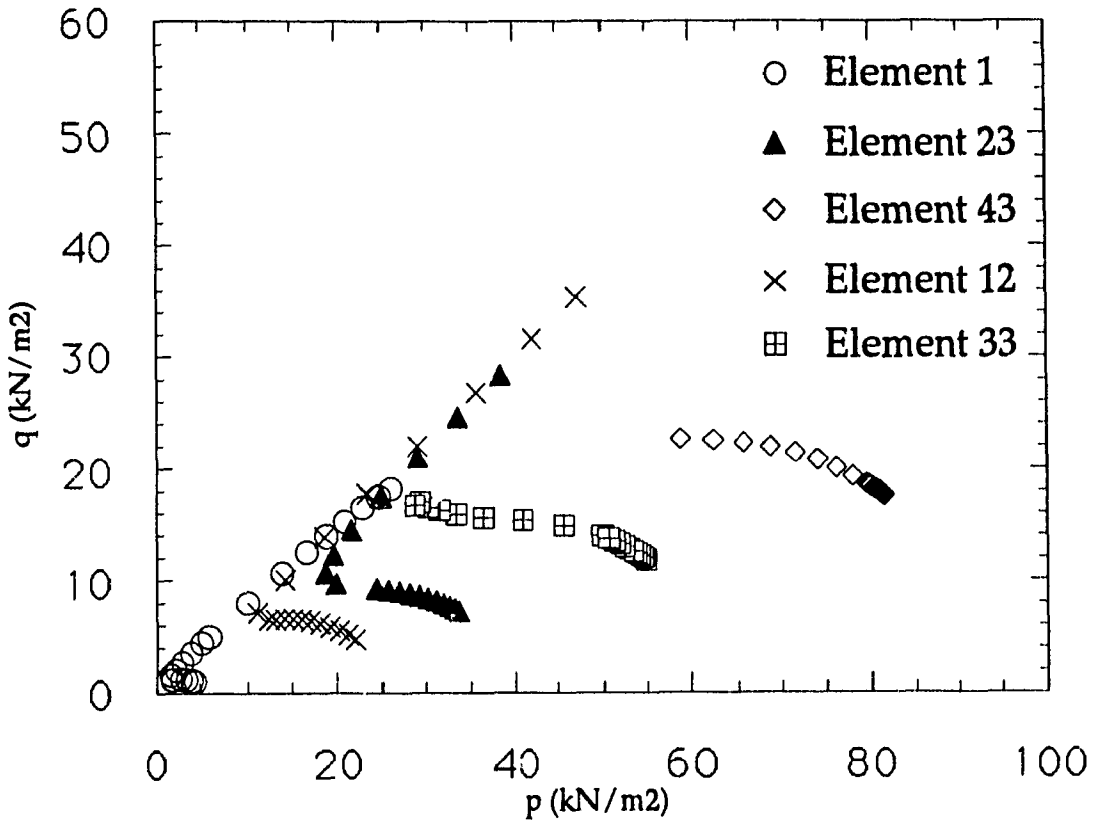

Figure 7.11 - Stress Paths for Undrained Behavior of Loose Material at Several Depths

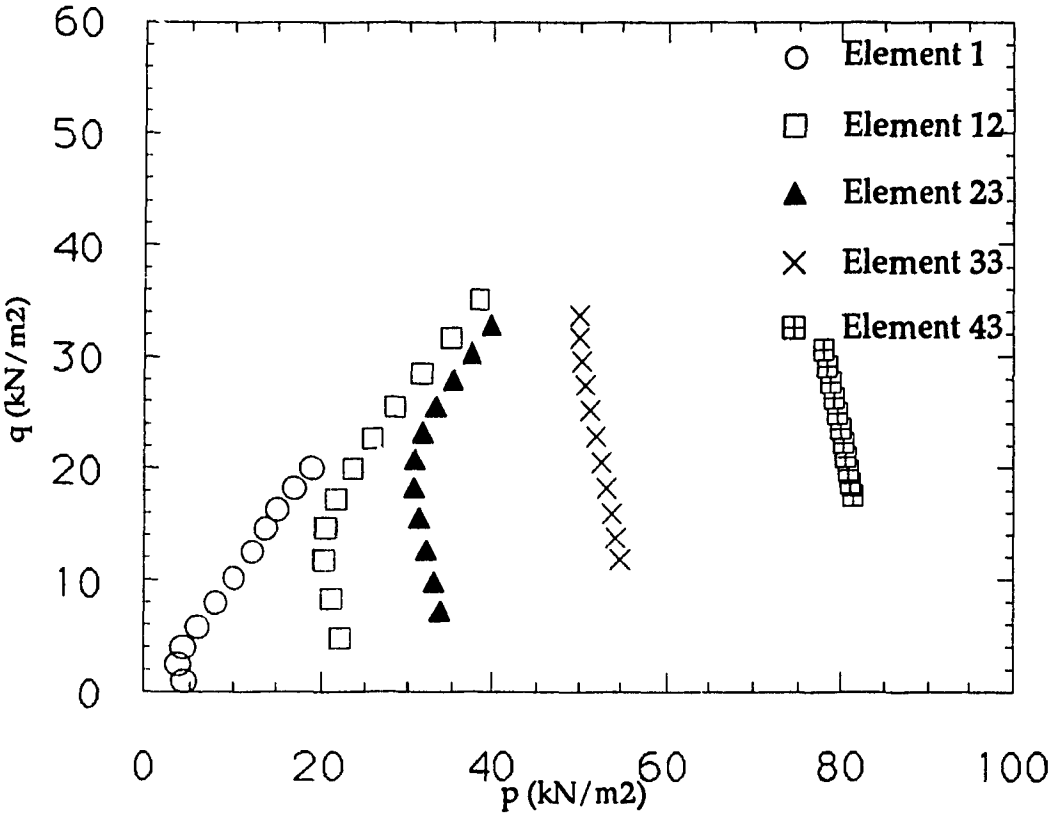

Figure 7.12 - Stress Paths for Undrained Behavior of Dense Material at Several Depths

From these figures, it can be concluded that, as expected, loose material generates higher positive pore pressure than dense material.

Finally, Figures 7.13, 7.14, 7.15, 7.16, 7.17 and 7.18 shown comparison of stress paths for drained, partly drained and undrained behavior for respectively loose and dense cohesionless material, corresponding to rapid, relatively rapid and slow loading of the footing. The elements represented here are located at several depths, directly below the loading area, as well as laterally to the loaded area.

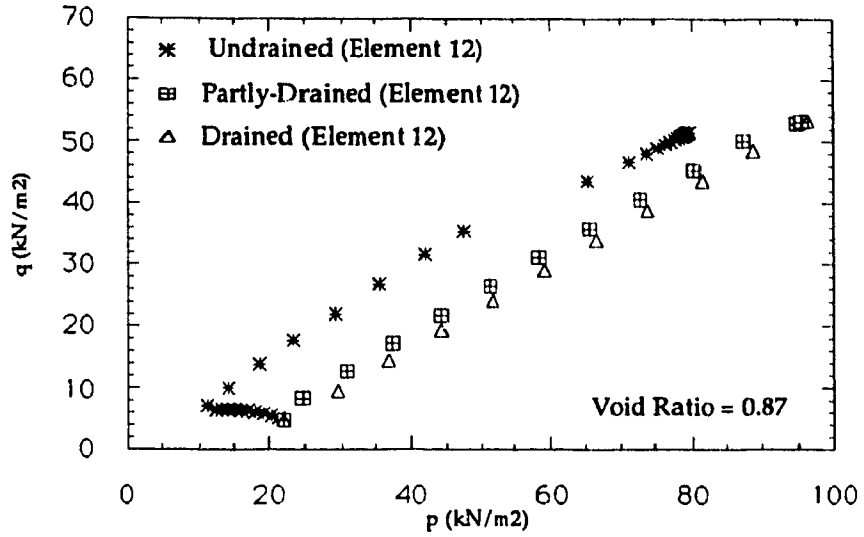

Figure 7.13 - Influence of Rate of Loading of the Footing on the Stress Paths (Element 12) for Slow (Drained), Relatively Fast (Partly Drained) and Fast (Undrained) Loading of Loose (e = 0.87) Material

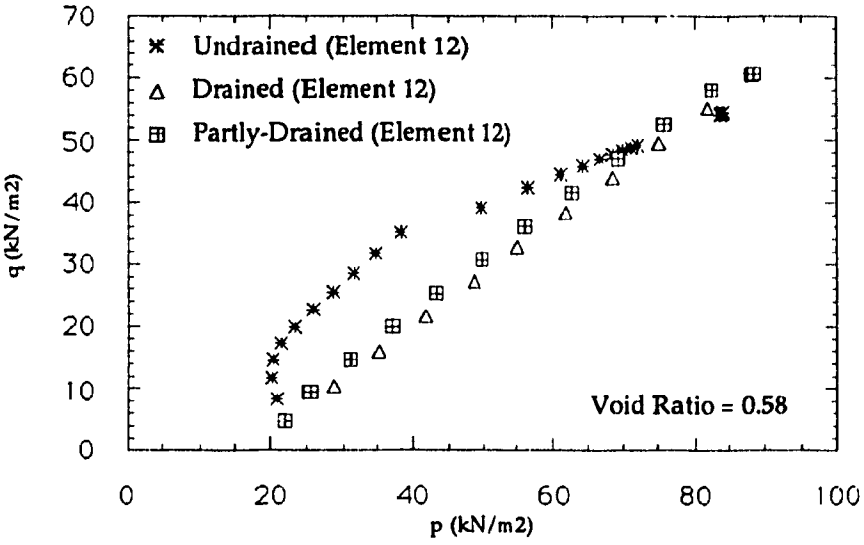

Figure 7.14 - Influence of Rate of Loading of the Footing on the Stress Paths (Element 12) for Slow (Drained), Relatively Fast (Partly Drained) and Fast (Undrained) Loading of Dense (e = 0.58) Material

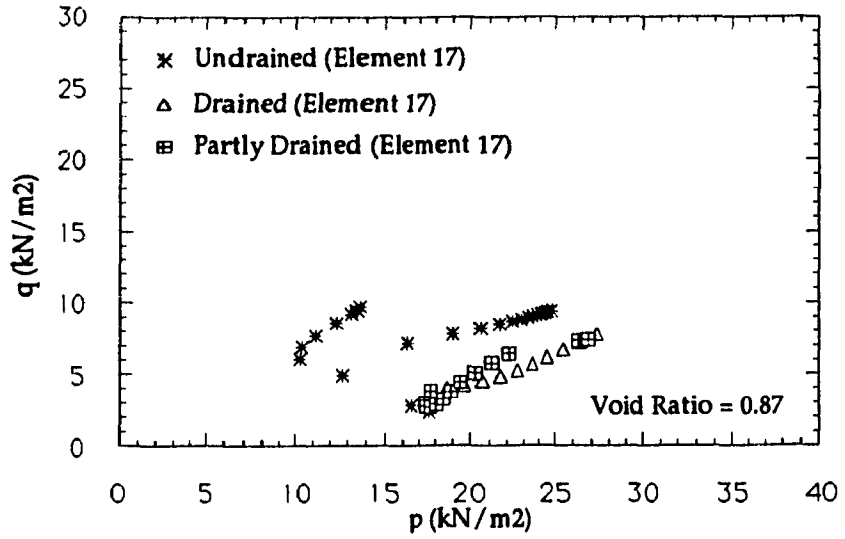

Figure 7.15 - Influence of Rate of Loading of the Footing on the Stress Paths (Element 17) for Slow (Drained), Relatively Fast (Partly Drained) and Fast (Undrained) Loading of Loose (e = 0.87) Material

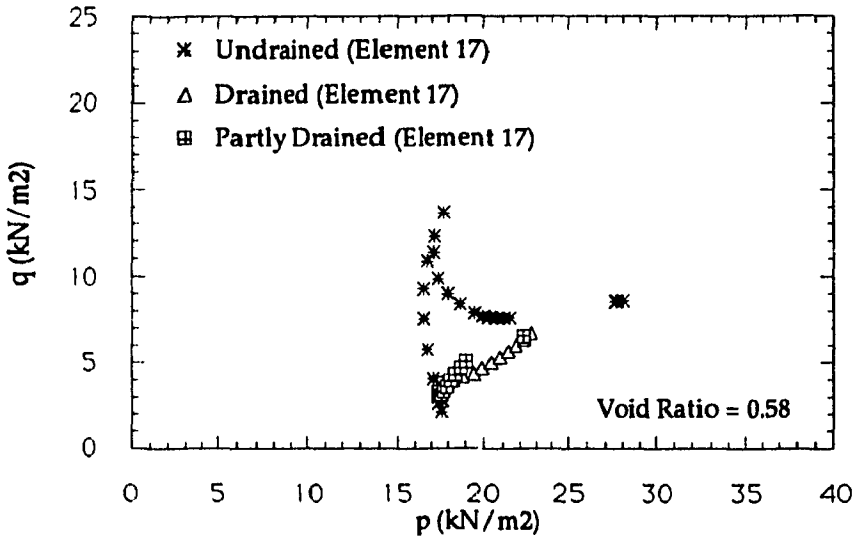

Figure 7.16 - Influence of Rate of Loading of the Footing on the Stress Paths (Element 17) for Slow (Drained), Relatively Fast (Partly Drained) and Fast (Undrained) Loading of Dense (e = 0.58) Material

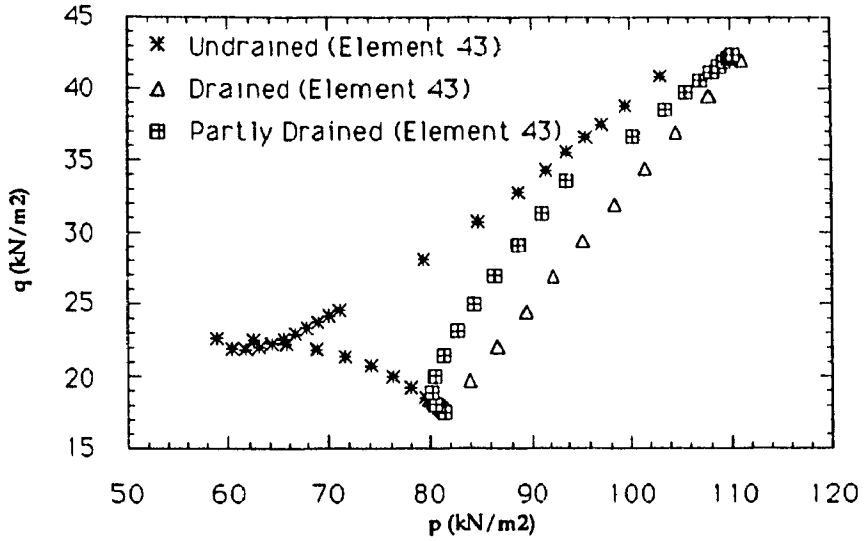

Figure 7.17 - Influence of Rate of Loading of the Footing on the Stress Paths (Element 43) for Slow (Drained), Relatively Fast (Partly Drained) and Fast (Undrained) Loading of Loose (e = 0.87) Material

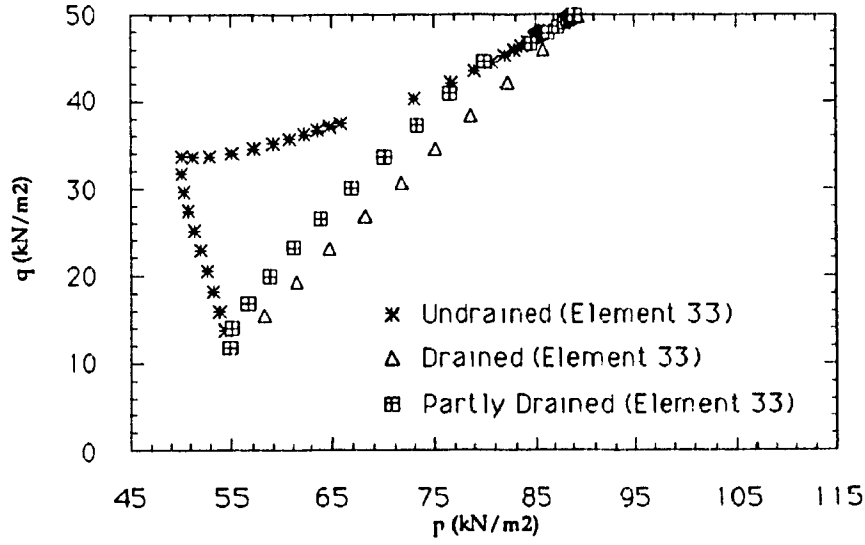

Figure 7.18 - Influence of Rate of Loading of the Footing on the Stress Paths (Element 33) for Slow (Drained), Relatively Fast (Partly Drained) and Fast (Undrained) Loading of Dense (e = 0.58) Material

Due to the fact that during undrained loading the stress path of some elements meet the State Boundary Surface and coincide with it for some distance, there is a discrepancy between the end points of the undrained stress paths, after consolidation, and drained and partly drained stress paths, whose final position is practically the same. These differences are more pronounced near the surface loading and decrease with depth, being more accentuated in loose material.

The differences occur because it is not possible for stress paths to be located outside the State Boundary Surface. This restricts them to a certain region forcing then redistribution of stresses to other elements near the ones affected.

The importance of these findings is that even though there is a difference in the final stress path position, which is a function of the rate of loading of the footing, this discrepancy is not so important to be considered in practical applications.

In Appendix B, the contours of the ratio $\{q/[p\ g(\theta)]\}$, which expresses the proximity of a state of stress of reaching the State Boundary Surface, are presented for Fast (Undrained), Relatively Fast (Partly Drained) and Slow (Drained) rate of loading.

CHAPTER 8

COMPARISON BETWEEN FIELD DATA AND NUMERICAL ANALYSIS FOR THE SARAMENHA CASE HISTORY

8.1. Introduction

The complete soil formation process (transportation of sediments, sedimentation, and consolidation) is numerically studied for the Saramenha Case History. The site condition is described in Chapter 3. Comparisons between the analytical solutions obtained by the coupled use of the developed programs CONSED and CONFDEF, and the field data, as reported by Villar (1990), are presented. Finally, the results are discussed in detail.

8.2. Comparisons Between Field Data and Numerical Results

To verify and give credibility to the developed theory, the Saramenha Case History is studied.

8.2.1. Geometry of the Problem and the Necessary Parameters for Its Solution

The study of the Saramenha Case History will be restricted to the Second Disposal Point, for a 10 year period, from the beginning of 1979 until August of 1988. It was during this period that most of the field data was obtained. An average of 175000 tons of solid waste was disposed yearly, with an average concentration of C = 0.00056. The geometry of the region was described in Chapter 3, with all the necessary technical data.

For convenience certain data are repeated below:

The Average Unit Weight of the Solids $\gamma^s = 30$ kN/m^3

The Total Unit Weight is 13.4 kN/m^3

The Submerged Unit Weight is 3.4 kN/m^3

The coefficient of lateral stress at rest adopted is $K_o = 0.5$.

The average fall velocity of the sediments in the sediment-water mixture being transported is 0.00009 m/s, as reported by Abreu (1989).

The relation between the permeability coefficient and the void ratio is given by Equation 3.1 in Section 3.3.

The parameters of the constitutive relation developed in Chapter 5 and implemented in the Finite Deformation Theory developed in Chapter 6 are obtained through the trial and error process of getting numerically (using the same mesh presented in Figure 7.1) the best possible approximation for the special *laboratory* tests run in the bauxite tailings material, reported by Azevedo (1990) and detailed in Appendix F.

In Figure 8.1 the comparison between laboratory data of the unidimensional consolidation test with constant rate of deformation (Appendix F) and the numerical simulation of the same test are shown for the best fitted approximation. The constitutive relation parameters for this simulation are:

$E_0 = 10$ kN/m2	$A = 1.0$	$\nu = 0.3$	$\mu = 0.75$
$\delta = 0.1$	$e_0 = 1.3$	$L = 0.088$	$R = 0.68$
$S = 0.08$	$T = 0.45$	$W = 1.33$	$\xi = 2.0$

Table 8.1 - Parameters of the Constitutive Relation for Saramenha's Case

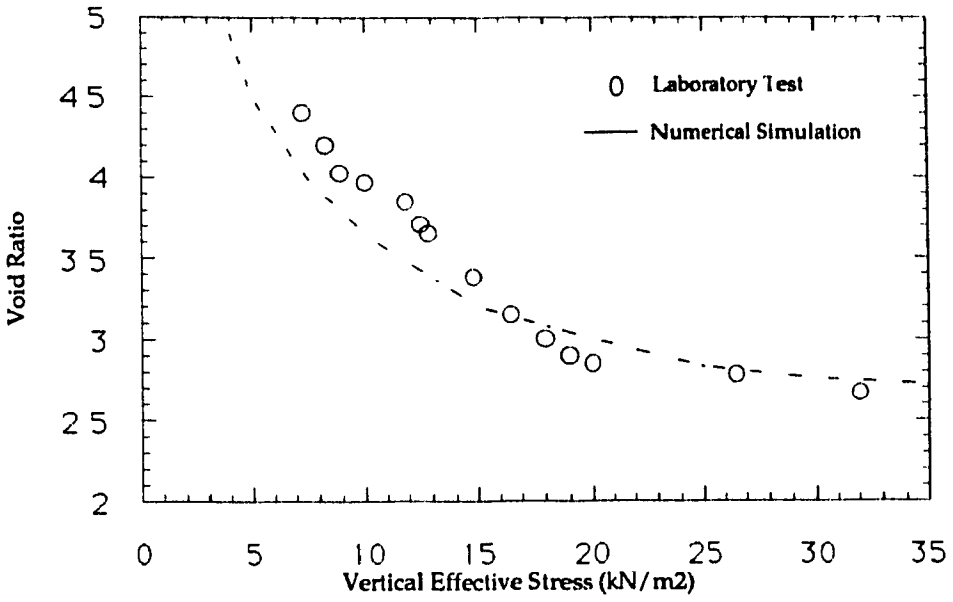

Figure 8.1 - Comparison between Laboratory Data of the Unidimensional Consolidation Test with Constant Rate of Deformation and its Numerical Simulation

To begin the analysis, the reservoir, starting at the second disposal point, is divided in seven sections, with intervals (Δx) of 80 meters between the sections, as shown in Figure 8.2.

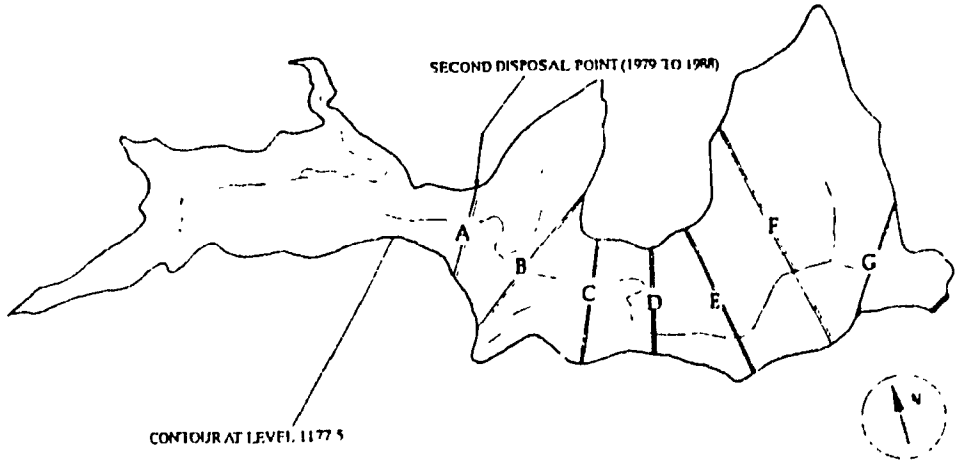

Figure 8.2 - Positions of Cross Sections Analyzed in the Reservoir

A Topographical Plan View of the Reservoir in its 1979 condition is presented in Figure 8.3.

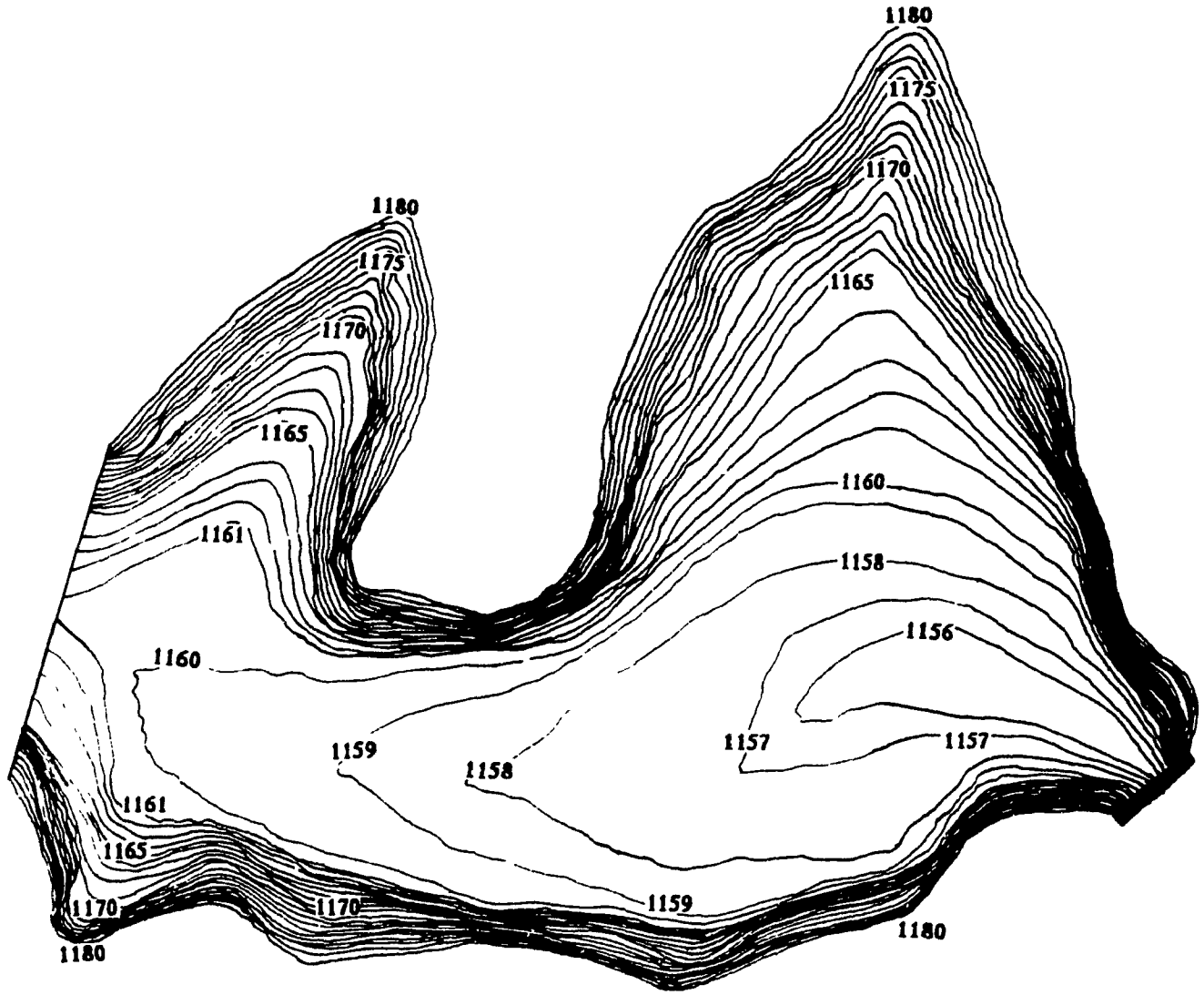

Figure 8.3 - Topographical Plan View of the Reservoir in 1979

The seven cross-sections being studied, with the original profile (1974) and the sedimented profile existing at the beginning of 1979, are presented in Figures 8.4 to 8.10.

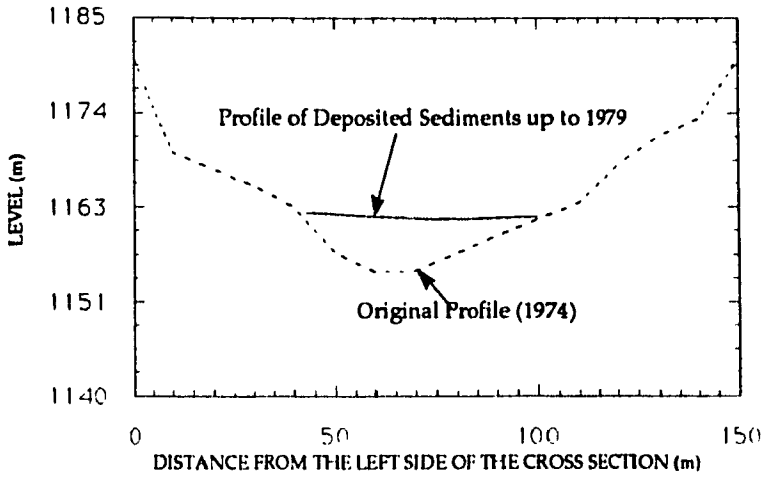

Figure 8.4 - Cross Section A (Disposal Point)

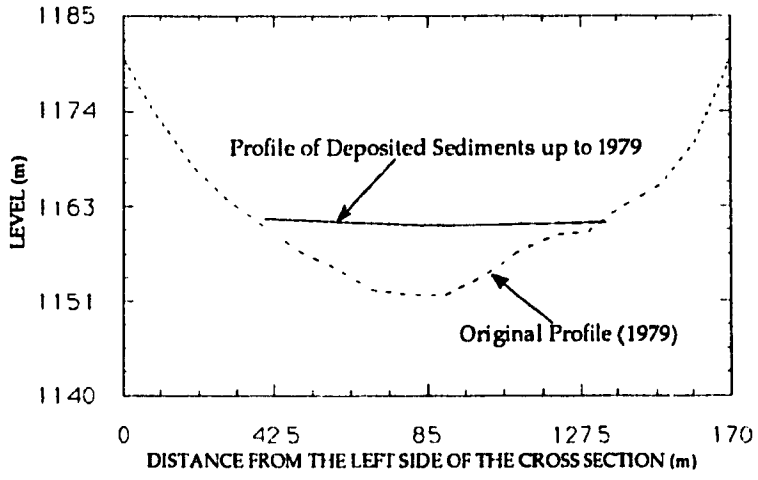

Figure 8.5 - Cross Section B

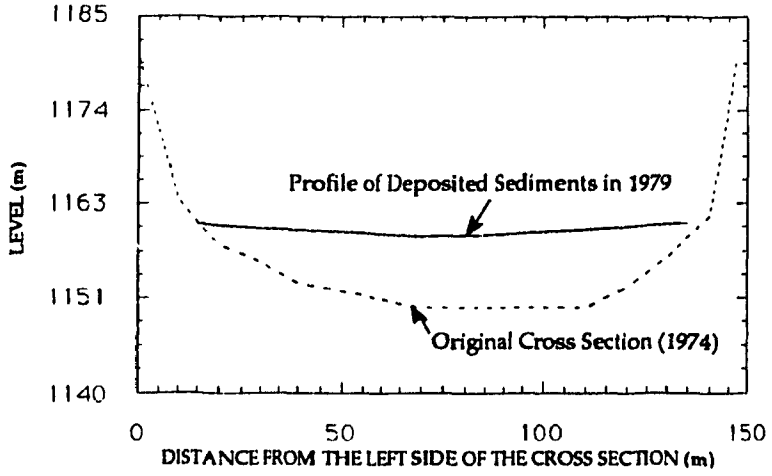

Figure 8.6 - Cross Section C (Equal to Cross Section 1 where Measurements were made)

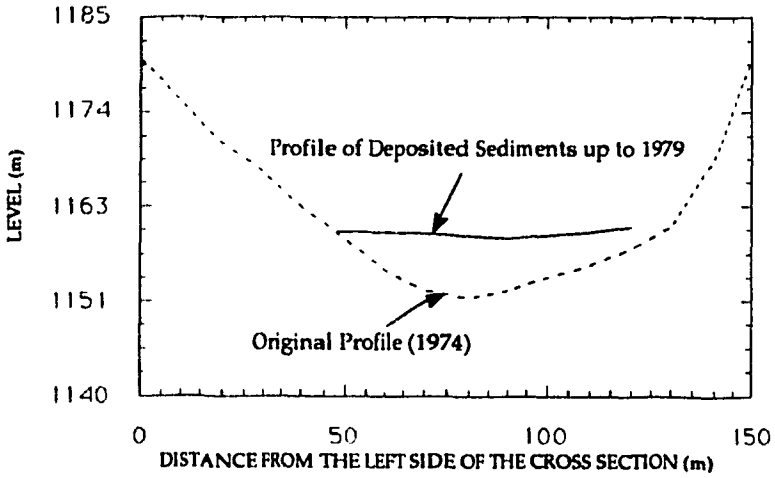

Figure 8.7 - Cross Section D

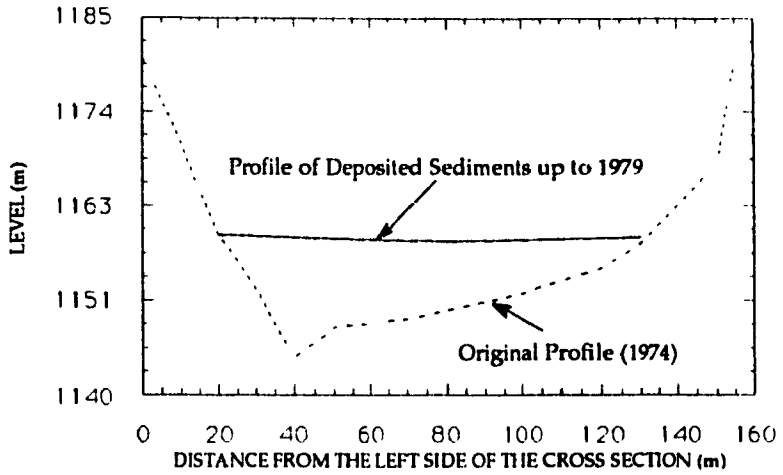

Figure 8.8 - Cross Section E

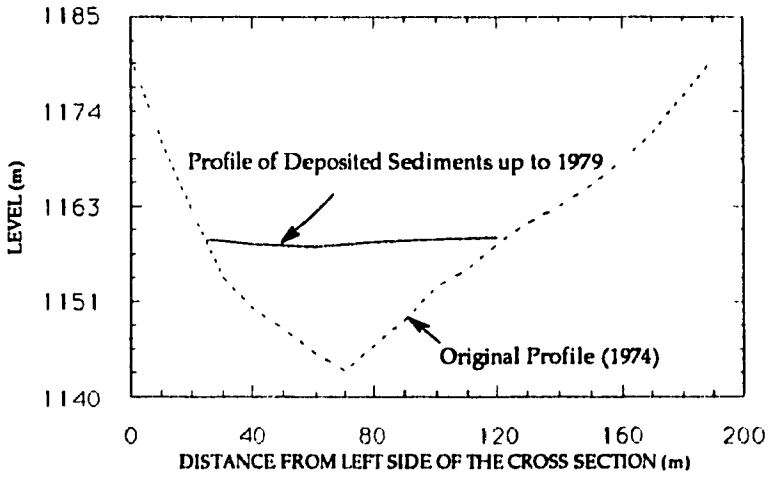

Figure 8.9 - Cross Section F

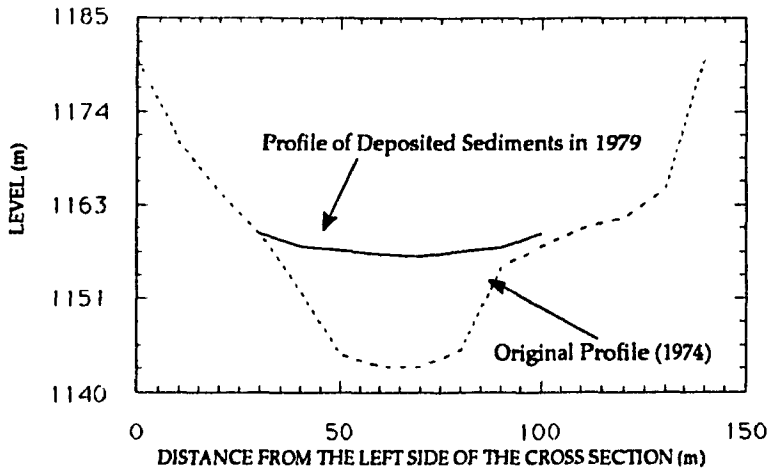

Figure 8.10 - Cross Section G (Equal to Cross Section 2 where Measurements were made)

8.2.2. Numerical Coupling of Sedimentation and Consolidation Processes

After having defined the geometry of the problem, as well as the parameters for the transportation of sediments, sedimentation and consolidation processes, the coupling of this processes is made as follows:

The transportation of sediments and sedimentation processes are run (program CONSED) for a predetermined period of time and a layer of sedimented material is obtained as a result in each cross section. Layers with the determined thickness are built in their respective sections in the finite deformation consolidation process (program CONFDEF). All the sections are studied and as a result the consolidation, a new geometry is obtained. This is used for updating and proceeding to the next step of the program CONSED, which again provides the input for the program CONFDEF. The process is repeated to obtain the history of the build up of the deposit in the reservoir. The time interval of each step in the program CONSED was $\Delta t = 3600$ seconds. It is important to mention that for each step the boundary conditions change and that both programs are able, in the sequence just mentioned above, to deal with these changes.

8.2.3. Saramenha's Sedimentation and Consolidation Analysis

The Initial Finite Element Mesh of each section of the reservoir was drawn following the boundaries of the cross section. Note that the thickness of each built layer might need to be modified in the entrance data of the Code CONFDEF, according to the amount of material that sediments in the considered period of time, once that in the initial mesh the inactive layers of elements were given an initial thickness value, which not necessarily agrees with the one obtained for a certain period of time by the program CONSED.

After the completion of the numerical analysis made for the Saramenha Case, comparison between the field and numerical profiles of deposited material was made. These are presented in Figures 8.11 and 8.12, for cross sections C and G. Comparison is also made of the longitudinal section of the reservoir, as shown in figure 8.13.

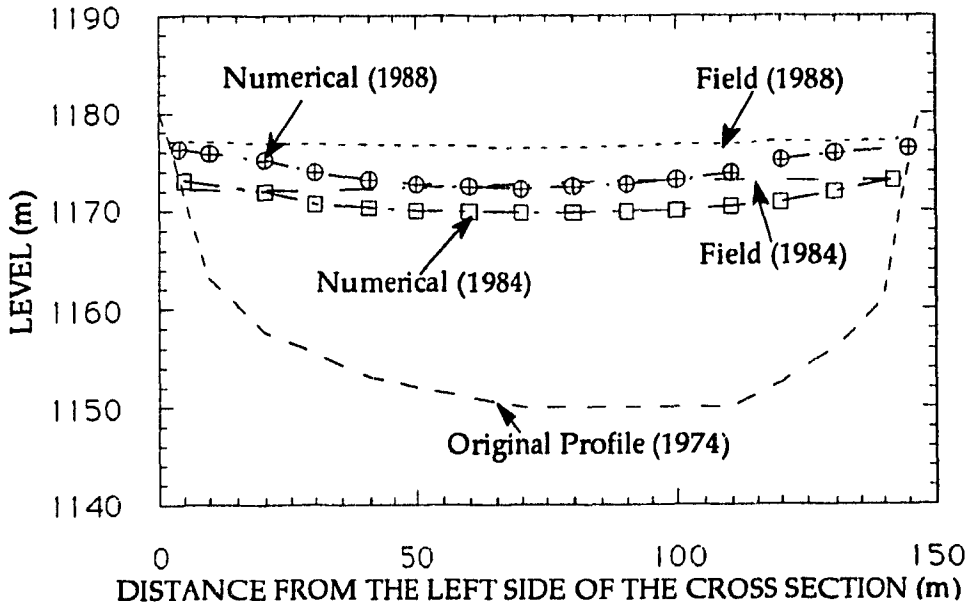

Figure 8.11 - Comparison between field and Numerical Profiles of Deposited Material for Cross Section C

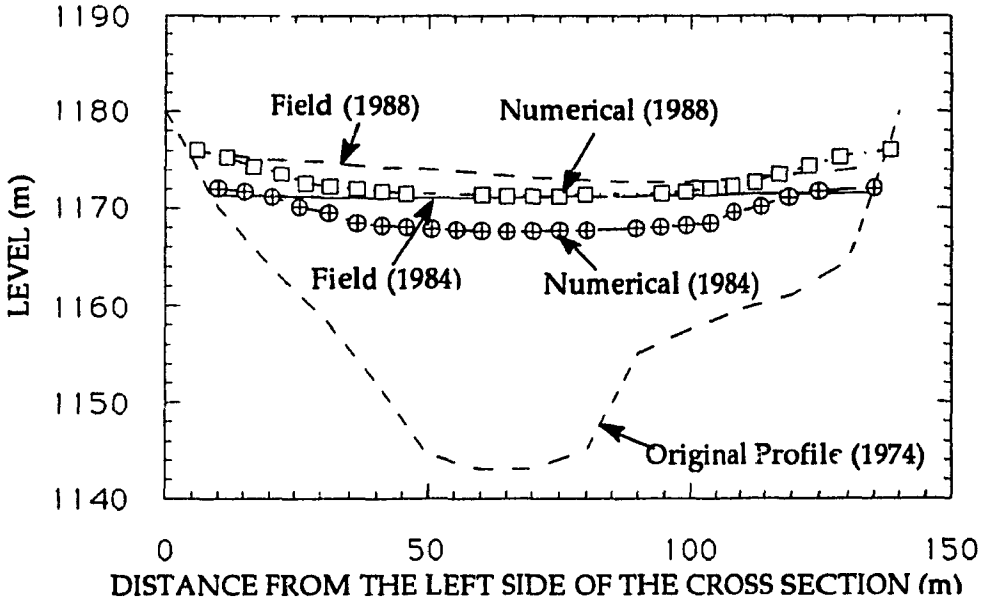

Figure 8.12 - Comparison between field and Numerical Profiles of Deposited Material for Cross Section G

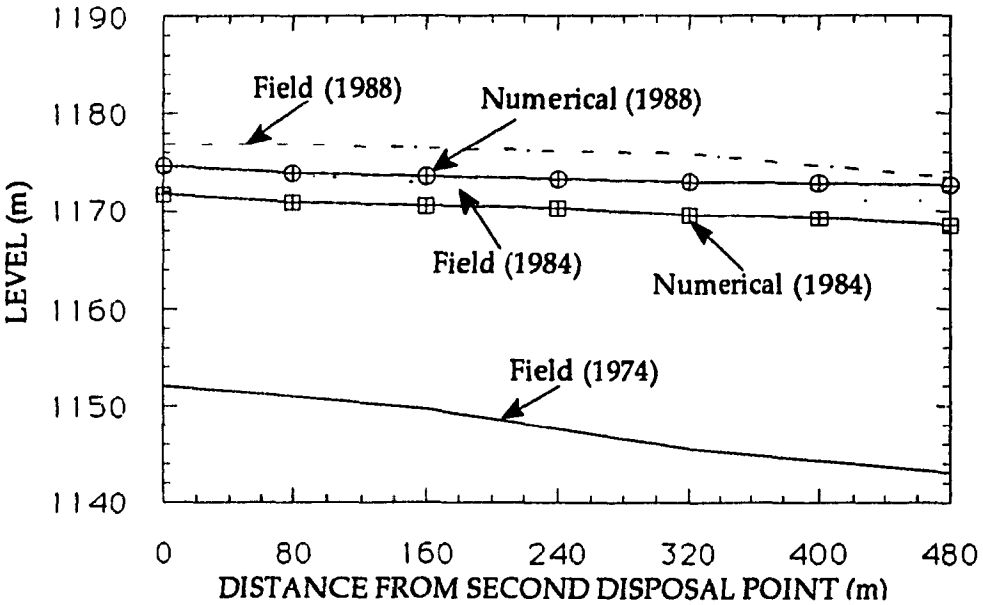

Figure 8.13 - Comparison Between Field and Numerical Longitudinally Deposited Material

The average rise of the red slime with time in each section,is shown in Figure 8.14. The relationship between time and level of sedimented material for all of the seven sections is clearly shown.

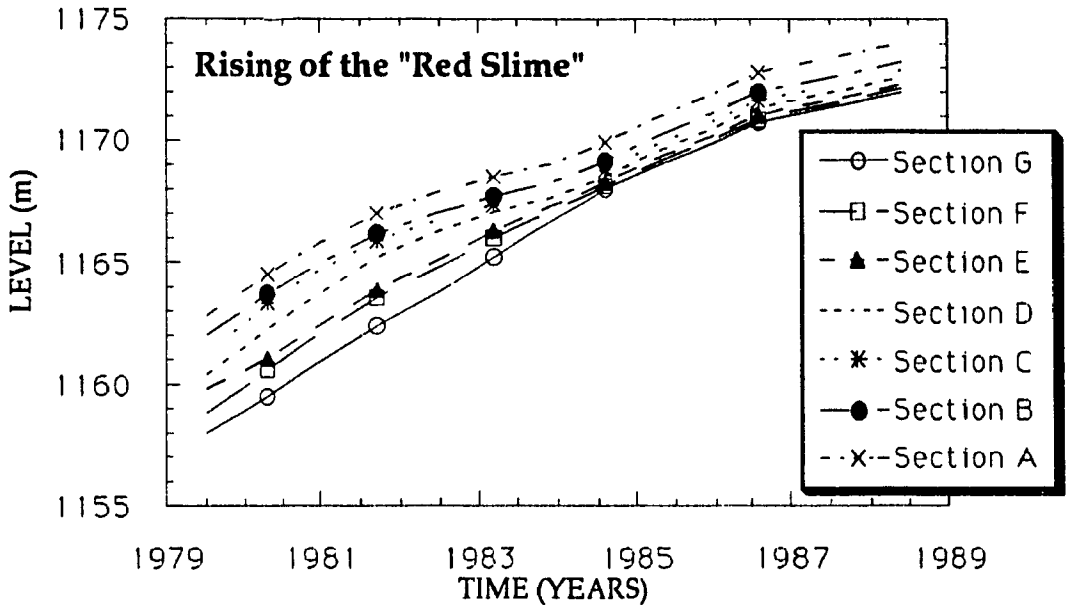

Figure 8.14 - Average Increase of Deposited Sediments with Time

The numerically simulated topographical plan view of the reservoir in 1983, 1985 and 1988 are shown respectively in Figures 8.15 to 8.17 inclusive.

Note that for the middle of section G, the field and numerical values of the profiles of void ratio with depth and stresses (effective and total) with depth are compared and presented in Figures 8.18 and 8.19, respectively.

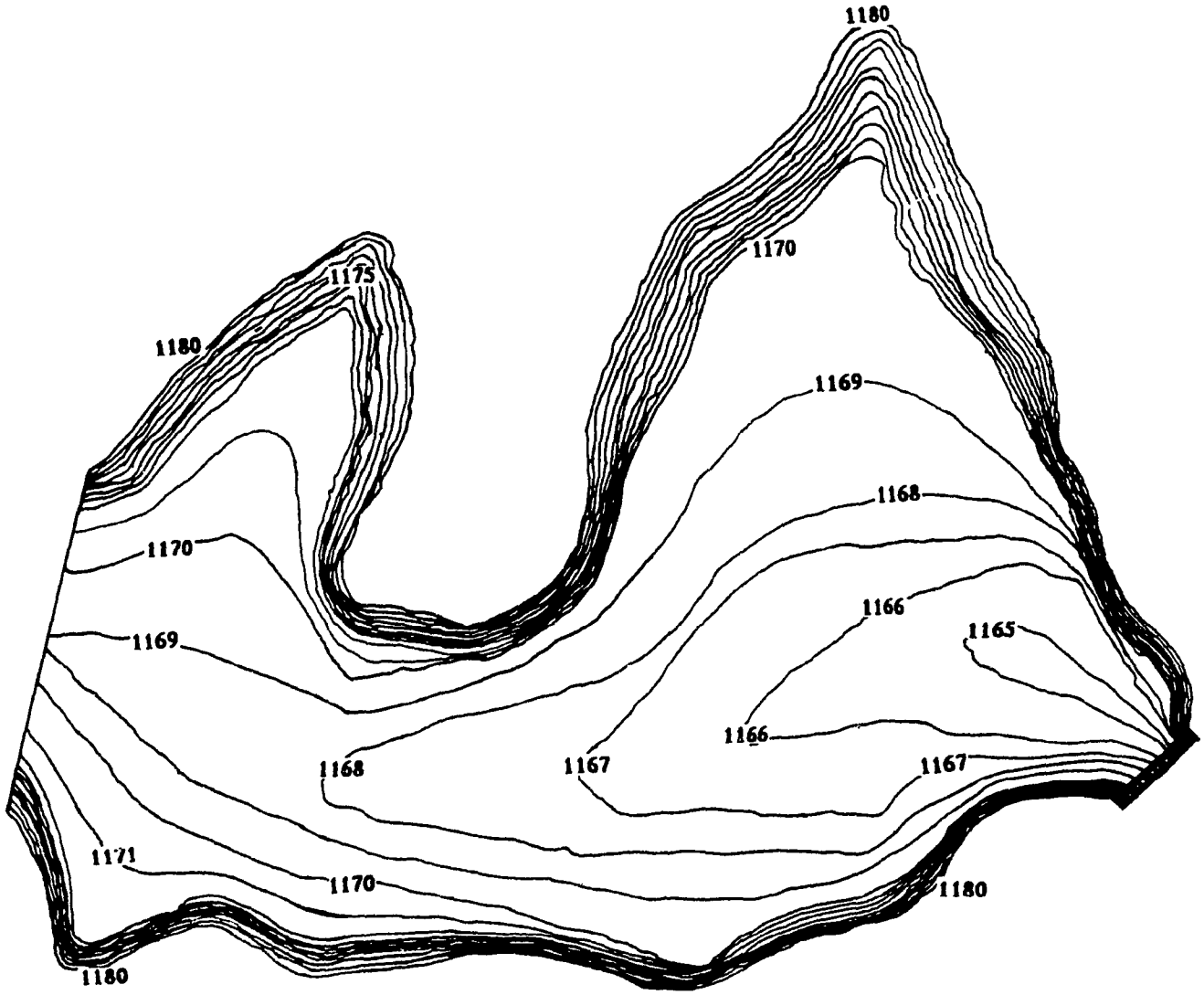

Figure 8.15 - Numerically Simulated Topographical Plan View of the Reservoir in 1983

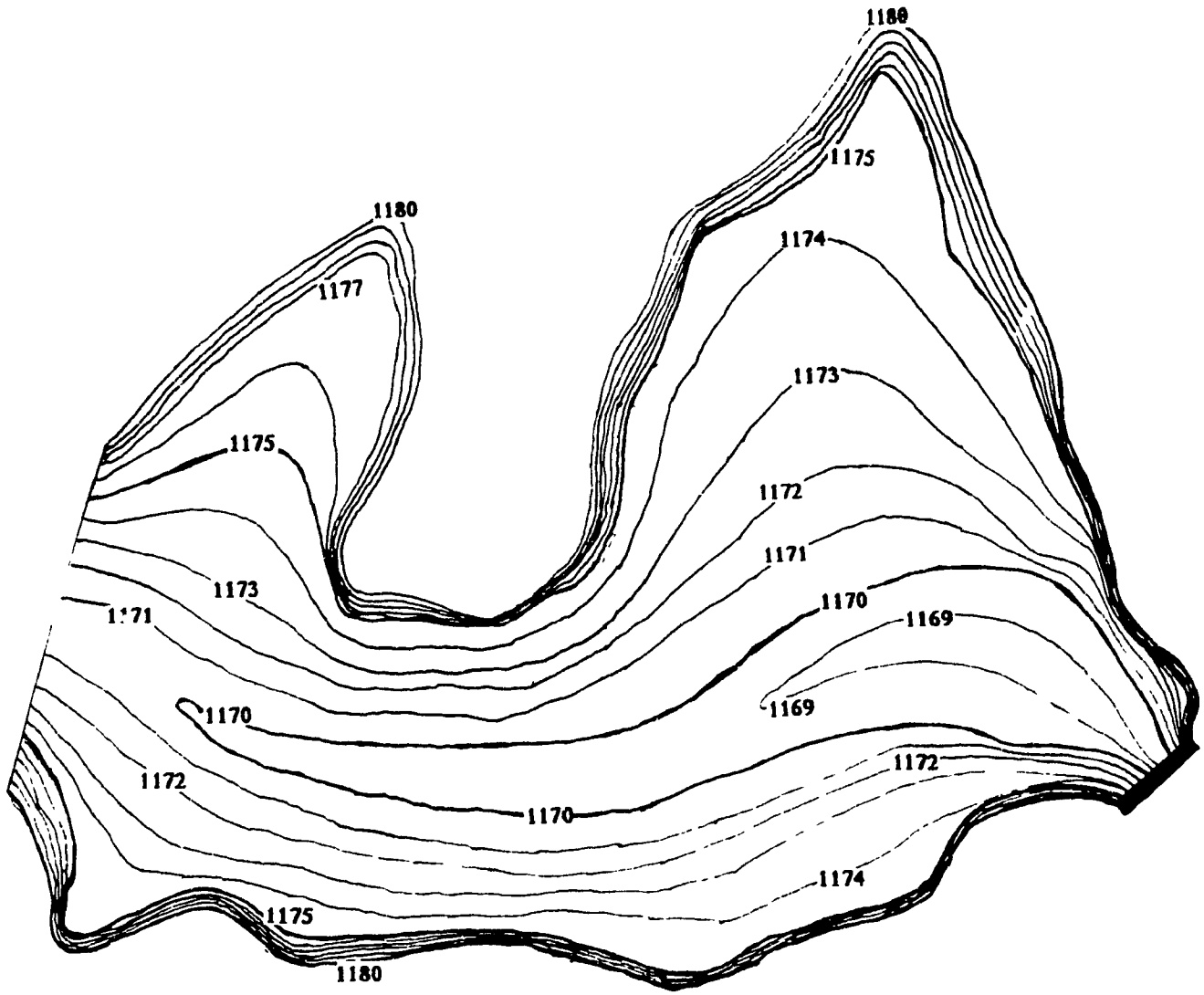

Figure 8.16 - Numerically Simulated Topographical Plan View of the Reservoir in 1985

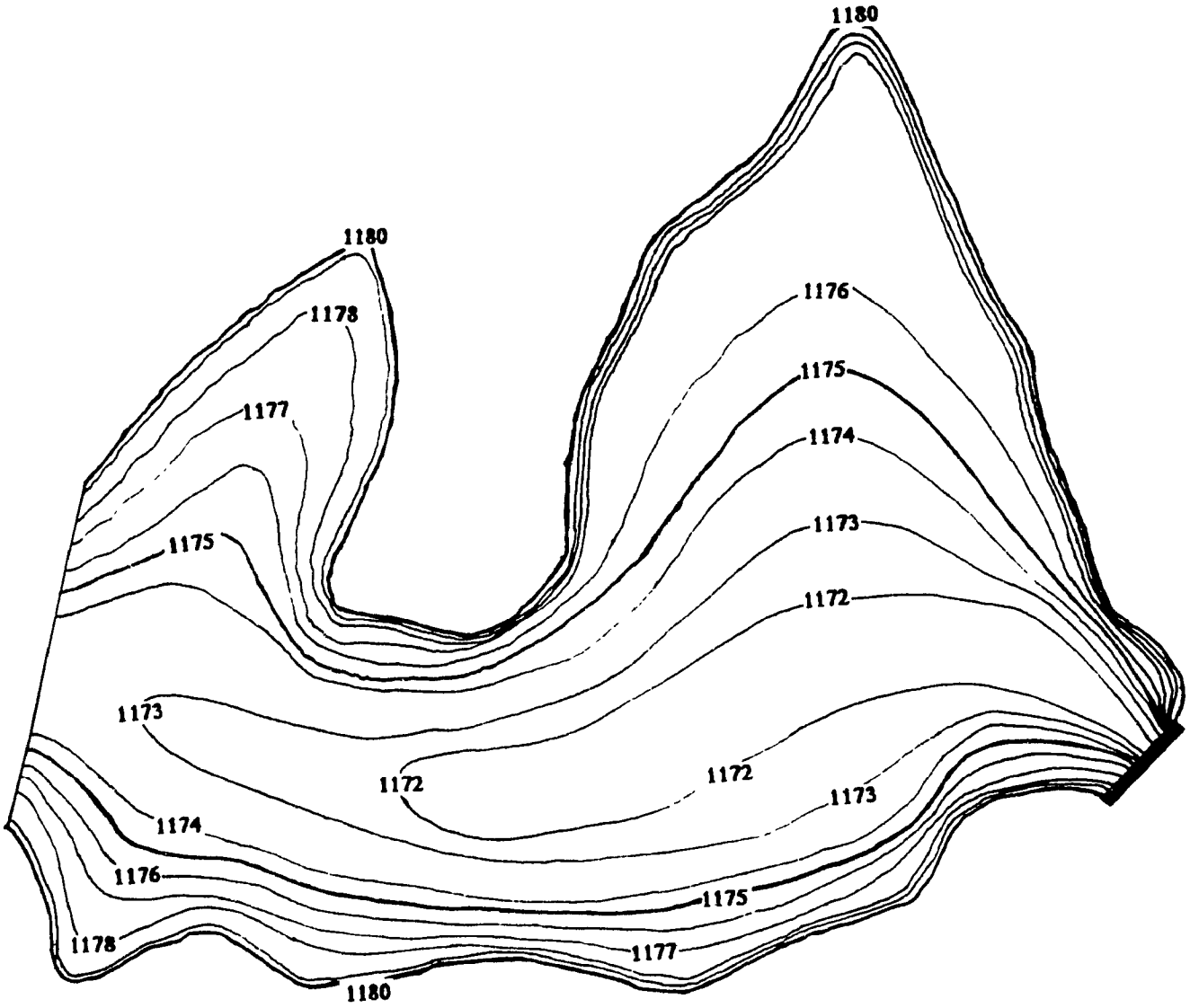

Figure 8.17 - Numerically Simulated Topographical Plan View of the Reservoir in 1988

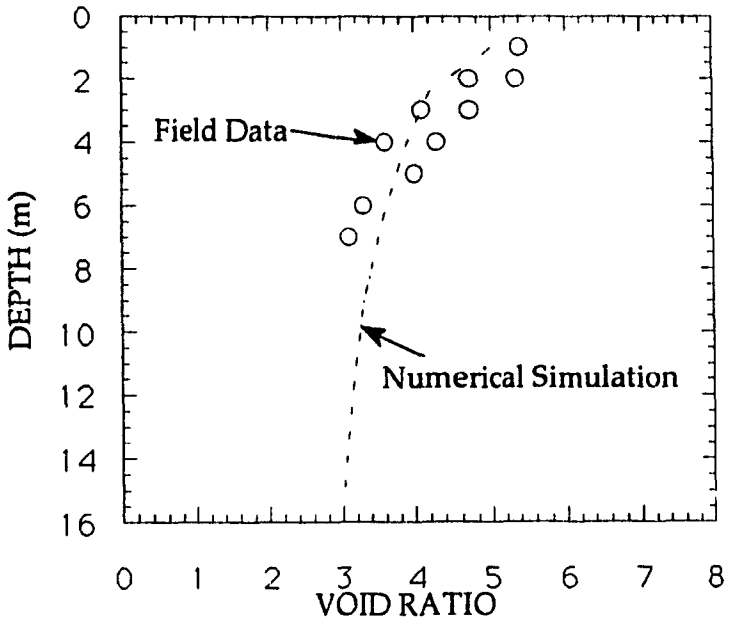

Figure 8.18 - Comparison Between Field and Numerical Values of Variation of Void Ratio with Depth

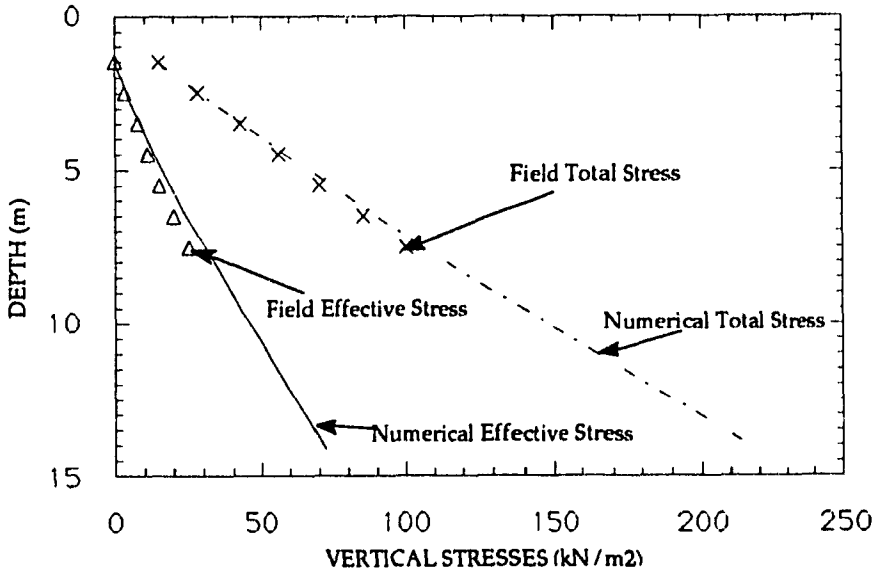

Figure 8.19 - Comparison Between Field and Numerical Values of Variation of Total and Effective Stresses with Depth

In Figure 8.20 the numerically simulated profiles of the pore pressure is presented for the center of section G.

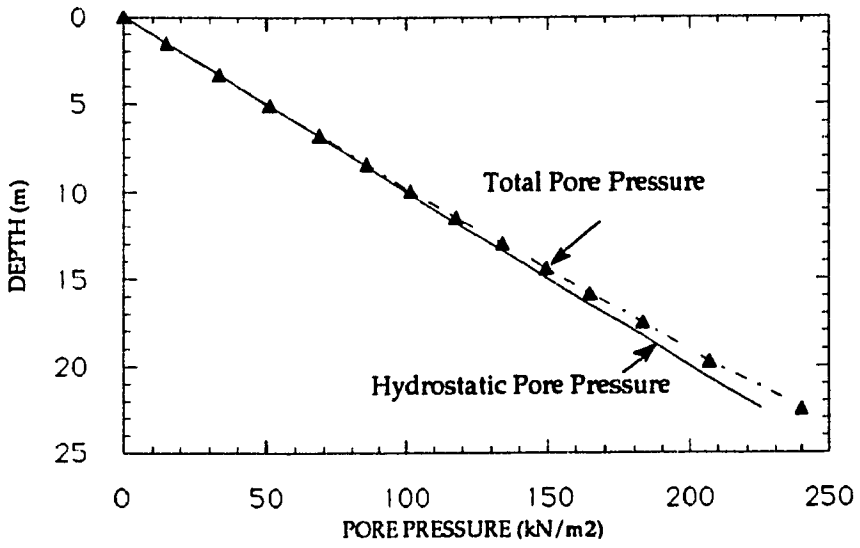

Figure 8.20 - Hydrostatic and Total Pore Pressure Profiles for Section G

Finally, in Figures 8.21 and 8.22 the stress paths of two elements located respectively in the middle and near the lateral boundary of cross section G are presented for the period of 1979 to 1988:

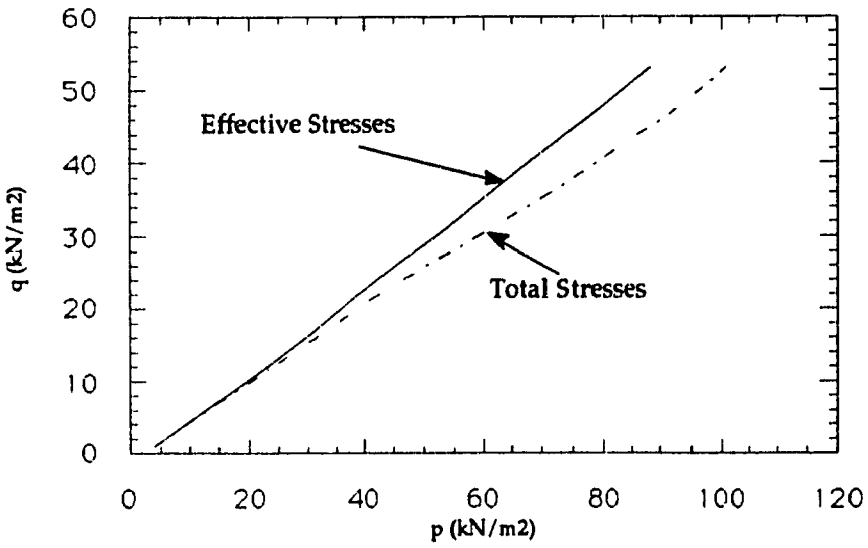

Figure 8.21 - Stress Path of Element Located in the Middle of Cross Section G

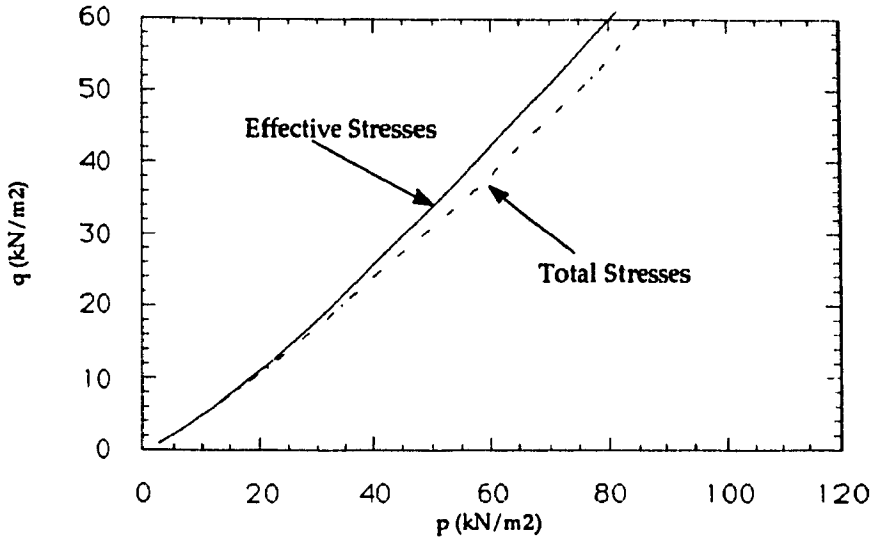

Figure 8.22 - Stress Path of Element Located Near the Lateral Boundary of Cross Section G

In Appendix C, the sequential changing of format (due to finite deformation considerations and layers build up with time) of the Finite Element Mesh of Cross Section G at several years is shown.

Laboratory test used for the calibration of soil parameters might have been subject to disturbance and the results might not truly reflect the properties of the material. For this reason it was decided to run a second set of analysis, changing the soil parameters of the stress-strain relation, characterizing now a stiffer soil. The new solution for the Saramenha Case History is obtained and comparisons between the new numerical results and the field values are presented in Appendix D.

8.3. Discussion of Results

The comparisons between the field and analytical cross sectional profiles of deposited sediments up to 1988, presented in Figures 8.11 and 8.12, are

quantitatively, as well as qualitatively, reasonable, with some discrepancy at the middle of cross section C.

The amount of material deposited up to 1988 in a longitudinal profile measured in the middle of each cross section is also compared, as can be seen in Figure 8.13, and the conclusions are that qualitatively a good agreement is obtained, but quantitatively the prediction by numerical analysis of the amount of deposited material is on the low side.

The increasing of elevation of the sediments deposited in the seven cross sections analyzed are presented in Figure 8.14. It can be concluded that during the period of 1979 to 1984, when the water level was kept at elevation 1173, the rate of sedimentation was gradually reduced. The rate of deposition was kept constant during 1984 and 1987, when the water level was increased to elevation 1175 and then gradually decreased once again after that time. Another point to be raised about Figure 8.14 is that the bed inclination is considerably reduced with time.

In Figures 8.15 to 8.17 the topographical plan view of the whole reservoir shows the modifications of the reservoir due to the filling with time. It is important to verify that the reduction of the rate of sedimentation with time is due to the decrease of the area of sediment-laden fluid (A) and consequent increase of the mean velocity (V) of the mixture.

In Figure 8.18, the comparison between the field measurements and the numerical analysis for the variation of the void ratio with depth shows them to be in reasonable agreement for practical purposes. It is important to emphasize the necessity of the geometrical non-linearity considerations to obtain a good agreement between field and numerical data in cases of very compressible materials.

The curves from the numerical analysis match the measured effective and total vertical stresses well, as can be seen in Figure 8.19, proofing once again the effectiveness of the numerical simulation.

The stress path shown in Figure 8.21, for the middle of cross section G, is a typical Ko-Path, usual in one-dimensional consolidation because it does not

approach failure. The stress path presented in Figure 8.22, for an element near the boundaries, the shear stress is higher and the curvature shows a tendency to localized failure if the loading continues. This is probably due to the difference of stiffness of the material that constitutes the boundary, and the sediments deposited.

It finally can be concluded that the numerical tool developed in this work is proven to be, without doubt, good for modelling the soil formation case in reservoirs and can describe, with good precision, the behavior of the complete process, from transportation of sediments, through sedimentation and consolidation, simultaneously.

CHAPTER 9

CONCLUSIONS AND SUGGESTIONS FOR FURTHER STUDY

9.1. Conclusions

The main aim of this work was the creation of a model capable of studying the complete process of soil formation in real life problems, without being restricted to vertically oriented one-dimensional problems.

The study presented is thought to be fundamentally of value as well as practically applicable. It is not only of interest in the field of Geotechnical Engineering, but probably also in Environmental Engineering.

The complete soil formation process was mathematically modelled by combining the three phases which were investigated. They are:

- The behavior of sediments in transportation and deposition. This is accomplished through the development, study and solution of the partial differential equations that control these phenomena, for specific boundary conditions.

- The development of a material constitutive model capable of representing the main characteristics of soil behavior during simple as well as complicated loading processes, taking into consideration the change of the state of the soil. Thus it can model the soil behavior from the first intergranular contact up to the ultimate state. After evaluating the model parameters, numerical simulations of laboratory tests carried out. These include modelling the behavior of samples under several stress paths for drained, partly drained and undrained situations, virgin and cyclic loading up to the point that ultimate state is achieved.

- The development of a coupled consolidation theory without restricting the deformation magnitude. The Eulerian System of Coordinates is used.

The specific conclusions arrived at are :

Loading rate appears to influence the superficial displacements of loose material in the case of shallow foundation lying over a soil layer, but the discrepancy of the results is not large, demonstrating the relative lack of importance of the loading history, a view held generally in the past, but without any proof.

The variation of the permeability coefficient with void ratio is shown to be an important factor that must be considered during simulation of very soft material behavior under loading conditions which cause large deformation. This confirms the earlier findings by Schiffman et al., (1984).

The coupled phenomena of transportation of sediments, sedimentation and consolidation developed in this work forms the foundation of soil formation in a reservoir. The analytical procedure is applied to the case history of Saramenha's Reservoir. In this connection the results indicated :

The value of the void ratio versus depth is shown through numerical simulation to approach a constant value at greater depths.

The rate of sedimentation is reduced with time due to the decrease of area of sediment-laden fluid (A) and consequent increase of mean velocity (V) of the mixture, which causes the reduction of the capacity of deposition of sediments.

In the center line of a cross section the K_o Stress Path is well defined, but the same cannot be said for that nearest to the boundaries of the cross section. Thus the use of an adequate and proper modelling scheme, as the one developed in this thesis, is mandatory, to be able to simulate accuratelly the field problem.

9.2. Suggestions for Further Study

It is suggested that special laboratory tests, such as plane strain and true triaxial tests, as well as conventional axysimmetrical triaxials tests, should be conducted

in the future. These tests are required for a better understanding of the parameters of the constitutive model based on state parameters, and to enhance calibration procedures.

Some more field measurements, like vertical and horizontal displacements at several depths, as well as vertical and horizontal stresses near the boundaries of the cross sections are essential for a better understanding of the field process.

Parametric studies are also suggested (variation of one or several parameters) to check the influence of each parameter in the soil formation process.

The extension of the model from the use of one average size of particulate sediment to several sizes may be necessary for cases where the grain distribution is not as uniform as the case of the bauxite tailings studied in this thesis.

The consideration of anisotropy in the constitutive relation is another suggestion for further study. The problem will become more complex, once that the state of a sample will be represented by a point in a twelve dimensional state space.

REFERENCES

Abbott, M. B. (1979) - "Computational Hydraulics: Elements of the Theory of Free Surface Flows", Pitman Publishing Limited, London , Great Britain, p. 326.

Abreu, F. R. S. (1989) - "Numerical Model For the Calculation of Disposal of Waste of Industries", M.Sc. Thesis, Catholic University of Rio de Janeiro, Brazil, p. 152. (in Portuguese).

Adachi, T. , Oka, F. and Tange, Y. (1982) - "Finite Element Analysis of Two-Dimensional Consolidation Using an Elasto-Viscoplastic Constitutive Equation", Numerical Methods in Geomechanics, Edmonton, Canada, pp. 287-296.

Alcan of Brasil Limited (1989) - Saramenha's Surveying Maps and Data of Disposed Material.

Almeida, M. S. S. and Ortigão, J. A. R. (1982) - " Performance and Finite Element Analysis of a Trial Embankment on Soft Clay", Proceedings International Symposium on Numerical Models in Geomechanics, Zurich.

Azevedo, R. F. (1990) - Report on the Behavior of Bauxite Tailings under Unidimensional Consolidation Tests, Catholic University of Rio de Janeiro, Rio de Janeiro, Brazil (in Portuguese).

Banerjee, P. K. and Fathallah, R. C. (1979) - "An Eulerian Formulation of the Finite Element Method for Predicting the Stresses and Pore Water Pressures Around a Driven Pile", Third Int. Conf. Num. Meth. in Geomechanics, pp. 1053-1060.

Been, K. (1980) - "Stress-Strain Behavior of Cohesive Soil Deposited Under Water", Ph.D. Thesis, University of Oxford, Great Britain.

Biot, M. A. (1941) - "General Theory of Three Dimensional Consolidation", Journal of Applied Physics, vol. 12, pp. 155-164.

Booker, J. R. and Small, J. C. (1975) - "An Investigation of the Stability of Numerical Solutions of Biot's Equation of Consolidation", International Journal of Solids and Structures, vol. 11, pp. 907-917.

Borland, W. M. and Miller, C. R. (1960) - "Distribution of Sediments in Large Reservoirs", Transactions ASCE, vol. 125, pp. 166-180.

Burd, H. J. and Houlsby, G. T. (1986) - "A Large Strain Finite Element Formulation for One-Dimensional Membrane Elements", Computers and Geotechnics, vol. 2, pp. 3-22.

Carter, J. P. , Small, J. C. and Booker, J. R. (1976) - "A Theory of Finite Elastic Consolidation", Int. J. Solids Struct., vol. 13, pp. 467-478.

Carter, J. P. , Booker, J. R. and Davis, E. H. (1977) - "Finite Deformation of an Elasto-Plastic Soil", International Journal for Numerical and Analytical Methods in Geomechanics , vol. 1, pp. 25-43.

Castro, G. and Poulos, S. J. (1977) - "Factors Affecting Liquefaction and Cyclic Mobility", J. of the Geoth. Eng. Division, ASCE, vol. 103, nº GT6, pp. 501-516.

Chang, C. S. and Duncan, J. M. (1983) - "Consolidation Analysis for Partly Saturated Clay by Using an Elasto-Plastic Effective Stress-Strain Model", International Journal and Analytical Methods in Geomechanics, vol. 7, pp. 39-55.

Chang, F. F. M. and Richards, D. L. (1971) - "Deposition of Sediment in Transient Flow", Journal of the Hydraulics Division, ASCE, vol. 97, nº HY6, pp. 837-849.

Chow, V. T. (1959) - "Open-Channel Hydraulics", McGraw-Hill Book Company Inc, New York, USA, p.680.

Coe, H. S. and Clevenger, G. H. (1916) - "Methods for Determining the Capacities of Slime-Settling Tanks", Transactions of the American Institution of Mining Engineers, vol. 55, p. 356.

Consoli, N. C. (1987) - "Field and Analytical Behavior of an Experimental Excavation", M.Sc. Thesis, Catholic University of Rio de Janeiro, Brazil, p. 153. (in Portuguese)

Consoli, N. C. and Poorooshasb, H. B. (1991) - "Flow of Cohesionless Granular Media; A Unified Approach", Constitutive Laws for Engineering Materials, Recent Advances and Industrial and Infrastructure Applications, Proceedings of the Third International Conference on Constitutive Laws for Engineering Materials: Theory and Applications, held January 7-12, in Tucson, Arizona, USA, pp. 25-28.

Cunge, J. A. , Holly, F. M. , Jr. and Verwey, A. (1980) - "Practical Aspects of Computational River Hydraulics", Pitman Publishing Limited, London , Great Britain, p. 420.

Cryer, C. W. (1963)- "A Comparison of the Three-Dimensional Consolidation Theories of Biot and Terzaghi", Quaterly Journal of Mechanics and Applied Mathematics, vol. 16, pp. 401-412.

Davis, E. H. and Raymond, G. P. (1965) - "A Non-Linear Theory of Consolidation", Geotechnique, vol. 15, pp. 161-173.

Dafalias, Y. F. and Popov (1975) - "A model of Non-Linear Hardening Material for Complex I oading, Acta Mechanica, vol. 21, pp. 173-192.

Dluzewski, J. M. (1988) - "Total Formulation For Large Strains in Soils", Computers and Geotechnics, nº 5, pp. 197-211.

Drucker, D. C. (1951) - "A More Fundamental Approach to Plastic Stress-Strain Relations', Proc. First U. S. Natl. Congr. Appl. Mech., ASME, pp. 487-491.

Drucker, D. C. and Prager, W. (1952) - "Soil Mechanics and Plastic Analysis or Limit Design", Quaterly Journal of Applied Mathematics, vol. 10, pp. 157-165.

Drucker, D. C. , Gibson, R. E. and Henkel, D. J. (1957) - "Soil Mechanics and Work Hardening Theories of Plasticity", Transactions ASCE, vol. 122, pp. 338-346.

Duncan, J. M. and Chang, C. Y. (1970) - "Non-Linear Analysis of Stress and Strain of Soils", Journal of the Soil Mechanics and Foundations Division", ASCE, vol. 96, pp. 1629-1653.

Emir, M. Z. (1991) - " The Mechanical Behavior of Soft Clays under Vibration Loading from Vehicle Traffic", Ph.D. Thesis, Concordia University, Montreal, Quebec, Canada, p.187.

Fernandez, R. M. and Christian, J. T. (1971) - "Finite Element Analysis of Large Strain in Soils", NASA Report R71-37, MIT.

Fung, Y. C. (1965) - "Foundations of Solid Mechanics", Prentice Hall.

Gibson, R. E. , England, G. L. and Hussey, M. J. L. (1967) - "The Theory of One-Dimensional Consolidation of Saturated Clays", Geotechnique, vol. 17, pp. 261-273.

Green, A. E. and Naghdi, P. M. (1965) - "A General Theory of an Elasto-Plastic Continuum", Arch. Rat. Mech. Anal., vol. 18, pp. 251-281.

Hencky, H. (1925) - "Zur Theorie Plastischer Deformationen und der Hierdurch im Material Hervorgerufenen Nebenspannungen", Proceedings of the First International Congress on Applied Mechanics, Delft, Technische Boekhandel en Druckerij, J. Waltman, pp. 312-317.

Hibbitt, H. D. , Marçal, P. V. and Rice, J. R. (1970) - "A Finite Element Formulation for Problems of Large Strain and Large Displacement", Int. J. Sol. Struct., vol. 6, pp. 1060-1086.

Hill, R. (1950) - "The Mathematical Theory of Plasticity", Oxford University Press, Great Britain, p. 355.

Hill, R. (1962) - "Uniqueness and Extremum Principles in Self-Adjoint Problems of Continuum Mechanics", J. Mech. Phys. Solids, vol. 10, pp. 185-194.

Imai, G. (1980) - "Settling Behavior of Clay Suspensions", Soils and Foundations, vol. 20, nº 2, pp. 61-77.

Iwagaki, Y. (1956) - "On The River Bed Variation and Its Stability", Proceedings of the Sixth National Congress for Applied Mechanics, pp. 361-366.

Janbu, N. (1963) - "Soil Compressibility as Determined by Oedometer and Triaxial Tests", Proceedings of the European Conference on Soil Mechanics and Foundation Engineering, vol. 1, pp. 19-25.

Kaplan, W. (1959) - "Advanced Calculus", Fifth Edition, Addison-Wesley Publishing Company Inc, Massachusets, USA, p.679.

Kinch, E. J. (1952) - "A Theory of Sedimentation", Transactions of the Faraday Society, vol. 48, pp. 168-176.

King, I. P. (1965) - "Finite Element Analysis of Two-Dimensional Time Dependent Problems", Ph.D. Thesis, University of California at Berkeley.

Kiousis, P. D. Voyiadjis, G. Z. and Tumay, M. T. (1986) - "A Large Strain Theory for the Two-Dimensional Problems in Geomechanics", Int. J. Num. Anal. Meth. Geomechanics, vol. 10, pp. 17-39.

Kondner, R. L. and Zelasko, J. S. (1963) - "A Hyperbolic Stress-Strain Formulation for Sands", Proceedings of the Second Pan-American Conference on Soil Mechanics and Foundation Engineering, vol. 1, pp. 289-324.

Lade, P. V. and Duncan, J. M. (1975) - "Elasto-Plastic Stress-Strain Theory for Cohesionless Soil", Int. J. Geoth. Eng. Division, ASCE, vol. 101, nº GT 10, pp. 1037-1053.

Lade, P. V. (1977) - "Elasto-Plastic Stress-Strain Theory for Cohesionless Soil with Curved Yield Surfaces", Int. J. of Solids and Structures, vol. 13, pp 1019-1035.

Lambe, T. W. and Whitman, R. V. (1979) - "Soil Mechanics, SI Version", John Wiley & Sons Inc , USA, p. 553.

Lane, E. W. and Kalinske, A. A. (1942) - "Engineering Calculations of Suspended Sediment", Transactions American Geophysical Union, vol. 22, pp. 603-607.

Lee, K. L. and Seed, H. B. (1967) - "Drained Strength Characteristics of Sands", Journal of the Soil Mechanics and Foundations Division", ASCE, vol. 93, nº SM6, pp. 117-141.

Lee, E. H. (1969) - "Elastic-Plastic Deformations at Finite Strains, J. Appl. Mech. Trans., ASME, vol. 38, pp. 1-6.

Levy, M. (1870) - "Memoire sur les Equations Generales des Mouvements Interieurs des Corps Solides Ductiles au dela des Limits ou l'Elasticite pourrait les Ramener a le Premier Etat", Compt. Rend., 70, pp. 1323-1325.

Lewis, W. K. , Gilliland, E. R. and Bauer, W. C. (1949) - "Characteristics of Fluidized Particles", Industrial Engineering Chemistry, vol. 41, pp. 1104-1117.

Liggett, J. A. and Cunge, J. A. (1975) - "Numerical Methods of Solution of the Unsteady Flow Equations", Unsteady Flow in Open Channels, vol. 1, chapter 4, edited by Mahmood and Yevjevich, Water Resources Publications, Colorado, USA.

Lyn, D. A. (1987) "Unsteady Sediment-Transport Modeling", ASCE, Journal of Hydraulic Engineering, vol. 113, nº 1, pp. 1-15.

Lyn, D. A. and Goodwin, P. (1987) - "Stability of a General Preissmann Scheme", ASCE, Journal of Hydraulic Engineering, vol. 113, nº 1, pp. 16-28.

Magnan, J. P. , Belkeziz, A. , Humpert, P. and Mouratidis, A. (1982) - Finite Element Analysis of Soil Consolidation with Special Reference to the Case of Strain Hardening Elasto-Plastic Stress-Strain Models", Numerical Methods in Geomechanics, Canada, pp. 327-336.

Mandel, J. (1953) - "Consolidation des Sols (Etude Mathematique)", Geotechnique, vol. 3, pp. 287-299.

Mase, G. E. (1970) - "Theory and Problems of Continuum Mechanics", Schaum's Outline Series in Engineering, McGraw-Hill Book Company, p. 221.

McMeeking, R. M. and Rice, J. R. (1975) - "Finite Element Formulations for Problems of Large Elastic-Plastic Deformation", Int. J. Sol. Struct. , vol. 11, pp. 601-616.

McRoberts, E. C. and Nixon, J. F. (1976) - "A Theory of Soil Sedimentation", Canadian Geotechnical Journal, nº 13, pp. 294-310.

Meijer, K. L. (1984) - "Comparison of Finite and Infinitesimal Strain Consolidation by Numerical Experiments", Int. J. Num. Anal. Meth. Geomechanics, vol. 8, pp. 531-548.

Middleton, G. V. and Southard, J. B. (1977) - "Mechanics of Sediment Movement", S. E. P. M. Short Course nº 3, Binghamton, New York, USA.

Mikasa, M. (1965) - "The Consolidation of Soft Clay: A New Consolidation Theory and Its Application", Japanese Society of Civil Engineering, pp. 21-26.

Mroz, Z. (1967) - "On the Description of Anisotropic Hardening", J. Mech. Phys. Solids, vol. 15, pp. 163-175.

Mroz, Z. , Norris, V. A. and Zienkiewicz, O. C. (1979) - "Application of an Anisotropic Hardening Model in Analysis of Elasto-Plastic Deformation of Soils", Geotechnique, nº 29, pp. 1-34.

Osaimi, A. E. and Clough, G. W. (1979) - "Pore-Pressure Dissipation During Excavation", Journal of the Geotechnical Division, ASCE, vol. 105, GT. 4, pp. 481-498.

Osias, J. R. and Swedlow, J. L. (1974) - "Finite Elasto-Plastic Deformation", Int. J. Solids Structures, vol. 10, pp. 321-339.

Paulet, M. (1971) - "An Interpretation of Reservoir Sedimentation as a Function of Watershed Characteristics", Ph.D. Thesis, Purdue University, USA.

Poorooshasb, H. B. (1961) - "The Properties of Soils and Other Granular Media in Simple Shear", Ph.D. Thesis, University of Cambridge.

Poorooshasb, H. B., Holubec, I. and Sherbourne, A. N. (1966) - "Yielding and Flow of Sand in Triaxial Compression: Part I", Canadian Geotechnical Journal, III, 4, pp. 179-190.

Poorooshasb, H. B., Holubec, I. and Sherbourne, A. N. (1967) - "Yielding and Flow of Sand in Triaxial Compression: Parts II and III", Canadian Geotechnical Journal, IV, 4, pp. 376-397.

Poorooshasb H. B. and Pietruszczak, S. (1985) - "On Yielding Flow of Sand; A Generalized Two-Surface Model", Computers and Geotechnics, vol. 1, pp. 33-58.

Poorooshasb H. B. and Pietruszczak, S. (1986) - "A Generalized Flow Theory For Sand", Soils and Foundations, vol. 26, nº 2, pp. 1-15.

Poorooshasb, H. B. (1988) - "M.I.T. Lecture Notes".

Poorooshasb, H. B. and Consoli, N. C. (1991) - "The Ultimate State", Proceedings of the Pan-American Conference of Soil Mechanics and Foundation Engineering, Santiago, Chile, August, 1991.

Poskitt, T. J. (1969) - "A Note on the Consolidation of Clay with Variable Permeability and Compressibility", Geotechnique, vol. 19, pp. 234-252.

Prager, W. (1961) - "An Elementary Discussion of Definitions of Stress Rate", Quart. Appl. Math., vol. 18, pp. 403-407.

Prandtl, L. (1924) - "Spannungsverteilung in Plastischen Koerpern", Proceedings of the First Congress on Applied Mechanics, Delft, pp. 43-54.

Prevost, J. H. (1978) - "Plasticity Theory for Soil Stress Behavior", J. Eng. Mech. Div., ASCE, vol. 104, pp. 1177-1194.

Rahuel, J. L., Holly, F. M., Chollet, J. P., Belleudy, P. J. and Yang, G. (1989) - "Modeling of Riverbed Evolution for Bedload Sediment Mixtures", ASCE, Journal of Hydraulic Engineering, vol. 115, nº 11, pp. 1521-1542.

Rendulic, L. (1936) - "Poronziffer und Porenwasserdruck in Tonen", Der Bauingenieur, vol. 17, pp. 559-564.

Roscoe, K. H., Schofield, A. N. and Wroth, C. P. (1958) - "On the Yielding of Soils", Geotechnique, vol. 8, pp. 22-53.

Roscoe, K. H., Schofield, A, N. and Thurairajah, A. (1963) - "Yielding of Clays in States Wetter than Critical", Geotechnique, vol. 3, pp. 211-240.

Roscoe, K. H. and Burland, J. B. (1968) - "On the Generalized Stress-Strain Behavior of Wet Clay", Engineering Plasticity, Cambridge University Press, England, pp. 535-568.

Saint-Venant, B. (1870) - "Memoire sur L'Etablissement des Equations Differentieles des Mouvements Interieurs Operes dans les Corps Solides Ductiles au dela des Limites ou l'Elasticite pourrait les Ramener a leur Premier Etat", Compt. Rend., 70, pp. 473-480.

Sandhu, R. S. and Wilson, E. L. (1969) - "Finite Element Analysis of Flow in Saturated Porous Elastic Media", Journal of Engineering Mechanics, ASCE, vol. 95, pp. 641-652.

Sandhu, R. S. and Liu, H. (1979) - "Analysis of Consolidation of Viscoelastic Soils", Third International Conference on Numerical Methods in Geomechanics, Aachen, pp. 1255-1263.

Schiffman, R. L., Chen, T. and Jordan, J. C. (1969) - "An Analysis of Consolidation Theories", ASCE, Journal of Soil Mechanics and Foundation Engineering,pp. 285-312.

Schiffman R. L. (1980) - "One-Dimensional Finite Strain Consolidation", University of Colorado, Boulder, USA.

Schiffman, R. L., Pane, V. and Gibson, R. E. (1984) - "The Theory of One-Dimensional Consolidation of Saturated Clays : An Overview of Nonlinear Finite Strain Sedimentation and Consolidation", Symposium on Sedimentation/ Consolidation Models, McGill University, Montreal, Canada, pp. 1-29.

Seed, H. B. and Lee, K. L. (1966) - "Liquefaction of Saturated Sands During Cyclic Loading", Journal of the Soil Mechanics and Foundations Division", ASCE, vol. 92, nº SM6, pp. 105-134.

Segerlind,L. J. (1984) - "Applied Finite Element Analysis", Second Edition, John Wiley & Sons, p. 427.

Soares, E. F. (1975) - "A Deterministic-Stochastic Model for Sediment Storage in Large Reservoirs", Ph.D. Thesis, University of Waterloo, Canada.

Somasundaran, P. (1981) - "Thickening of Dewatering of Slow-Settling Mineral Suspensions", Mineral Processing, J. Laskowski Editor, Elsevier, Amsterdam, Netherlands, pp. 233-261.

Tan, T.-S., Yong, K.-Y., Leong, E.-C. and Lee, S. L. (1990) - "Behavior of Clay Slurry", Soils and Foundations, vol. 30, nº 4, pp. 105-118.

Terzaghi, K. (1923) - "Die Berechnung der Durchlassigkeitsziffer des Tones aus dem Verlauf der Hidrodynamischen Spannungserscheinungen", Akademie der Wissenchaften in Wein, vol. 132, pp. 125-138.

Tresca, H. (1864) - "Sur l'Ecoulement des Corps Solids Soumis a de Fortes Pression", Compt. Rend. 59, p. 754.

Truesdell, C. (1952) - "The Mechanical Foundations of Elasticity and Fluid Dynamics", J. Rat. Mechs. Analysis, vol. 1, p. 125.

Vanoni, V. A. (1984) - "Fifty Years of Sedimentation", ASCE, Journal of Hydraulic Engineering, vol. 110, nº 8, pp. 1022-1057.

Villar, L. F. S. (1990) - "Analysis of Behavior of Bauxite Residues: Field and Laboratory Experiments", M.Sc. Thesis, Catholic University of Rio de Janeiro, Brazil, p. 236. (in Portuguese).

Von Mises, R. (1913) - "Mechanik der Festen Koerper in Plastisch Deformablen Zustant", Goettinger Nachr., Math.- Phys., pp. 582-592.

William, K. J. and Warnke, E. P. (1975) - "Constitutive Models for the Triaxial Behavior of Concrete", Proc. Int. Ass. Bridge Struct. Engineering, vol. 19, pp. 1-30.

Yamada, Y. and Wifi, A. S. (1977) - "Large Strain Analysis of Some Geotechnical Problems by the Finite Element Method", Int. J. Num. Anal. Meth. Eng. , vol. 1, pp. 299-318.

Yang, Q. (1990) - "Wave Induced Response of Sea Floor Deposits: A Simple Model for Sands and Nonlinear Analysis by FEM", Ph.D. Thesis, Concordia University, Montreal, Canada, p. 197.

Zeng, G. X. and Gong, X. N. (1985) - "Consolidation Analysis of the Soft Clay Ground Beneath Large Steel Oil Tank", Fifth International Conference on Numerical Methods in Geomechanics, Nagoia, Japan, pp. 613-620.

Zienkiewicz, O. C. and Nayak, G. C. (1971) - "A General Approach to Problems of Plasticity and Large Deformation Using Isoparametric Elements", Procedure Conference on Matrix Methods in Structural Mechanics, Wright-Patterson A. F. Base, Ohio.

Zienkiewicz, O. C. and Naylor, D. J. (1971) - "The Adaptation of Critical State Soil Mechanics Theory for Use in Finite Elements", Roscoe Memorial Symposium, Great Bretain, pp. 537-547.

Zienkiewicz, O. C. (1977) - "The Finite Element Method", Third Edition, McGraw Hill Publishing Company, London.

Zienkiewicz, O. C. and Mroz, Z. (1984) - "Generalized Plasticity Formulation and Applications to Geomechanics", Mechanics of Engineering Materials, Chapter 33, edited by Desai and Gallagher, John Wiley & Sons Ltd, pp. 655-679.

APPENDIX A

CAUCHY'S, LAGRANGE'S AND KIRCHOFF'S STRESS TENSORS

A brief review of the difference of the three kinds of stress {Cauchy(σ_{ij}), Lagrange(T_{ij}) and Kirchoff(S_{ij})} normally used in large deformation analysis, as well as the connection to each other is presented as follows:

- Cauchy's stress tensor is a tensor which is referred to the strained state (deformed configuration), while Lagrangian and Kirchoff stress tensors are always referred to the initial state (original configuration) in a way that is physically artificial though mathematically consistent;

- The Cauchy stress tensor σ_{ij} is symmetric. The relation between the Lagrangian and Cauchy stress tensors is given by:

$$T_{ij} = \det\left|\frac{\partial x_m}{\partial X_l}\right| \left[\frac{\partial X_j}{\partial x_n}\right] \sigma_{ni} \qquad (A.1)$$

which is not symmetric. The Lagrangian tensor would be inconvenient to use in a stress-strain law in which the strain tensor is always symmetric.

- The relation between the Kirchoff and Cauchy stress tensors is given by:

$$S_{ij} = \det\left|\frac{\partial x_m}{\partial X_l}\right| \left[\frac{\partial X_i}{\partial x_\kappa}\right]\left[\frac{\partial X_j}{\partial x_\omega}\right] \sigma_{\kappa\,\omega} \qquad (A.2)$$

which is symmetric. The Kirchoff stress tensor is more suitable for use in a stress-strain law in which the strain tensor is always symmetric.

- Consequently the relation between Kirchoff and Lagrange stress tensors is given by:

$$S_{ij} = \left[\frac{\partial X_j}{\partial x_\omega}\right] T_{i\,\omega} \qquad \text{(A.3)}$$

APPENDIX B

CONTOURS OF RATIO OF STRESS {q/[p g(θ)]} IN A SHALLOW FOUNDATION ANALYSIS

B.1. Introduction

The value of the ratio of stress {q/[p g(θ)]} is intended to express the proximity of the state of stress at some point in the stress field to the State Boundary Surface.

B.2. Undrained Loading and After Loading (Consolidation) Ratio of Stress Contours

The contours of the ratio {q/[p g(θ)]} during undrained loading of the shallow foundation represented in Section 7.6, for the case of loose (e = 0.87) and dense (e = 0.58) material is presented respectively in Figures B.1 and B.2. After undrained loading behavior, the pore pressure in the region is allowed to consolidate, and in Figures B.3 and B.4 the contours after full consolidation are presented for void ratio=0.87 and 0.58 respectively.

If comparison is made between Figures B.1 (loose material) and B.2 (dense material) for the undrained behavior at the end of loading it can be noticed that a pronounced difference in the value of maximum ratio of stress exists. This occurs because, as can be seen in Figure 5.3 of Section 5.2.1.1, the State Boundary Surface, which encloses all the possible states a sample of a cohesionless medium may assume, is bigger for denser materials.

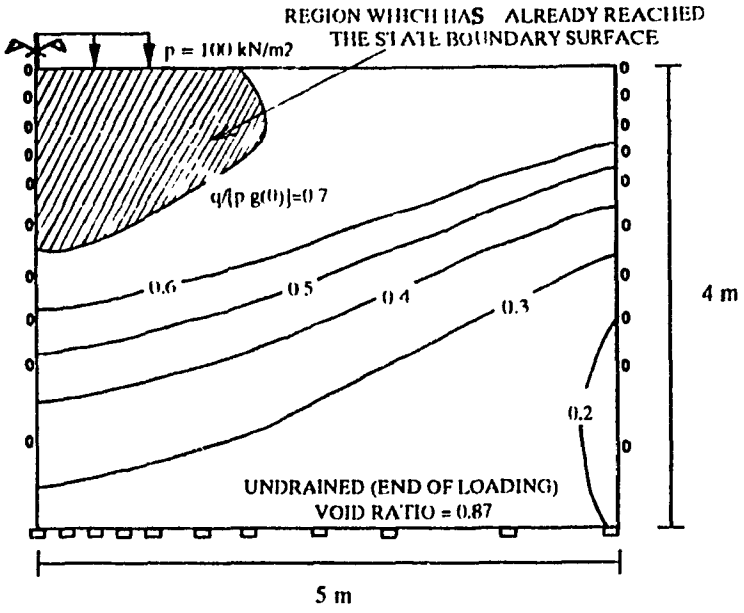

Figure B.1 - Contours of {q/[p g(θ)]} for the End of Undrained Loading and Void Ratio = 0.87

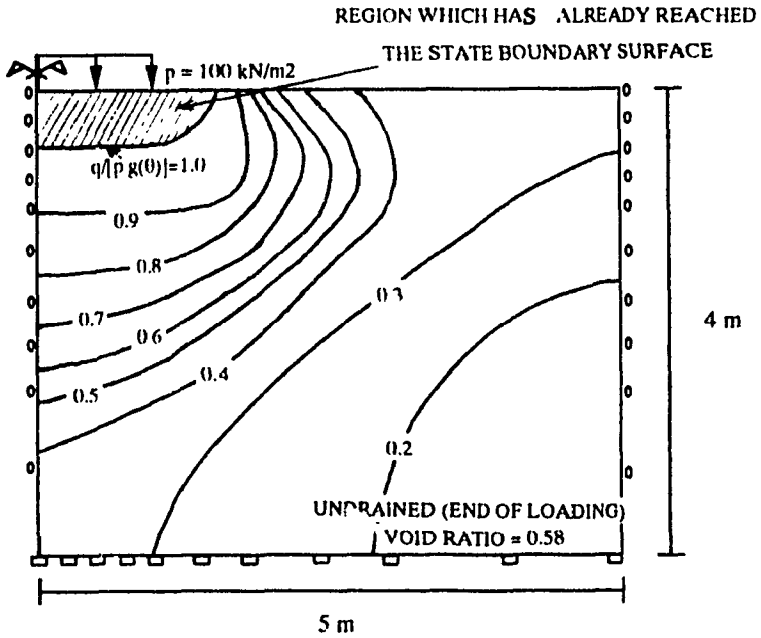

Figure B.2 - Contours of {q/[p g(θ)]} for the End of Undrained Loading and Void Ratio = 0.58

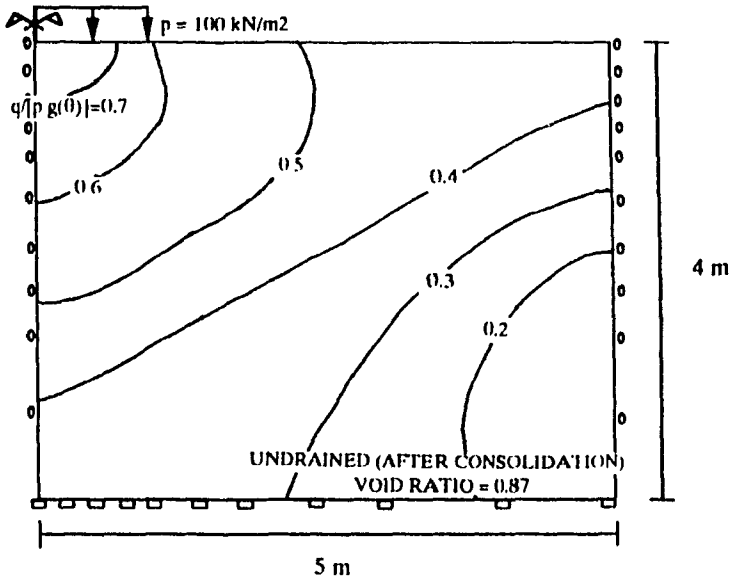

Figure B.3 - Contours of {q/[p g(θ)]} After Consolidation of the Pore Pressure Built During Undrained Loading and Void Ratio = 0.87

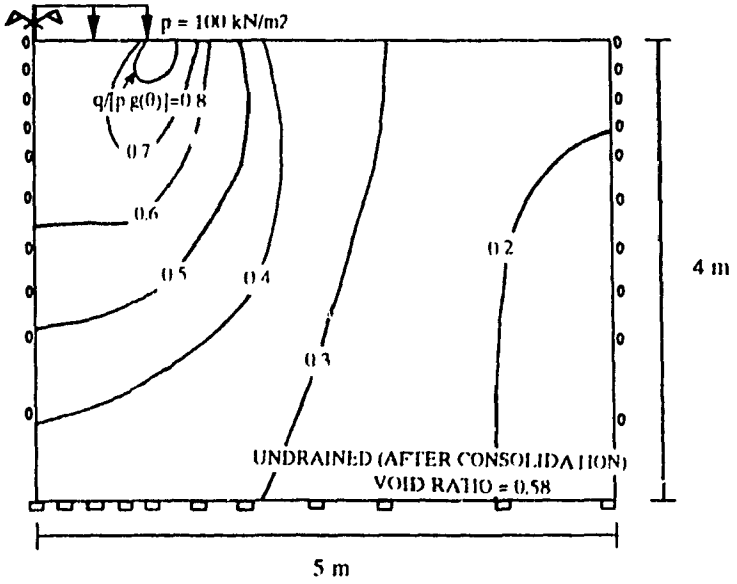

Figure B.4 - Contours of {q/[p g(θ)]} After Consolidation of the Pore Pressure Built During Undrained Loading and Void Ratio = 0.58

The region which have already reached the State Boundary Surface at the end of undrained loading (shaded area) for the case of loose material (e=0.87) is larger than for dense material (e=0.58).

After the consolidation of the pore pressure built during undrained loading, the ratio of stress decreases for both loose (Figure B.3) and dense(Figure B.4) materials.

B.3. Drained and Partly Drained Loading Ratio of Stress Contours

The contours of $\{q/[p\ g(\theta)]\}$ value during drained loading of the shallow foundation represented in Section 7.6, for the case of loose (e = 0.87) and dense (e = 0.58) material is presented in Figures B.6 and B.7 respectively. After undrained loading behavior, the pore pressure in the region is allowed to consolidate, and in Figures B.3 and B.4 the contours after full consolidation are presented for void ratio=0.87 and 0.58 respectively.

The difference in magnitude of the value of maximum ratio of stress for the drained loading is apparent if comparison is made between Figures B.5 (loose material) and B.6 (dense material), but it is of small value and it can be noticed that neither loose nor dense drained loading reaches the State Boundary Surface at any point of the stress field.

In Figures B.7 (e=0.87) and B.8 (e=0.58), the difference in magnitude of the value of maximum ratio of stress for the partly drained loading, as in the case of drained loading, is of small value and it can be noticed that neither loose nor dense partly drained loading reaches the State Boundary Surface at any point of the stress field.

If comparisons are made between drained and partly drained loading, it can be noticed that for the same void ratio, the contours patterns are very similar.

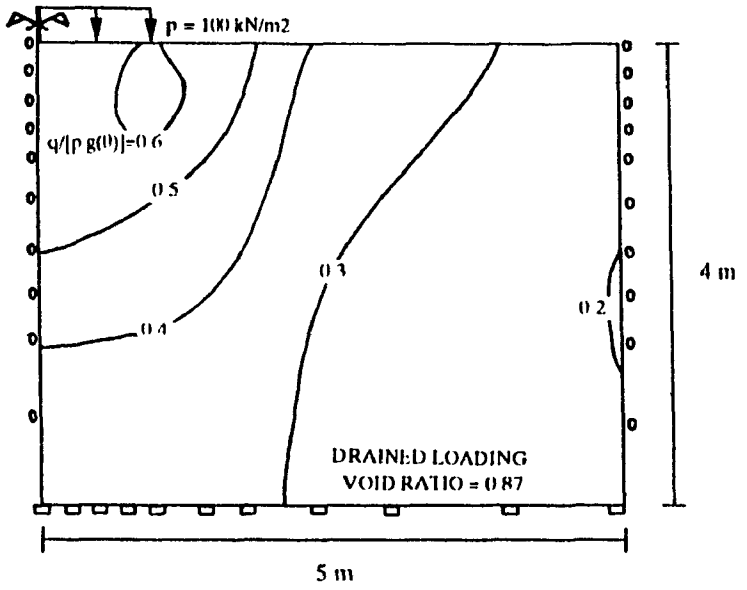

Figure B.5 - Contours of {q/[p g(θ)]} for Drained Loading and Void Ratio=0.87

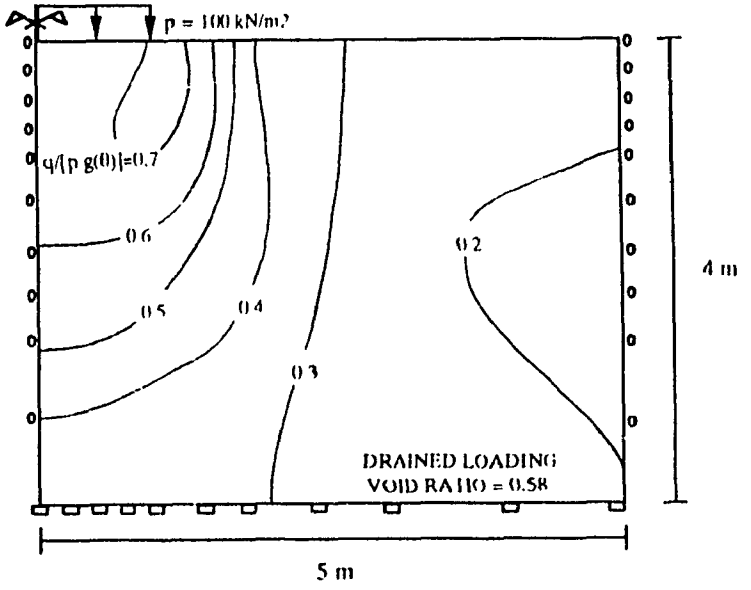

Figure B.6 - Contours of {q/[p g(θ)]} for Drained Loading and Void Ratio=0.58

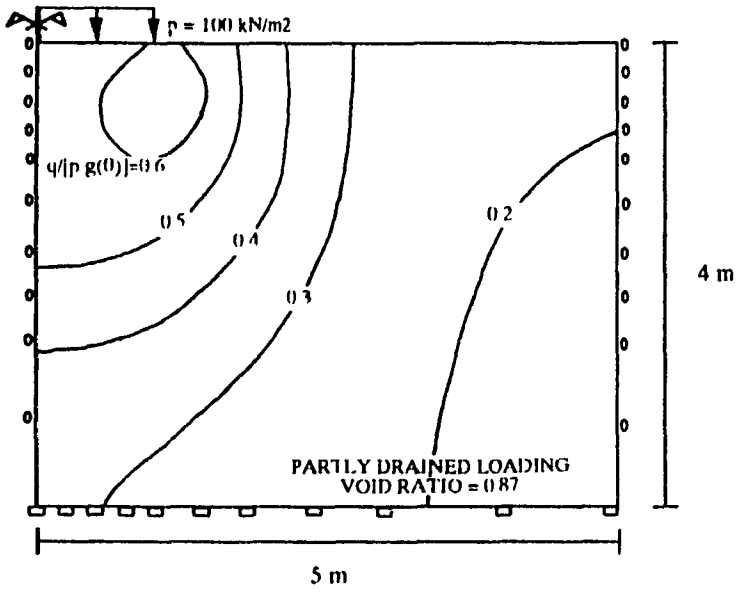

Figure B.7 - Contours of {q/[p g(θ)]} for the End of Partly Drained Loading and Void Ratio = 0.87

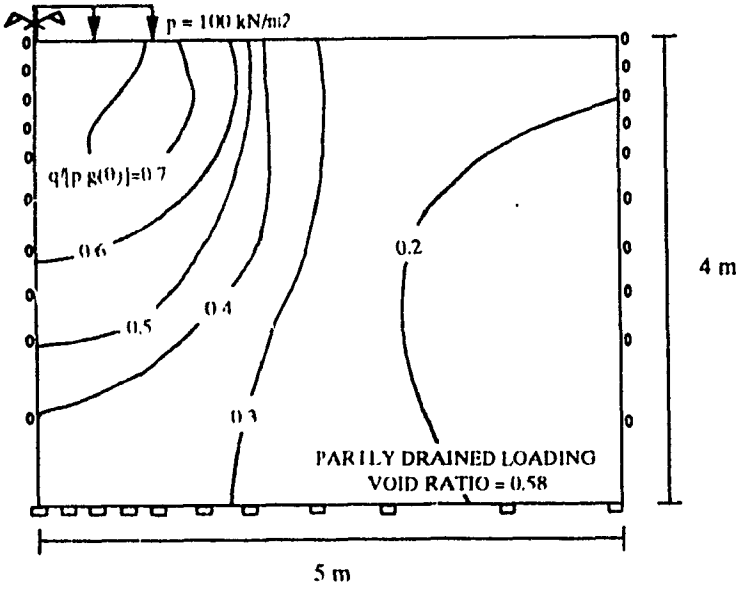

Figure B.8 - Contours of {q/[p g(θ)]} for the End of Partly Drained Loading and Void Ratio = 0.58

APPENDIX C

SEQUENTIAL CROSS SECTIONAL MESHES CHARACTERIZING THE FILLING OF THE SARAMENHA RESERVOIR

Considering Section G of the Saramenha Reservoir, the mesh of the this cross section is presented at several stages (1979, 1982, 1984 and 1988), with the respective boundary conditions, for the complete understanding of the reservoir filling with time.

All lateral boundary nodes are restrained in X and Y directions, except for nodes indicated as "•", which are free to move in the Y direction, as may be seen in Figures C.3 and C.4.

The drainage always occurs through the top nodes of the elements located in the top layer.

The results of the analysis show that during consolidation the deposit flows towards the center of the reservoir. Note that in Figures C.2, C.3 and C.4, the alignment of successive nodes deviates from the vertical, especially close to the edge of the reservoir.

All the meshes containing the active elements in the sequential years of 1979, 1982, 1984 and 1988 are shown in Figures C.1, C.2, C.3 and C.4 respectively, as follows:

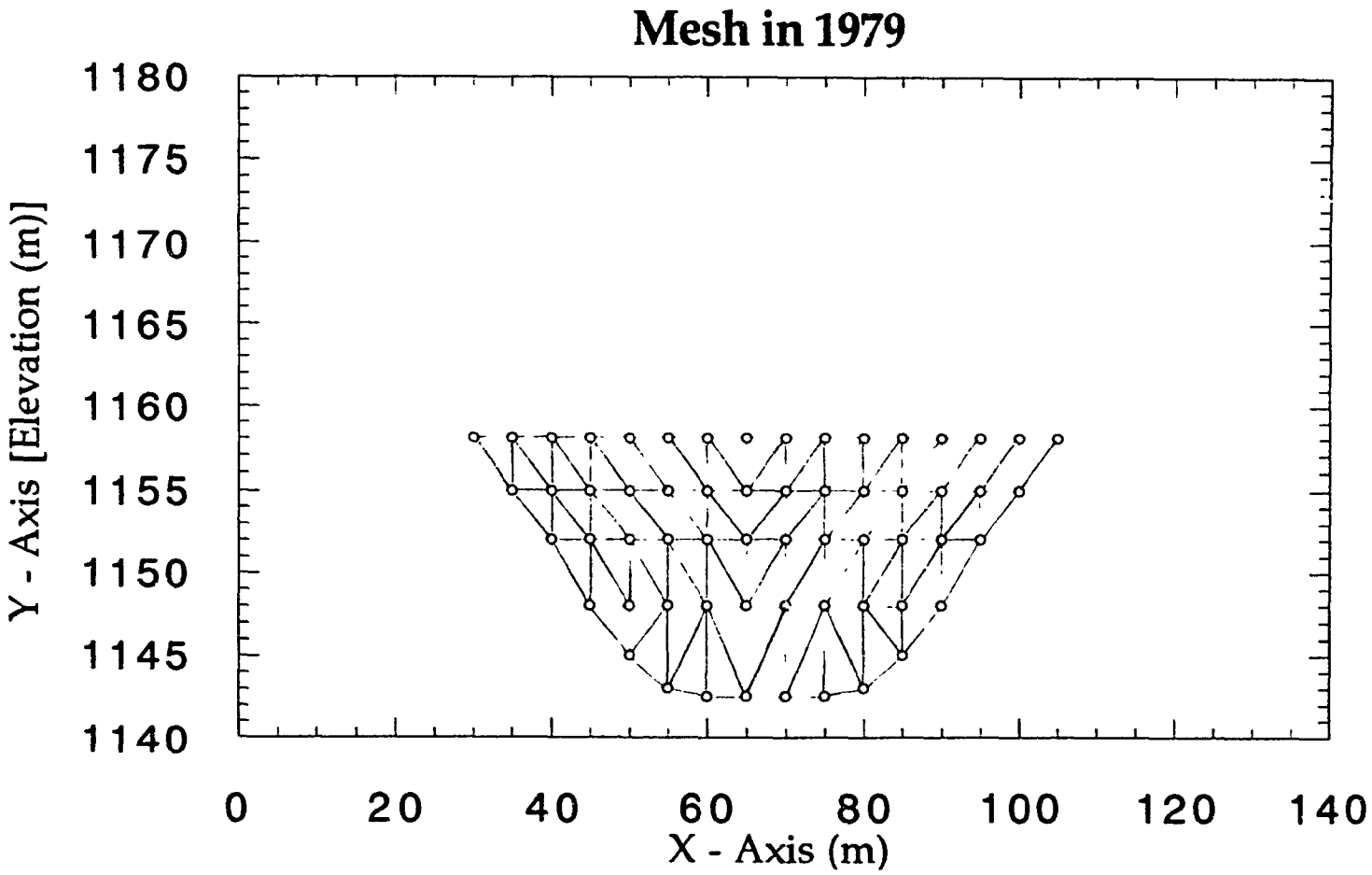

Figure C.1 - Active Mesh in 1979

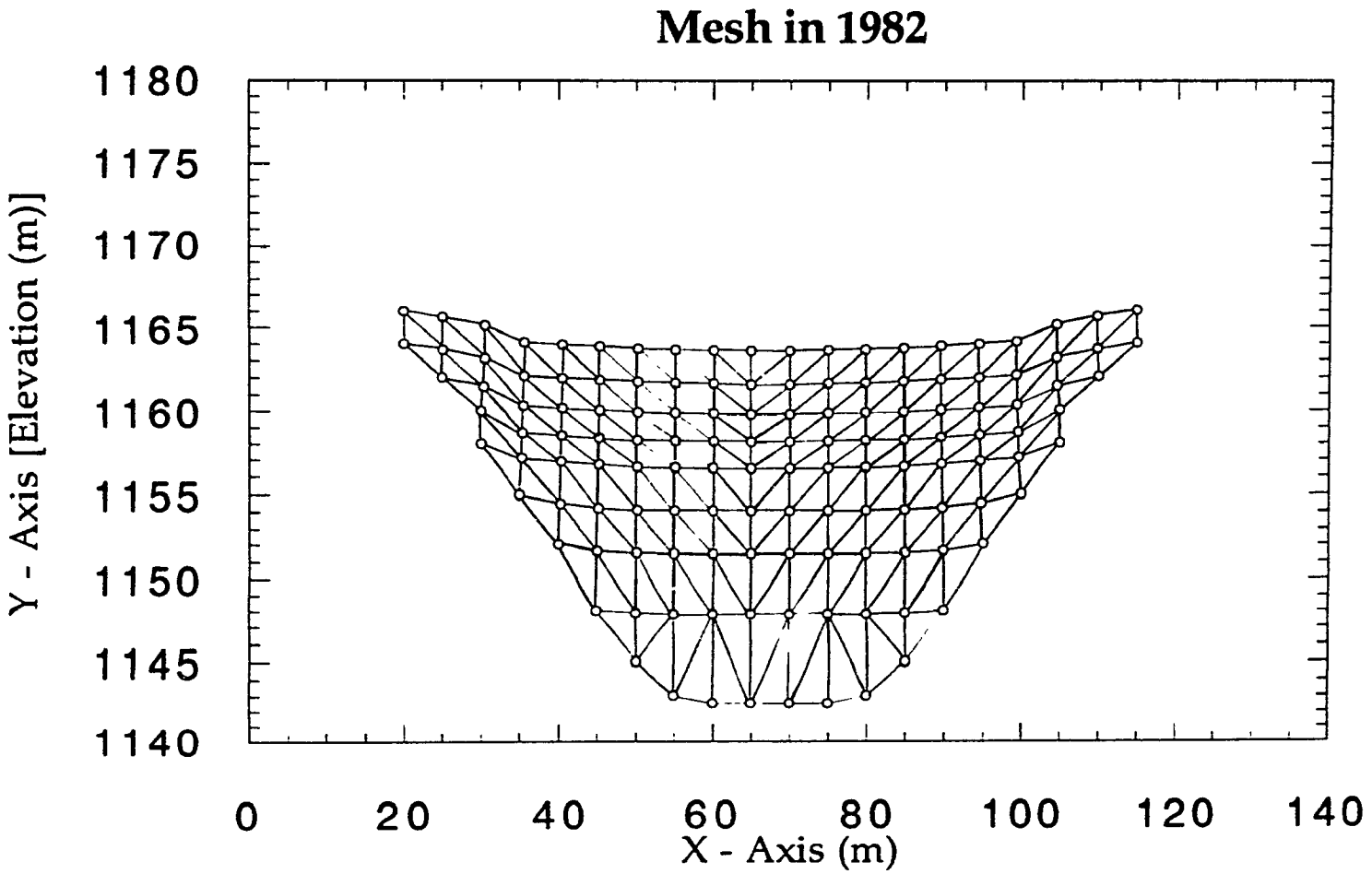

Figure C.2 - Active Mesh in 1982

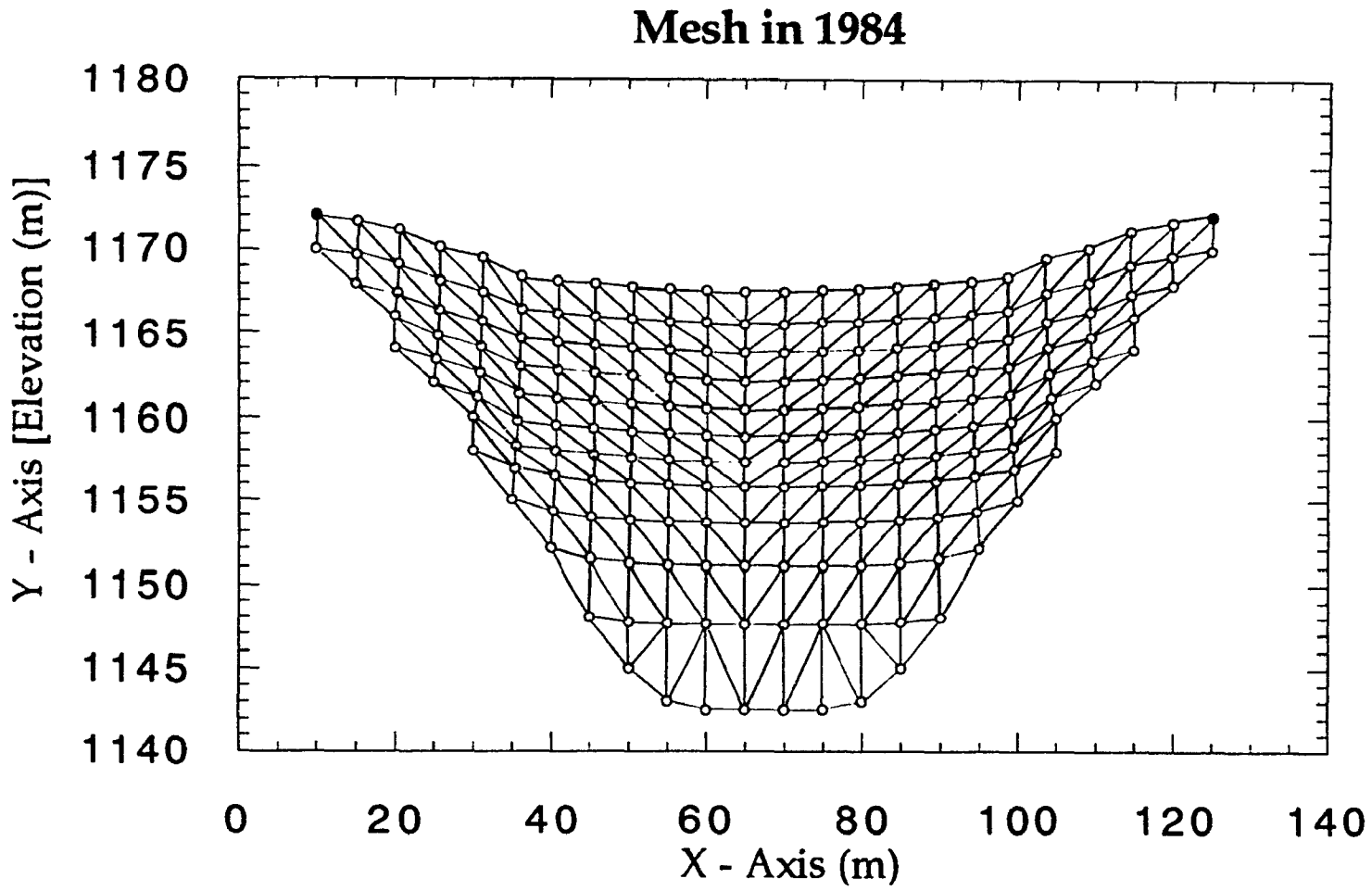

Figure C.3 - Active Mesh in 1984

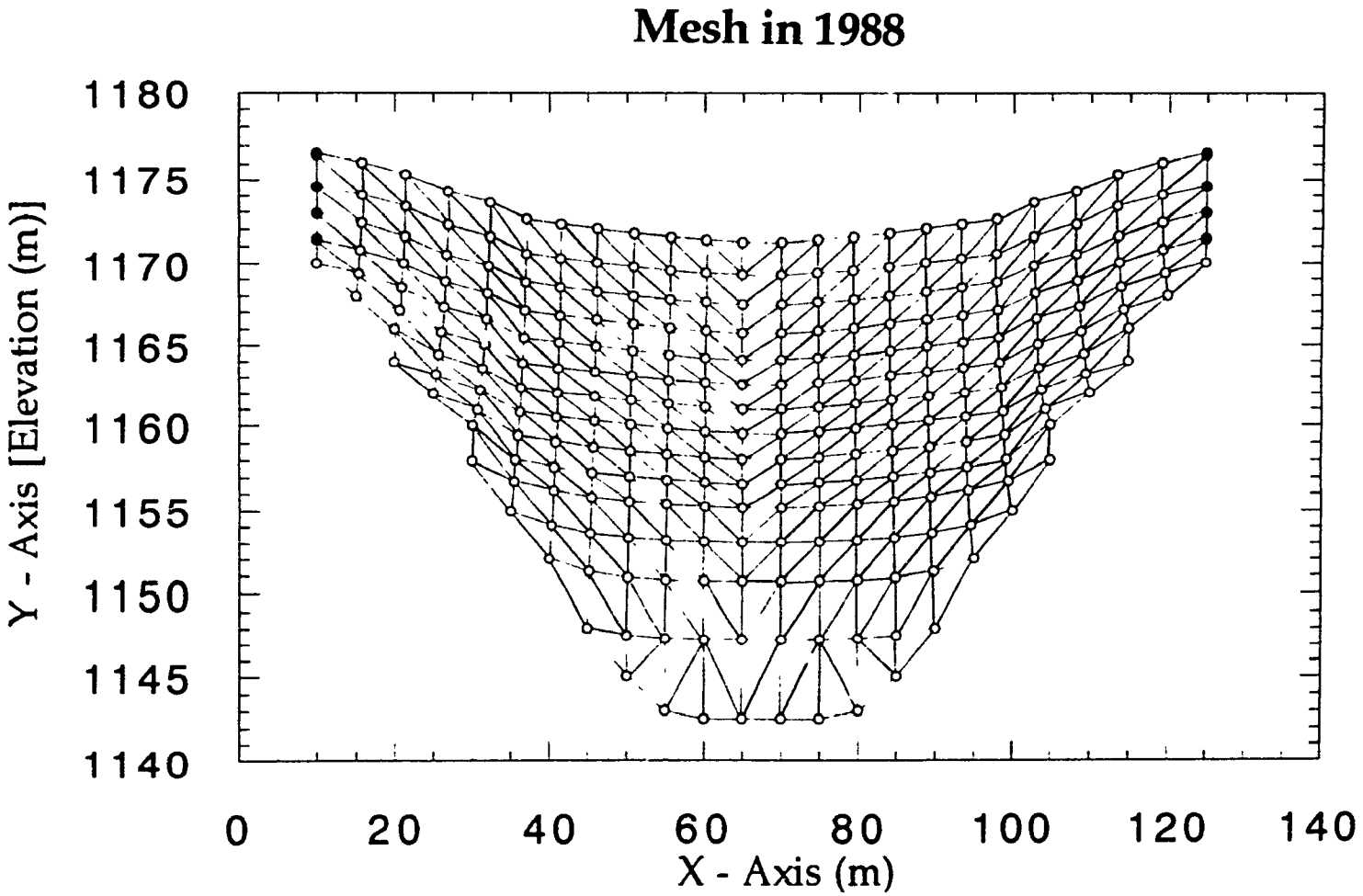

Figure C.4 - Active Mesh in 1988

APPENDIX D

PARAMETRIC NUMERICAL ANALYSIS FOR THE SARAMENHA CASE HISTORY

D.1. Introduction

A brief parametric analysis of the Saramenha Case History was made with soil parameters of the stress-strain relation assumed stiffer than those used in the laboratory tests. The sedimentation parameters were kept the same. This was done to determine whether the variation between the numerical predictions and the field observation could be caused by the fact that the laboratory test used for the calibration of the soil parameters may have been subject to disturbance and the results may not truly reflect the properties of the material.

D.2. New Saramenha Case History Analysis

The sedimentation and consolidation processes were run with the new parameters in the same way described previously in Chapter 8, with the reservoir divided in seven sections, with intervals of 80 meters between the sections, starting at the second disposal point, as shown in Figure 8.2.

Except for parameters E_o, A, R, S and T, which were changed with the objective of representing a stiffer material than the one represented by the parameters based in the laboratory data presented by Azevedo (1990), all the other parameters were the same as the ones used in the original simulation presented in Table 8.1.

The constitutive relation parameters for this new simulation were:

$E_0 = 20\ kN/m2$	$A = 0.4$	$\nu = 0.3$	$\mu = 0.75$
$\delta = 0.1$	$e_0 = 1.3$	$L = 0.088$	$R = 0.18$
$S = 0.008$	$T = 0.50$	$W = 1.33$	$\xi = 2.0$

Table D.1 - New Parameters of the Constitutive Relation for Saramenha's Case considering a Stiffer Material

Comparisons between the numerical results and field measurements are presented, as follows:

First, a comparison between the field and numerical profiles of deposited material is presented in Figures D.1 and D.2 for cross sections C and G (Figure 8.2) . The longitudinal profile of deposition of the reservoir is shown in Figure D.3.

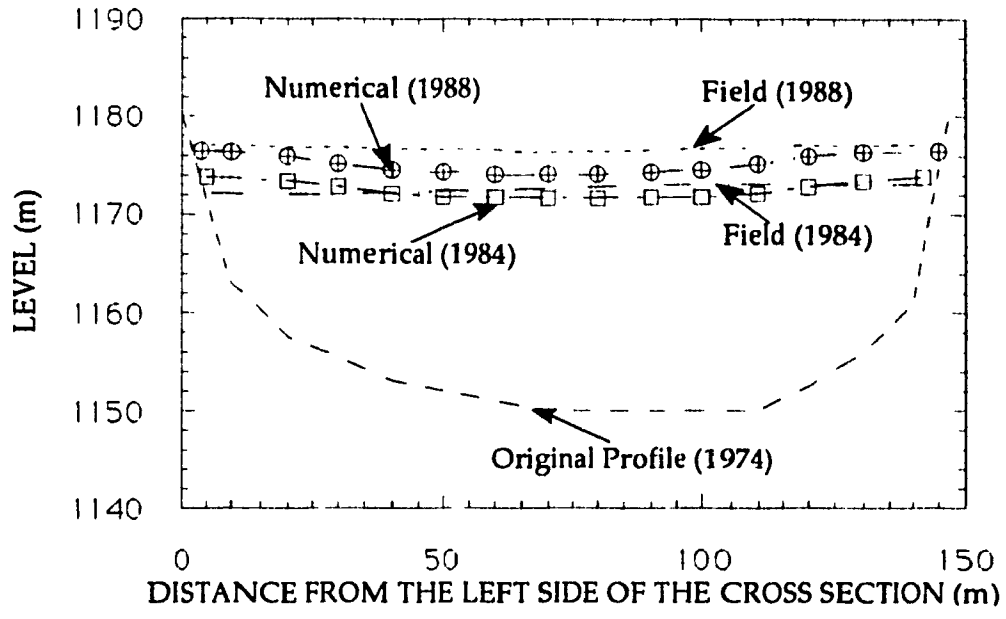

Figure D.1 - Comparison between Field and Numerical Profiles of Deposited Material for Cross Section C

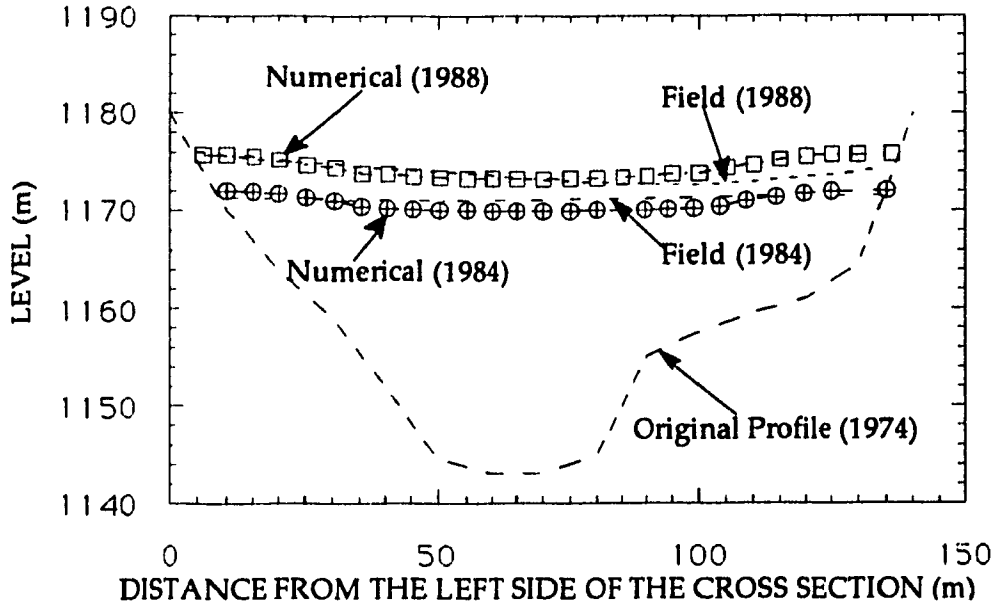

Figure D.2 - Comparison between field and Numerical Profiles of Deposited Material for Cross Section G

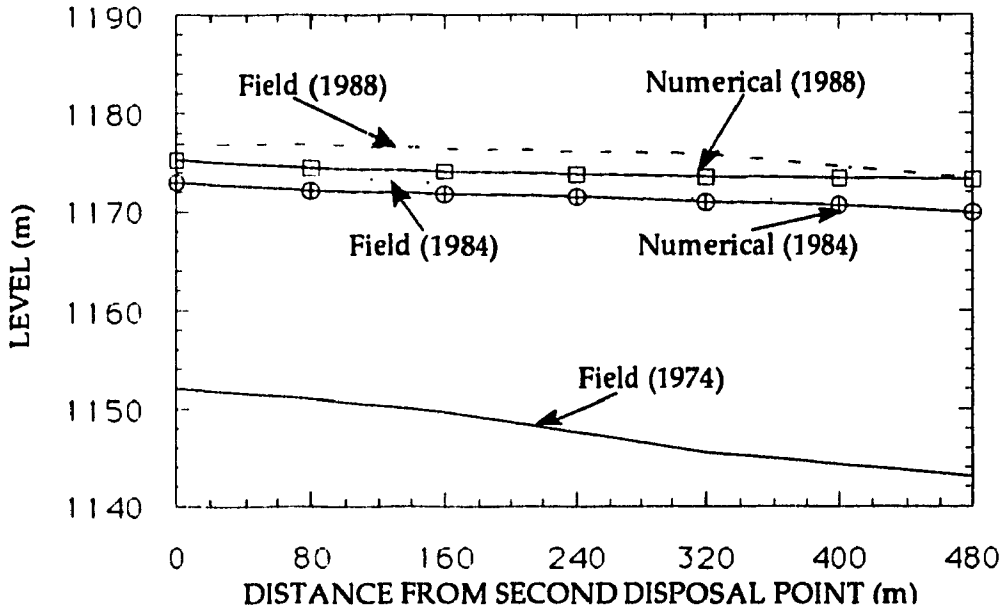

Figure D.3 - Comparison Between Field and Numerical Longitudinally Deposited Material

The average rise of the red slime with time in each section, is shown in Figure D.4. The relationship between time and level of sedimented material for all of the seven sections is clearly shown. Once again, the deposition of sediments is faster in the initial stages, up to 1982, when the cross sectional area of the sediment-fluid mixture is bigger and consequently the fluid velocity is smaller.

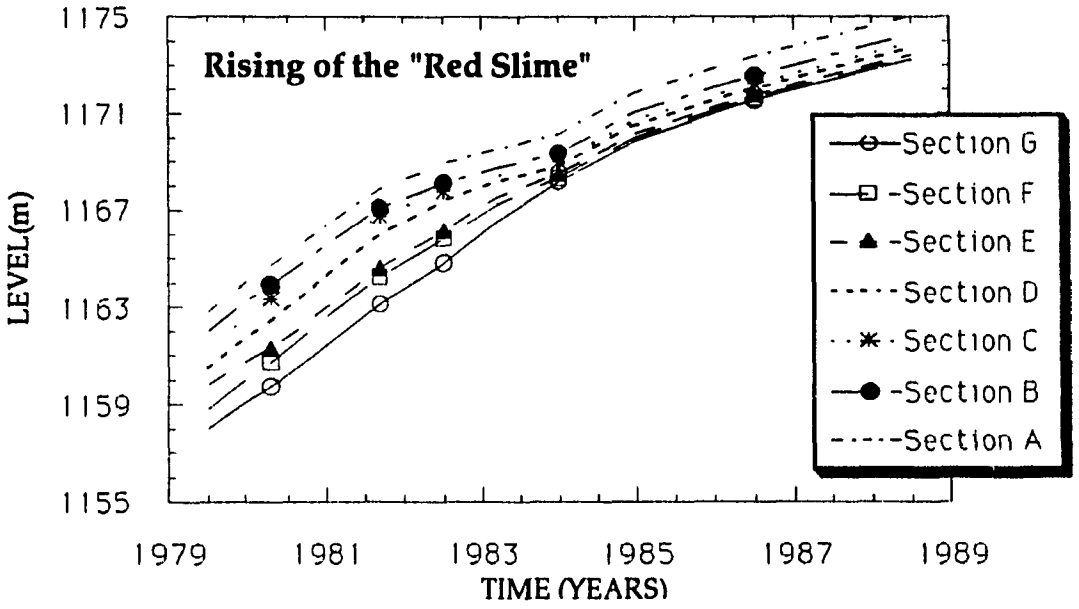

Figure D.4 - Average Increase of Deposited Sediments with Time

Note that for the middle of section G, the field and numerical values of the profiles of void ratio with depth and stresses (effective and total) with depth are compared and presented in Figures D.5 and D.6, respectively.

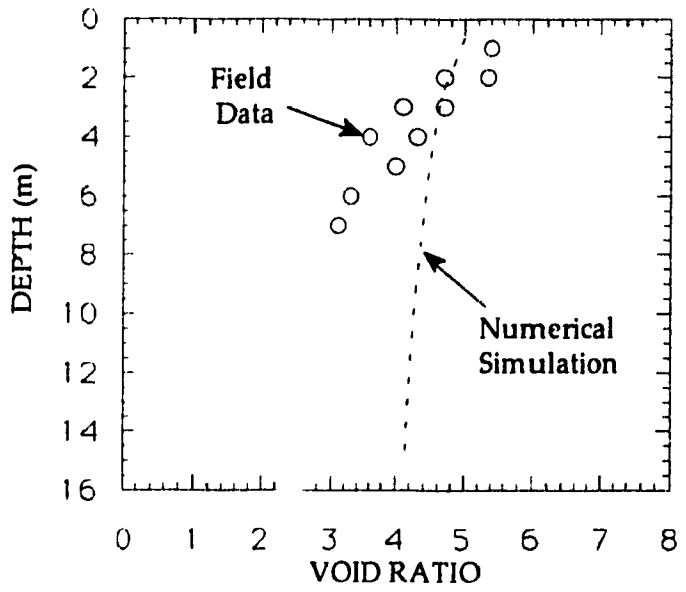

Figure D.5 - Comparison Between Field and Numerical Values of Variation of Void Ratio with Depth

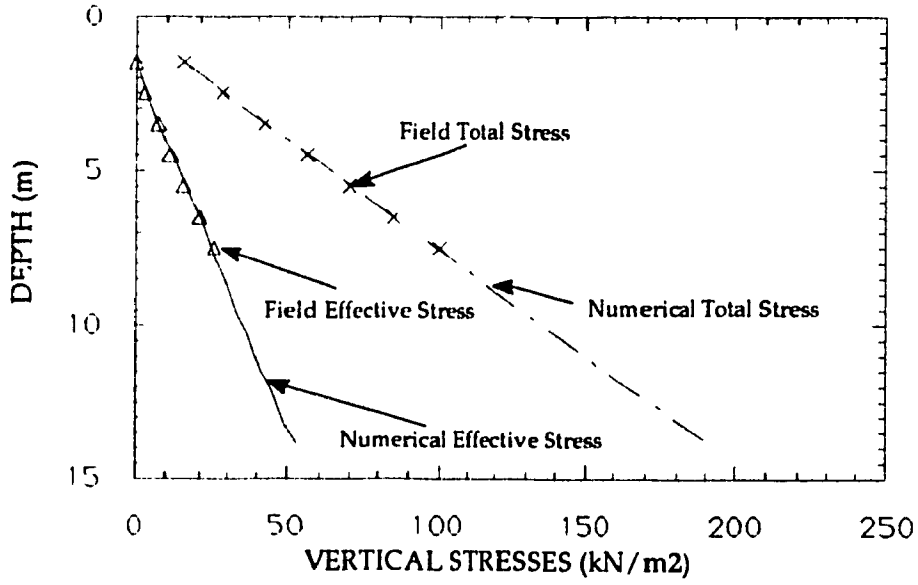

Figure D.6 - Comparison Between Field and Numerical Values of Variation of Total and Effective Stresses with Depth

D.3. Conclusions

It can be concluded that the simulation using the new constitutive parameters, characterizing stiffer material, gives a solution closer to the field results for the longitudinal profile and cross sections, as well as the stress profile, than the simulation executed in Chapter 8. However the new simulation does not give as good a correlation for void ratio profile as the previous one. This is as expected since the change in the void ratio with depth is smaller as the stiffness of the material increases.

In Figure D.4 it can be noticed that if comparison is made between this simulation, using constitutive relation parameters which characterize a stiffer material, and the simulation represented in Figure 8.14, a faster rise of the slime occurs in the new simulation,. The general characteristics however, are practically the same.

APPENDIX E

CODES DEVELOPED IN THIS THESIS

E.1. Code CONSED

The Code CONSED (Concordia Sedimentation) was developed incorporating the theory presented in Chapter 4. The computer program, written in Fortran, was run on the VAX2 (VAX6510) of Concordia University. The average execution time for a typical problem of this work was around 400 CPU seconds for the sedimentation part of the problem.

E.2. Code CONDIR

The Code CONDIR (Concordia Direct Stress-Strain Relation) was developed incorporating the first part of the constitutive relation developed in Chapter 5, which was: given the present state of a sample and a stress increment, the strain increment is then obtained. The computer program, written in Fortran, was run on the VAX2 (VAX6510) of Concordia University. The average execution time for a typical problem of this work was around 10 minutes CPU time.

E.3. Code CONINV

The Code CONINV (Concordia Inverse Stress-Strain Relation) was developed incorporating the second part of the constitutive relation developed in Chapter 5, which was: given the present state of a sample and a strain increment, the stress increment is then obtained. The computer program, written in Fortran, was run on the VAX2 (VAX6510) of Concordia University. The average execution time for a typical problem of this work was around 10 minutes CPU time.

E.4. Code CONFDEF

The Code CONFDEF (Concordia Finite Deformation) was developed incorporating the Finite Deformation Theory, applied to the solution of Coupled Consolidation problems, presented in Chapter 6. The computer program, written in Fortran, was run on the VAX2 (VAX6510) of Concordia University. The average execution time for a typical problem of this work was around 2 hours CPU time for each cross section.

E.5. Conclusion

This Codes are available for consultation in an extra volume which will be kept in the archives of the Geotechnical Computational Laboratory of the Civil Engineering Department of Concordia University. Any further information can be obtained from Dr. H. B. Poorooshasb or Dr. M. M. Douglass.

APPENDIX F

UNIDIMENSIONAL CONSOLIDATION TESTS WITH CONSTANT RATE OF DEFORMATION

F.1. Introduction

This Appendix shows the results of unidimensional tests with constant rate of deformation performed in the waste residuals of the bauxite mine located in Saramenha, Brazil, as reported by Azevedo in 1990. The tests were made to predict the behavior as well as to obtain the properties of the bauxite waste material when it is subjected to a K_0 stress path, for a better understanding of the consolidation process.

F.2. Laboratory Tests

In order to obtain the consolidation properties of the bauxite tailings, a serie of samples were tested under unidimensional tests, with different initial void ratio and water content and small rate of deformation (as seen in Table F.1).

Test	Rate of Deformation (mm/s)	Initial Void Ratio	Initial Water Content (%)
1	0.0001	4.65	132.11
2	0.000075	5.01	142.35
3	0.000050	5.22	148.40

Table F.1 - Properties of Material of the Serie of Unid nensional Consolidation Tests performed in Bauxite Tailings Samples

By using slow velocity testing, one acquire an uniform consolidation in the whole sample, avoiding the variation of the void ratio on it.

The figures F.1 to F.3 show the variation of the void ratio with the vertical effective stress, which is an essential factor in the calibration of the constitutive relation for the soil. The variation of permeability with void ratio (figures F.4 and F.5), also represents an important data for materials which have a significant volumetric deformation as the case of the bauxite tailings studied in the present work.

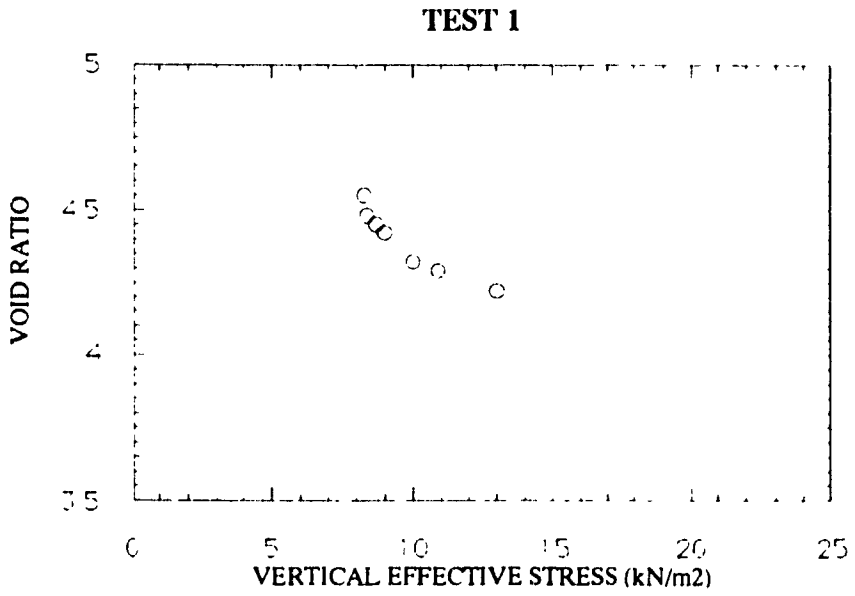

Figure F.1 - Void Ratio versus Vertical Effective Stress for Test 1

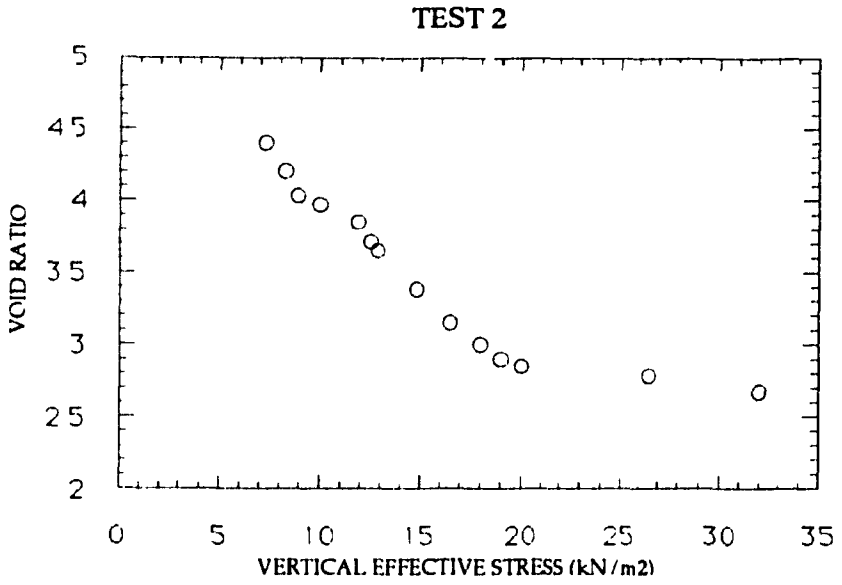

Figure F.2 - Void Ratio versus Vertical Effective Stress for Test 2

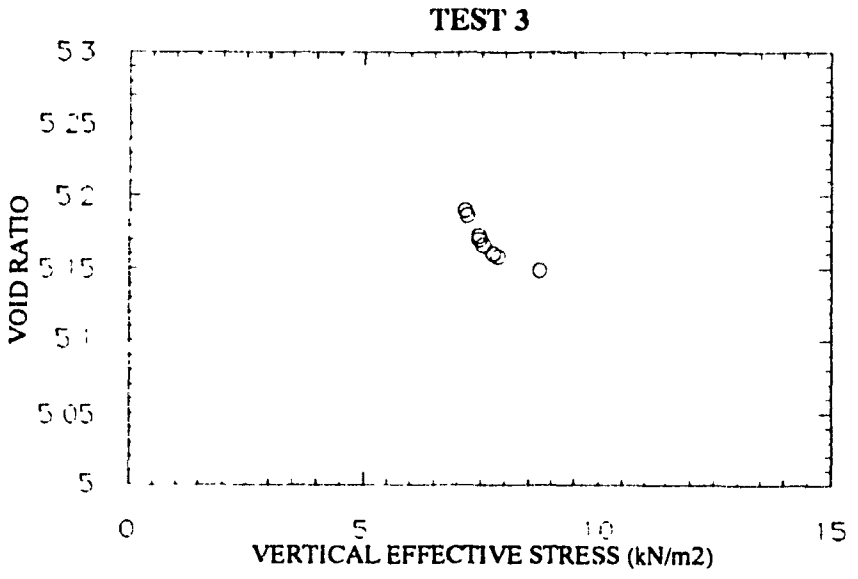

Figure F.3 - Void Ratio versus Vertical Effective Stress for Test 3

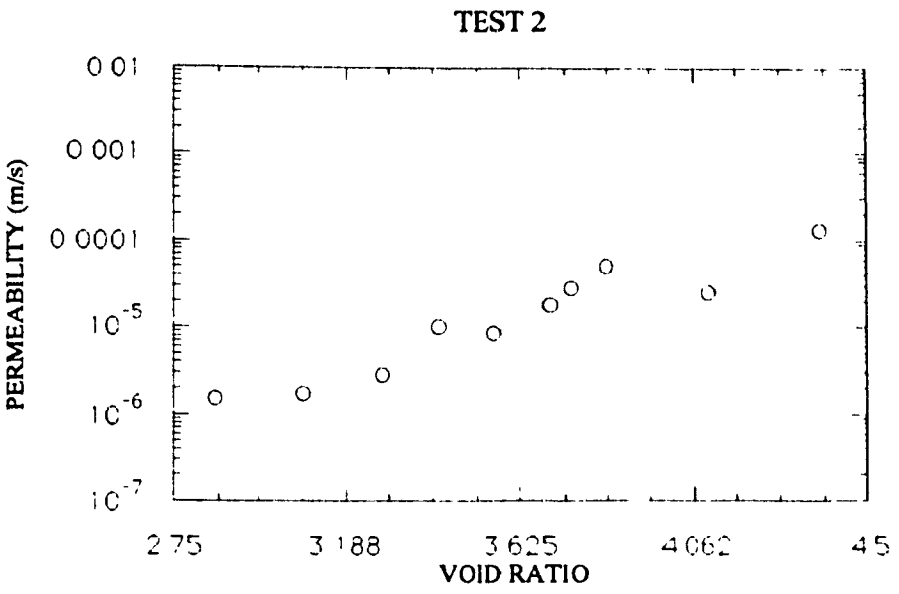

Figure F.4 - Permeability versus Void Ratio for Test 2

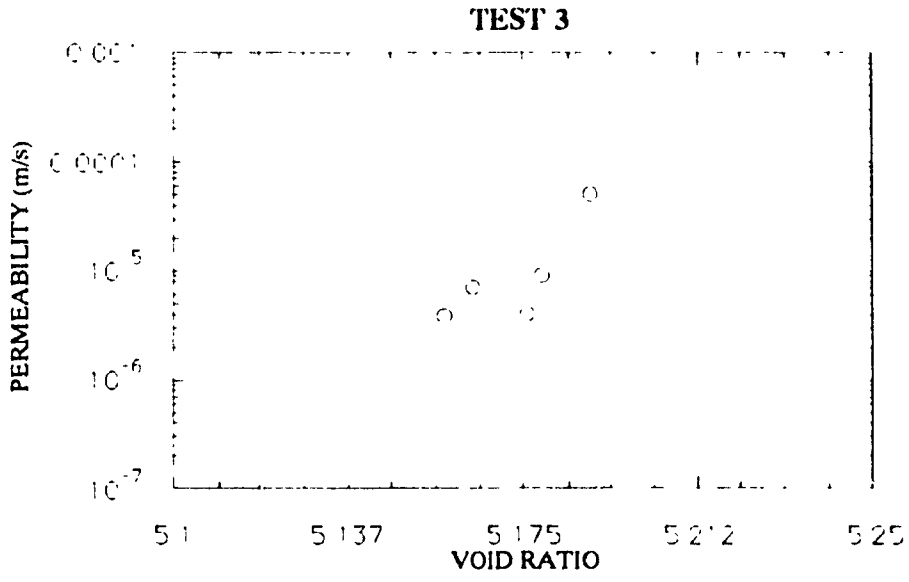

Figure F.5 - Permeability versus Void Ratio for Test 3